

NASA TECHNICAL NOTE

NASA TN D-5630



NASA TN D-5630

CASE FILE
COPY

EXAMPLES OF THE USEFULNESS
OF SATELLITE DATA IN GENERAL
ATMOSPHERIC CIRCULATION RESEARCH

Part I - Monthly Global Atmospheric Circulation
Characteristics as Reflected in TIROS VII
Radiometric Measurements

by

Lewis J. Allison

Goddard Space Flight Center

Earl R. Kreins

USAF Environmental Technical Applications Center

Fredric A. Godshall

Environmental Science Services Administration

Guenter Warnecke

Goddard Space Flight Center

NATIONAL AERONAUTICS AND SPACE ADMINISTRATION • WASHINGTON, D. C. • DECEMBER 1969

1. Report No. NASA TN D-5630	2. Government Accession No.	3. Recipient's Catalog No.	
4. Title and Subtitle Examples of the Usefulness of Satellite Data in General Atmospheric Circulation Research—Part I, Monthly Global Atmospheric Circulation Characteristics as Reflected in TIROS VII Radiometric Measurements		5. Report Date December 1969	
		6. Performing Organization Code	
7. Author(s) Lewis J. Allison, Earl R. Kreins, Fredric A. Godshall, and Guenter Warnecke		8. Performing Organization Report No. G-959	
9. Performing Organization Name and Address Goddard Space Flight Center Greenbelt, Maryland 20771		10. Work Unit No. 160-44-03-02-51	
		11. Contract or Grant No.	
		13. Type of Report and Period Covered Technical Note	
12. Sponsoring Agency Name and Address National Aeronautics and Space Administration Washington, D. C. 20546		14. Sponsoring Agency Code	
15. Supplementary Notes			
16. Abstract A climatological analysis was made of TIROS VII 8-12 micron radiation data for the period June 19, 1963, through December 31, 1964. Patterns in TIROS VII quasi-global maps of monthly mean equivalent black-body temperatures in the "window" region appear to be well related to conventional cloud cover observations, the major Northern Hemisphere ridge-trough positions, the seasonal movement of the intertropical zone of convergence, and large-scale monsoonal circulation patterns over India and southeast Asia.			
17. Key Words Suggested by Author Atmospheric circulation Climatological data from TIROS VII Global atmospheric circulation TIROS VII climatological data		18. Distribution Statement Unclassified—Unlimited	
19. Security Classif. (of this report) Unclassified	20. Security Classif. (of this page) Unclassified	21. No. of Pages 80	22. Price* \$3.00

*For sale by the Clearinghouse for Federal Scientific and Technical Information
Springfield, Virginia 22151

Page intentionally left blank

Page intentionally left blank

CONTENTS

INTRODUCTION	1
DESCRIPTION OF THE SATELLITE RADIATION MEASUREMENTS	2
TIROS VII Radiation Experiment	2
Computer Mapping Procedure	3
Radiation Data Coverage	4
METHODS OF ANALYSIS	10
Radiation Data	10
Supplementary Climatological Data	11
MONTHLY CLIMATOLOGICAL DISCUSSION	12
June 19-30, 1963	12
July 1963	13
August 1963	14
September 1963	15
October 1963	16
November 1963	16
December 1963	17
January 1964	18
February 1964	19
March 1964	20
April 1964	21
May 1964	22
June 1964	23
July 1964	24
August 1964	25
September 1964	26
October 1964	26
November 1964	27
December 1964	27
CONCLUSIONS	28
ACKNOWLEDGMENTS	30
References	31

- Appendix A—(a) Maps of monthly mean equivalent blackbody temperature, June 1963-December 1964, from TIROS VII radiometric measurements in the 8-12 micron window.
- (b) Maps of mean monthly cloud coverage from surface observations, of the monthly range of the position of the ITC, of the principal axes of the 700-mb maximum winds with isotachs (except June 1963), and of the mean monthly trough positions, June 1963-December 1964.
- (c) Monthly mean surface streamlines in the tropics, ITC positions, and precipitation frequency and amounts, based upon long-term climatological data.....

EXAMPLES OF THE USEFULNESS OF SATELLITE DATA IN GENERAL ATMOSPHERIC CIRCULATION RESEARCH

PART I

MONTHLY GLOBAL ATMOSPHERIC CIRCULATION CHARACTERISTICS AS REFLECTED IN TIROS VII RADIOMETRIC MEASUREMENTS

by

Lewis J. Allison
Goddard Space Flight Center

Earl R. Kreins, Major, USAF^{*}
USAF Environmental Technical Applications Center

Fredric A. Godshall[†]
Environmental Science Services Administration

Guenter Warnecke[‡]
Goddard Space Flight Center

INTRODUCTION

The applicability of radiometric measurements from meteorological satellites for various meteorological and climatological purposes has been documented in a large number of publications since the first successful radiation experiment on TIROS II in 1962. Emphasis was generally given to synoptic applications (Fritz and Winston, 1962; Rao and Winston, 1963; Allison et al., 1964, 1966; Allison and Warnecke, 1966, 1967; Widger et al., 1966), or to problems of the atmospheric or planetary radiation balance (Winston and Rao, 1962; Bandeen et al., 1965; House, 1965; Anderson, 1966; Möller, 1967; Hanson et al., 1967; Vonder Haar, 1968; Raschke et al., 1968; Raschke, 1968). Only recently, steps were taken to summarize satellite observations in order to derive characteristics of large-scale, i.e. planetary-scale, atmospheric general circulation and its monthly or year-to-year variations (Winston, 1969; Winston and Taylor, 1967; Taylor and Winston, 1968; Sadler, 1968; Kreins and Allison, 1969).

^{*}Air Weather Service member temporarily attached to Goddard Space Flight Center. Present affiliation: Headquarters, U. S. Air Force, Joint Meteorological Satellite Program Office, Washington, D. C.

[†]Environmental Data Service, ESSA, Silver Spring, Maryland.

[‡]On leave from the Free University of Berlin, Germany, as NAS-NRC Senior Postdoctoral Resident Research Associate with NASA.

This paper is one of a series in which satellite observations, both infrared and television, will be analyzed in the form of monthly mean charts, in order to investigate and demonstrate the degree of usefulness of these data for the observation, description, and understanding of variations in large-scale parameters in the general circulation of the earth's atmosphere.

In this first paper, quasi-global maps of monthly mean equivalent blackbody temperature in the 8-12 micron "window" region are presented in atlas form. These maps were derived for the period of the TIROS VII medium-resolution infrared radiometer experiment from June 19, 1963, through December 31, 1964. Northern Hemisphere surface cloud observations are summarized in the form of monthly means for the same period. In addition, the mean position of the ITC (intertropical convergence zone) is presented for each month of the year. A brief meteorological and climatological discussion is presented to aid in the interpretation of the radiation data.

DESCRIPTION OF THE SATELLITE RADIATION MEASUREMENTS

TIROS VII Radiation Experiment

The TIROS VII meteorological satellite, launched on June 19, 1963, contained a five-channel medium-resolution scanning radiometer. The optical axis of the radiometer was at a fixed angle of 45° from the spin axis of the satellite. The radiometer viewed in two collinear directions, 180° apart. The spinning motion of the satellite at the rate of about 10 rpm, combined with the orbital motion, with the spin axis approximately fixed with respect to inertial space, produced a rather complicated pattern of scanning. The instantaneous field of view of the radiometer subtended an angle of 5° , which intercepts a spot about 55 km in diameter when viewing the nadir from the TIROS VII mean orbital height of 635 km. The orbital inclination of the spacecraft was 58.2° , preventing observations poleward of about 60° latitude.

The energy received by the infrared channels of the radiometer was converted into units of equivalent blackbody temperature (in $^{\circ}\text{K}$). Equivalent blackbody temperature, T_{BB} , is defined as that temperature of an isothermal blackbody filling the field of view (as in the laboratory calibration) which causes the same response from the radiometer as does the generally non-Planckian spectral distribution of the radiation emerging from the top of the atmosphere in the direction of the satellite.

A detailed description of the radiometer, the data processing, the scanning modes, the pre-launch calibration, and an observed degradation in the calibration after launch and methods of correcting for this degradation is contained in the TIROS VII Radiation Data Catalog and Users' manual (Staff Members, 1964a, 1964b, 1965 and 1966). Readers interested in additional information concerning the analysis and interpretation of TIROS VII radiation data for a single day on a quasi-global basis are referred to Allison and Warnecke (1967) and other studies mentioned in the Introduction.

The channel used in this study responded to emitted radiation in the 8-12 micron (atmospheric "window") portion of the electromagnetic spectrum, where gaseous absorption in the atmosphere is minimal and therefore the radiation originates mainly from the earth's surface and/or clouds.

Computer Mapping Procedure

The individual equivalent blackbody temperature measurements were averaged by an IBM 7094 computer over a field of equally-spaced grid points, superimposed on a Mercator projection with a resolution of 5° of longitude per mesh interval. Because of the nature of the map projection, the span of latitude between adjacent grid points is variable, ranging from 5° at the equator to about 2.5° at latitude 60° . A simple filter having three weights in both the meridional and zonal directions was passed over the grid array to smooth out perturbations due to spatial and temporal sampling bias in the data, resulting from the interrogation pattern and history of the satellite. The weight array of the 3×3 filter was the following:

.0625	.1250	.0625
.1250	.2500	.1250
.0625	.1250	.0625

The weighted temperature was assigned to the central value. The computer was instructed to reject all data with scan nadir angles greater than 40° , to lessen limb-darkening effects. Also, to avoid mislocation of data (Allison and Warnecke, 1966), a provision was added that, whenever the minimum nadir angle occurring within a scan was greater than 38° , all data from the entire scan were rejected. All ambiguous portions of what is known as the "alternating open scanning mode" were thus eliminated, as well as most of the "closed scanning mode" (see Staff Members, 1964a, for further details).

It was mentioned above that the calibration of the radiometer was observed to degrade while in orbit. A quantitative study of the degradation history was carried out, and correction nomograms were published in the TIROS VII Manual (Staff Members, 1964a, 1964b, 1965, 1966). These corrections were applied in the computer processing of these maps. The degradation with time was sufficiently slow to permit applying mean degradation corrections over six to nine days during each monthly period. As an example, the corrections applied for instrumental degradation of the TIROS VII $8-12\mu$ channel for January 21-22, 1964, orbits 3195 through 3203, are shown in Table 1.

Table 1

Corrections for Instrumental Degradation of
TIROS VII $8-12\mu$ Channel Applied to Data
for January 21-22, 1964.

(The corrected T_{BB} is obtained by algebraically
adding ΔT to the observed T_{BB} .)

T_{BB} ($^{\circ}$ K)	ΔT ($^{\circ}$ K)
200	+3.8
210	+4.2
220	+4.5
230	+4.8
240	+5.2
250	+5.6
260	+6.1
270	+6.6
280	+7.2
290	+7.6
300	+8.2

Radiation Data Coverage

For the purpose of this study, the data from the 8-12 micron channel were compiled into one 12-day map (June 19-30, 1963) and 18 monthly maps (July 1, 1963 through December 31, 1964) of mean equivalent blackbody temperature (see Appendix A, Figures A1(a) through A19(a) - "(a)" figures only).

The term "monthly maps" is, however, a misnomer insofar as TIROS VII orbital coverage over the world from 60°N to 60°S varied daily because of operational and instrumental factors caused by ground stations, and other such factors aboard the satellite; and because of the applied specifications for rejection of questionable data. Hence daily coverage over this large region varied greatly, and true monthly radiation maps, i.e. maps based on data equally distributed in space and time, were not obtained.

As an example, Table 2 indicates the variation by months in TIROS VII orbital coverage over the Indian Ocean (20°E to 155°E, 45°N to 50°S).

Table 2

Number of TIROS VII Orbits Per Month
Providing Useful Radiation Data Over the Indian Ocean.

1963		1964		1964	
Month	Orbits	Month	Orbits	Month	Orbits
June	60	January	150	July	60
July	160	February	140	August	70
August	150	March	155	September	45
September	145	April	135	October	70
October	170	May	100	November	110
November	130	June	60	December	60
December	105				

The periods of highest and lowest data coverage were October 1963 and September 1964, respectively. A further breakdown of weekly orbital coverage within 60° latitude and 60° longitude blocks from the equator to 60°N and 60°S is shown in Table 3.

Table 3

Orbital Coverage: June 19, 1963 to December 31, 1964.

(A unit in this table consists of 60 degrees of orbital coverage.)
(N and S indicate Northern and Southern hemispheres, respectively.)

1963		30°W–30°E	30°E–90°E	90°E–150°E	150°E–150°W	150°W–90°W	90°W–30°W
June 19-24	N	9	6	7	14	15	14
	S	10	13	18	10	6	4
June 25-30	N	13	10	10	13	19	20
	S	12	19	21	14	8	6
July 1-6	N	10	7	7	12	15	16
	S	9	13	15	10	6	4
July 7-12	N	13	9	11	17	21	19
	S	14	20	21	14	7	7
July 13-18	N	14	10	11	17	20	23
	S	15	21	23	14	8	7
July 19-24	N	15	9	10	16	20	18
	S	15	23	25	16	8	7
July 25-29	N	12	7	10	18	20	16
	S	16	22	21	13	6	7
July 30-31	N	2	3	3	4	4	3
	S	3	6	6	4	2	2
August 1-6	N	9	7	6	10	12	3
	S	10	15	17	10	5	2
August 7-12	N	10	8	11	14	16	7
	S	13	20	20	12	7	8
August 13-18	N	7	7	7	11	10	7
	S	10	12	15	8	6	3
August 19-24	N	11	9	12	17	17	11
	S	15	21	20	12	8	8
August 25-30	N	14	10	10	14	16	10
	S	11	18	19	14	9	6
Sept 1-6	N	11	9	8	12	14	8
	S	8	15	19	14	9	3
Sept 7-12	N	12	10	7	12	12	7
	S	10	17	20	13	8	4
Sept 13-18	N	15	12	6	9	8	9
	S	8	15	19	15	8	4

Table 3 (Continued)

1963		30°W—30°E	30°E—90°E	90°E—150°E	150°E—150°W	150°W—90°W	90°W—30°W
Sept 19-24	N	14	11	8	12	11	7
	S	9	18	20	15	8	5
Sept 25-30	N	10	9	8	10	12	6
	S	9	14	16	12	7	5
Oct 1-6	N	13	11	8	13	12	8
	S	12	19	23	15	8	4
Oct 7-12	N	11	7	7	14	14	9
	S	11	17	18	12	6	5
Oct 13-18	N	14	8	5	12	9	11
	S	10	17	21	13	7	3
Oct 19-24	N	9	7	8	15	8	10
	S	12	18	19	10	6	5
Oct 25-31	N	16	13	12	18	12	14
	S	16	24	27	17	10	6
Nov 1-6	N	8	6	10	14	11	9
	S	12	17	16	9	4	6
Nov 7-12	N	9	3	6	14	15	16
	S	12	17	16	8	2	4
Nov 13-18	N	7	4	8	11	13	12
	S	10	14	12	6	3	5
Nov 19-24	N	14	9	9	15	16	14
	S	13	21	22	15	7	6
Nov 25-27	N	3	3	2	3	3	3
	S	3	5	7	5	2	1
Dec 1-6	N	4	4	7	10	5	7
	S	11	15	13	7	2	5
Dec 7-12	N	6	6	10	11	8	7
	S	10	14	14	8	10	5
Dec 13-18	N	6	4	9	13	8	6
	S	14	18	16	8	3	6
Dec 19-26	N	5	4	5	10	9	5
	S	8	12	14	9	6	2
Dec 27-31	N	8	7	6	6	8	3
	S	4	11	11	10	6	3

Table 3 (Continued)

1964		30°W–30°E	30°E–90°E	90°E–150°E	150°E–150°W	150°W–90°W	90°W–30°W
Jan 1-7	N	14	12	10	16	21	7
	S	16	24	25	16	9	5
Jan 8-14	N	16	13	8	17	17	10
	S	15	24	29	18	9	3
Jan 15-21	N	14	10	14	17	13	16
	S	18	24	28	15	8	9
Jan 22-31	N	28	22	15	27	26	28
	S	23	42	48	31	18	8
Feb 1-7	N	17	13	13	16	17	20
	S	16	22	24	16	10	8
Feb 8-14	N	11	7	6	12	12	14
	S	7	12	16	14	10	3
Feb 15-21	N	16	9	12	18	12	22
	S	17	26	24	14	7	8
Feb 22-28	N	15	12	8	11	15	10
	S	10	18	23	16	10	4
March 1-7	N	6	5	6	12	14	4
	S	8	11	12	7	4	3
March 8-14	N	12	10	9	14	13	5
	S	14	20	22	13	8	5
March 15-21	N	13	10	2	12	18	6
	S	18	24	26	15	10	7
March 22-28	N	18	14	12	17	17	8
	S	15	23	28	18	12	6
March 29-31	N	6	6	5	6	6	2
	S	6	8	11	7	5	3
April 1-7	N	19	13	12	17	11	12
	S	21	27	29	19	11	7
April 8-14	N	11	7	11	16	10	13
	S	17	22	21	11	7	7
April 15-21	N	8	5	11	16	14	9
	S	17	23	19	9	4	8
April 22-28	N	3	2	8	9	5	4
	S	9	14	9	5	1	5
April 29-30	N	6	7	2	2	1	1
	S	2	4	2	2	2	1

Table 3 (Continued)

1964		30°W–30°E	30°E–90°E	90°E–150°E	150°E–150°W	150°W–90°W	90°W–30°W
May 1-7	N	2	2	6	7	4	2
	S	6	10	8	5	1	2
May 8-15	N	6	3	8	12	10	5
	S	11	16	13	7	2	5
May 16-22	N	17	14	11	16	19	13
	S	15	22	26	18	11	7
May 23-29	N	7	7	8	10	10	5
	S	7	14	15	12	8	1
June 1-7	N	7	9	9	10	9	8
	S	9	14	15	11	8	6
June 8-14	N	8	8	7	8	5	9
	S	9	13	15	10	8	3
June 15-24	N	7	5	6	9	7	9
	S	9	13	12	7	2	4
June 25-30	N	2	3	5	6	5	3
	S	6	9	9	6	3	2
July 1-7	N	2	2	6	8	4	2
	S	8	13	10	6	1	2
July 8-14	N	2	2	6	9	5	3
	S	9	13	10	6	2	4
July 15-21	N	1	1	3	5	4	1
	S	5	10	9	5	0	1
July 22-28	N	2	2	4	9	5	2
	S	6	10	10	5	1	1
July 29-31	N	2	4	4	4	4	3
	S	2	4	5	5	3	2
August 1-7	N	6	6	6	8	8	5
	S	6	13	13	12	6	3
August 8-15	N	2	3	4	5	5	1
	S	3	8	6	6	2	0
August 16-22	N	3	5	6	7	7	4
	S	7	11	10	8	4	2
August 23-29	N	4	4	3	12	8	4
	S	9	11	14	5	3	1
August 30-31	N	0	1	1	3	3	2
	S	3	3	5	2	2	0

Table 3 (Continued)

1964		30°W–30°E	30°E–90°E	90°E–150°E	150°E–150°W	150°W–90°W	90°W–30°W
Sept 1-7	N	4	3	4	8	10	4
	S	7	9	11	6	4	2
Sept 8-14	N	2	2	5	6	7	2
	S	5	11	8	7	2	2
Sept 15-21	N	3	2	8	10	5	4
	S	8	12	8	4	1	4
Sept 26-30	N	0	0	1	1	1	0
	S	0	0	0	0	0	0
Oct 2-10	N	1	1	4	6	8	3
	S	3	8	5	4	1	2
Oct 12-17	N	6	6	7	8	8	5
	S	6	11	11	8	5	3
Oct 18-23	N	5	6	7	6	6	3
	S	5	9	10	8	7	3
Oct 24-29	N	9	8	5	7	6	6
	S	7	11	14	9	7	3
Oct 30-31	N	2	3	2	3	2	3
	S	3	5	5	3	2	2
Nov 1-6	N	4	5	7	11	3	6
	S	11	13	13	5	4	4
Nov 7-12	N	6	6	7	9	6	5
	S	6	12	11	8	5	3
Nov 13-18	N	4	4	5	7	5	2
	S	6	9	9	6	3	4
Nov 19-24	N	12	10	11	15	16	8
	S	13	20	21	13	7	6
Nov 25-30	N	7	7	7	10	10	4
	S	7	14	14	11	6	4
Dec 1-6	N	5	4	6	11	11	4
	S	9	14	13	8	4	2
Dec 7-12	N	2	1	4	8	7	2
	S	5	10	7	5	0	1
Dec 13-18	N	2	2	6	8	6	9
	S	5	9	6	4	2	1
Dec 19-24	N	0	0	4	7	6	2
	S	0	1	1	1	2	0
Dec 25-30	N	3	3	3	6	4	3
	S	3	5	10	5	4	1

METHODS OF ANALYSIS

Radiation Data

The monthly mean maps of equivalent blackbody temperature produced by the computer in the form of grid point data were analyzed by hand. Isotherms were drawn at intervals of 5°C. These maps are presented in Appendix A of this report (Figures A1(a) through A19(a)—"(a)" figures only). Dashed isotherms indicate areas where the number of individual measurements falling within the square represented by a grid point was less than 100. Isotherms were omitted in areas of no measurements, and these areas are marked "NO DATA." Regions having equivalent blackbody temperatures of 0°C or less were shaded to stress the presence of clouds. In the winter hemispheres, where freezing or colder air temperatures can be found at the surface, an ambiguity in the determination of cloud and/or earth's surface from radiation data can occur. Outside of the above-mentioned regions, the brightness values represent effective radiation height of the clouds, i.e. that height in the atmosphere where the ambient air temperature equals the equivalent blackbody temperature of the clouds. This is an approximation, as will be discussed below.

For a number of physical and technical reasons, some care must be used in interpreting the satellite measurements. In particular, thin cirrus clouds are partially transparent and thus permit radiation from below to be recorded by the TIROS radiometer. Under these conditions, effective radiation heights tend to fall below the top level of the high cloud layers. When either an opaque cloud layer or clear skies over a sea or land region homogeneously fill the field of view of the radiometer, a unique interpretation of the equivalent blackbody temperatures in terms of surface and/or cloud-top temperature becomes possible. If scattered to broken cloud decks of varying transparency or varying cloud-top altitude are viewed, the radiation originating from the ground and the various cloud layers contributes to the integrated intensity detected by the satellite, and a separation of the partial contributions is impossible without other supporting data. Godshall and Shenk (1969) have used the relation: $T_s = (AT_c + BT_g)/100$ to derive cloud-top temperatures from Nimbus MRIR* data. T_s is the equivalent blackbody temperature of the cloud top and surface together, measured by satellite radiometer; T_c is the cloud-top temperature; T_g is the temperature of the earth or sea surface; A is the percentage of cloud cover, and B = 100 - A, or the percentage of clear sky. This correction technique was not applied to the radiation data used in this report, because of a lack of global cloud cover data for the analysis periods.

In the 8-12 micron window, residual absorption of infrared energy, mainly by water vapor and ozone, can still cause the observed equivalent blackbody temperatures to be 8°C to 10°C colder than in the absence of tri-atomic gases. The cumulative effects of these factors could cause an error of up to 2,000 meters in the estimation of cloud-top height. Corrections for these effects have not been made in the computer program nor during the process of hand analysis.

The monthly maps of equivalent blackbody temperatures can include data taken during either daytime or nighttime. Nighttime and daytime data were combined, when both were available.

*Medium Resolution Infrared Radiometer.

Averaging processes will generally smooth out the diurnal variation of surface temperature and cloud-top heights in partially cloudy areas, particularly over land, where it is more pronounced. However, at times the presented data may be biased by the predominance of certain local times of observation.

Supplementary Climatological Data

For comparison purposes, maps of monthly mean total cloud amount for the period June 1963 through December 1968 were produced from conventional synoptic surface observations for the Northern Hemisphere. These maps are presented in Appendix A as Figures A1(b)-A19(b).

The data used in the preparation of these charts were obtained from the nephanalysis data tapes of the Air Force Global Weather Central (AFGWC), Offutt Air Force Base, Omaha, Nebraska, which are on file at the USAF Environmental Technical Applications Center (ETAC), Washington, D. C.

These data tapes contain daily values of total cloud cover for 0000 GMT and 1200 GMT for the grid points of the AFGWC Northern Hemisphere 1:30 million scale polar stereographic projection grid system. The AFGWC grid system consists of 2,397 (47 by 51) grid points; however, data are included for only 1,977 points of the grid with the corners ignored. Thus the region covered by the data grid is octagonal in shape with data extending from the North Pole to 10°N-15°N. Since the rectangular grid is superimposed on a polar projection, the grid spacing varies from 2-1/2 degrees latitude at 15°N to 3-1/2 degrees at 70°N.

Both the 0000 GMT and 1200 GMT data were used to compute the values for the monthly mean total cloud amount. The data were analyzed for tenths of cloud amount and then the map projection was transformed to a Mercator projection to make an easier comparison with the other climatological parameters presented. In addition, monthly positions of the ITC were obtained from daily minimum surface pressure and surface wind convergence data for the tropics (Berliner Wetterkarte, 1963-1964). The ranges of these positions were averaged monthly and combined with the AFGWC cloud cover data and included in Appendix A, Figures A1(b)-A19(b).

Figures A1(c)-A19(c) show the mean monthly climatological positions of the ITC and convergence lines in the tropics. Frequency of precipitation from total observations from ships at sea (the only data available over most oceanic regions) and amounts of precipitation (generally available only over large land masses where rain gauges are in use) are also shown. Oceanic surface wind and frequency of precipitation data were obtained from the National Weather Records Center, Asheville, N. C., from the following U. S. Weather Bureau card decks of climatological data:

Deck Number	Period
193	1854-1938
189	1939, 1945-1955
194	1856-1953
184	1953-1959

Deck Number	Period
192	1859-1939
115	1938-1948
116	1949-1959
110	1945-1951
195	1942-1945

The mean wind vectors and averages of precipitation percentage were analyzed over a 5° and 2° square of latitude-longitude, respectively.

Monthly surface wind data and amounts of precipitation (in mm from rain gauges) over Africa and South America were based upon data in *Air France Climatologie* (1963, 1965).

In this paper, the ITC is defined as a zone into which surface air streams from opposite hemispheres converge and where wind constancy is a minimum (Godshall, 1968; Simpson et al., 1968). From studies of ESSA satellite television and ATS spin-scan camera pictures over the Pacific, large variations in ITC cloudiness have been reported and it is inferred that trade wind convergence in some portions of the ITC may be weak and/or disorganized (Johnson, 1966; Warnecke et al., 1968; Kornfield and Hanson, 1968; Fujita, 1969).

The convergence lines associated with intra-hemispheric flow, shown by short dashes in Figures A1(c)-A19(c), were delineated in the climatological wind analysis by criteria similar to those used in defining the ITC.

MONTHLY CLIMATOLOGICAL DISCUSSION

Significant surface and upper air climatological features which occurred during the period of the TIROS VII satellite radiation measurements will be discussed in the following subsections.

June 19-30, 1963

The northern hemisphere monthly surface pressure map for June 1963 (Deutscher Wetterdienst, 1963; Meteorologische Abhandlungen, 1963) shows some interesting synoptic features which help to explain the cloud systems shown in the June 19-30, 1963, TIROS VII radiation data and June 1963 surface-observed cloud charts [Figures A1(a) and A1(b)]. A semicircular zone of low surface pressure along the edge of the strong Pacific subtropical high is shown extending from New Guinea, northwest to the Philippines and Formosa, then northeast across Japan and the North Pacific, and southeast to western Canada. Large areas of high cloudiness indicated by cold T_{BB} values (-10° to -15°C) are shown in this region. Three typhoons contributed additional cloudiness to the curved extratropical band of cloudiness mentioned above. 700-mb circulation featured troughs in the Central Pacific, eastern China, and western United States. A stronger than normal ridge over the

eastern United States, extending from the Great Lakes through Central Canada, is associated with warm T_{BB} values, decreased zonal westerlies, scattered cloudiness, and lack of rainfall (Dickson, 1963). Troughs off the east coast of Canada which extend into the Davis Strait are associated with T_{BB} values of -5° to -20°C . Heavy drought-breaking rains shown in the radiation and cloud data above occurred in Alabama, Georgia, and South Carolina, making June a record month for precipitation in this region.

A blocking ridge over the Norwegian Sea caused the lack of cloudiness over Central Europe, while a trough extending north-northwest from the Caspian Sea is reflected in increased cloudiness in Figures A1(a) and A1(b).

The onset of the southwest monsoon over India is indicated by a cloudy region, with T_{BB} values at -10° to -15°C , over the Andaman Sea (10° to 15°N , 90° to 100°E). Coupled with this significant feature is a zone of high temperatures (T_{BB} values of $+5^{\circ}$ to $+30^{\circ}\text{C}$) over north central India and the Ganges Valley. This condition was typical of the beginning of the monsoonal flow over India from the second week of June 1963 to the end of the month (Sikha, 1964).

Warm T_{BB} values ($+15^{\circ}$ to 35°C) are shown over the cloud-free "thermal low" regions of the Sahara, Kalahari, Arabian, Iranian, and Iraqi Deserts and east central Brazil. T_{BB} values of 5° to $+10^{\circ}\text{C}$ usually overlie the subtropical highs in both the northern and southern hemispheres. The Intertropical Zone of Convergence (ITC) is strongly indicated in the radiation analyses of cold T_{BB} values (-5° to -15°C) in the eastern-western Pacific and Atlantic Oceans and weakly indicated from 120°W to 150°W and 175°W to 175°E in the Pacific Ocean. The ITC cloud patterns inferred from the radiation data agreed qualitatively with the ITC precipitation data shown in Figure A1(c).

The South Pacific Convergence Zone, seen as cold T_{BB} values in the cloud region oriented northwest-southeast from New Guinea to the Fiji Islands, is related to stagnated Southern Hemisphere mid-latitude frontal systems (Gabites, 1943; Hill, 1963; Kornfield and Hanson, 1968). This zone appears to be a Southern Hemisphere counterpart to the mid-Pacific trough described by Sadler (1968). The warm ($+10^{\circ}$ to $+15^{\circ}\text{C}$) isotherms seen over the northwest Australian coast and southern Indonesia area are related to the cloud-suppressing effect of the subsiding Australian desert air which flows northwestward during the southeast monsoon.

Heavy cloudiness (-10° to -20°C , T_{BB} values) shown from 40° to 60°S is related to storm tracks during the Southern Hemisphere winter.

July 1963

The 700-mb ridges over Europe and the eastern Pacific Ocean intensified during July 1963, while the remainder of the Northern Hemisphere circulation appeared normal (O'Connor, 1963). The Aleutian Low had disappeared from the surface pressure chart, and the strong subtropical Pacific High had moved northward to near 37°N . Low-pressure systems of extratropical origin in the North Pacific Ocean were generally weak, and reports of gales were rare. Small areas of T_{BB} values from -10° to -15°C are shown in this region in July [Figure A2(a)] which are related to lower cloud top levels.

The 700-mb circulation showed that the mid-Pacific trough had shifted from 170°W-170°E to 165°E-145°E during the period from June to July, 1963. Other troughs were located off the east and west coasts of the United States and the eastern Atlantic Ocean.

Record drought still remained over Texas, and the upper Mississippi Valley. Large ridges existed over the east central Pacific, Europe, and south central Russia which are related to the lack of clouds and related warm T_{BB} values in these regions [Figures A2(a) and A2(b)].

The southwest monsoon over India and southeast Asia was well established in July and is shown by overcast cloudiness, heavy rainfall, and cold T_{BB} values of -10° to -20°C (Indian Journal of Meteorology, 1964, a). However, the area of the western Arabian Sea appears to be relatively cloud-free. Ramage (1966) discusses this feature and explains it as being the result of the interaction of the developing summer heat low over Arabia, Somalia, and northern India, the strength of low-level southwesterlies and upper easterlies, the low-level subsidence of dry desert air, and the concurrent upwelling of cold water along the Somali-Arabian coast.

High T_{BB} values (+10° to +20°C) and related cloud-free areas are seen over summer heat lows of the African and Middle East deserts. These surface equivalent blackbody temperatures appear higher during the previous month. This was probably the result of sparse satellite coverage and the predominance of daytime observations during the last 12 days of June (Table 3), while the mixture of day and nighttime measurements lowered the average during the following months.

Four typhoons and one tropical storm contributed to the ITC cloudiness (-5° to -15°C, T_{BB} values) between 10° and 20°N, from 150°E to the Philippines. The Intertropical Zone of Convergence (ITC) is more pronounced across the Pacific and Atlantic Oceans in July than in June, as shown in Figure A2(a) by the T_{BB} values of 0° to -5°C. The east-west oriented clouds over Central Africa, which normally are 100 to 500 miles south of the ITC, have intensified and reached higher levels as indicated by T_{BB} values of -10° to -20°C. The ITC location is in agreement with the climatological precipitation areas shown in Figure A2(c).

The high clouds (-10° to -15°C, T_{BB} values) of the previous month appear to have diminished from the Philippines to the New Guinea area during this month. The extension of the cloud fields from the Tasman Sea to the equator also was not as strong during July as it was in June 1963, possibly because of sparse data coverage.

Northern Australia and southern Indonesia are shown to be relatively cloud-free (+10° to +15°C isotherms) [Figure A2(a)], as they also appeared to be in June [Figure A1(a)].

August 1963

The previously strong Pacific anticyclone and the trough along the western U. S. coast weakened during August, and a strong ridge developed over Alaska and western Canada (O'Connor, 1963). These synoptic conditions are reflected in the large area of 1/10 to 5/10 cloud coverage and warm T_{BB} values over the United States and western Canada, shown in Figures A3(b) and A3(a) respectively. The 700-mb trough along the east coast of North America and west coast of Europe and Siberia

deepened with the intensification of the Atlantic and eastern Europe ridges. A decrease in cloudiness in these ridges is indicated in the above-mentioned figures.

An area of oceanic cloudiness north of 30°N latitude is shown to the east of the mid-Pacific trough. The high cloudiness in this region, -10° to -15°C in T_{BB} values, appears to have decreased in Figures A3(a) and A3(b). Two typhoons in the western Pacific added more than normal cloudiness, corresponding to 0° to -5°C, T_{BB} values, to the ITC east of the Philippines. The ITC shown in the Pacific and Atlantic oceans is in its most northerly position for the year and is strongly defined by cool T_{BB} values (0° to -10°C). This position agrees qualitatively with the climatological data [Figure A3(c)].

An area of cloudiness over Mexico and southwest United States (0° to -5°C, T_{BB} values) is related to heavy precipitation over Arizona, New Mexico, and Colorado. This anomalous rainfall was related to a persistent trough in the easterlies over Mexico into which considerable moisture from the Gulf of Mexico was supplied and which then moved over the southwestern United States. Generally drought conditions were increasingly serious west and east of the Rockies, related to subsiding northerly air from the 700-mb ridge. This condition is indicated by +5° to +10°C, T_{BB} values, and 3/10 to 5/10 cloudiness. The two cloudy areas (-5° to -10°, T_{BB} values) in the Atlantic from 45°W to 75°W between 28°N to approximately 40°N are related to the tracks of Hurricanes Beulah and Arlene during August.

The southwest monsoon over India and southeast Asia is strongly shown by typical heavy cloudiness (0° to -20°C, T_{BB} values) and 5/10 to 7/10 cloudiness in Figures A3(a) and A3(b). The trajectory of the dry warm subsiding desert air from Somaliland and Saudi Arabia may account for the decrease in cloudiness seen in the western Indian Ocean.

Large areas of the Middle East and North African deserts are outlined by warm (+10° to +25°C) T_{BB} values, while large cloud masses south of the ITC (0° to -10°C, T_{BB} values) appear in Central Africa.

The cloudiness of the South Pacific trough discussed under June 19-30, 1963, above, with T_{BB} values of -5 to -10°C, appears to have intensified and extends southeastward from New Guinea.

The cloud-free regions (+5° to +10°C, T_{BB} values) over northern Australia and southern Indonesia are typical of the location of the subtropical high in the winter season.

September 1963

During September, stronger than usual Gulf of Alaska and Icelandic troughs at the 700-mb level coupled with the strong subtropical anticyclones and intensified mid-latitude westerlies in the North Pacific and Atlantic oceans (O'Connor, 1963).

Large and slow-moving lows moved across from Kamchatka to the Aleutian Islands during this month, and these storms are reflected in the increased area of 7/10 to 9/10 cloudiness and T_{BB} values of -10° to -15°C. 700-mb troughs off the east and west coasts of the U. S. and a strong

ridge over North America intensified in response to the deep Gulf of Alaska and Davis Strait lows. These cloudy trough and cloud-free ridge areas are delineated by related surface cloud observations and respective T_{BB} values in Figures A4(b) and A4(a).

Four typhoons and two tropical storms in the western Pacific added considerable cloudiness (0° to $-20^{\circ}C$, T_{BB} values) north of the ITC from 160° to $140^{\circ}E$. The equivalent blackbody values ($+5$ to $+10^{\circ}C$, T_{BB}) over India and the low amount of surface-cloudiness observed indicate the weakening and withdrawal of the southwest monsoon in that region. Heavy cloudiness still persists from Malaysia southwestward across the equator to the Indian Ocean. The intense cloudiness noted with ITC activity along the Central American region agrees qualitatively with the climatological chart, Figure A4(c). Large cloud-free regions are indicated over Australia and South Africa ($+5$ to $+15^{\circ}C$, T_{BB} values), as storm tracks shifted farther south in the southern hemisphere.

October 1963

The Gulf of Alaska and Icelandic low regions experienced severe weather during October as several deep and extensive lows moved through from the west. The mean surface pressure in these regions was almost 10 mb below normal. Strong negative height anomalies at 700 mb were noted in this region, as indicated by heavy cloudiness (-10° to $-15^{\circ}C$, T_{BB} values), Figure A5(a). Unusually dry weather was observed under a 700-mb ridge which prevailed along the clearer Gulf and Atlantic coasts of the United States (Green, 1964).

With the intensification of zonal westerlies, increased surface-observed cloudiness was noted over the entire Pacific from 30° to $60^{\circ}N$ and Eurasia from 50° to $60^{\circ}N$ [Figure A5(b)], in accordance with the radiation data [Figure A5(a)].

Four typhoons formed in the western Pacific and created additional cloudiness in that area north of the ITC during this month.

The southwest monsoon continued to withdraw in slow stages from northeast India and remained confined to the southern regions. Several cyclones and depressions in the Bay of Bengal during October caused severe floods in the State of Madras, at the southeast tip of the Indian peninsula. Heavy cloudiness persisted from Malaysia southwest to the central Indian Ocean, and increased cloudiness was noted in the ITC in the Central Pacific [Figure A5(a)].

October is the beginning of the spring season in South America, and an increase in cloudiness (0° to $-15^{\circ}C$, T_{BB} values) is shown over the west central portion [Figure A5(a)].

The Australian continent is relatively cloud-free ($+10^{\circ}$ to $+25^{\circ}C$, T_{BB} values), while cyclonic activity (-10° to $-25^{\circ}C$, T_{BB} values) is indicated in the South Pacific between $160^{\circ}W$ and $100^{\circ}W$, 20° and $40^{\circ}S$ [Figure A5(a)].

November 1963

A deep 700-mb trough with large negative height anomalies developed off the east coast of the United States, in conjunction with a ridge over the west coast. Three major surface

storms developed in this region, as indicated by increased cloudiness in Figures A6(a) and A6(b).

The main core of the westerlies at 700 mb was positioned near its usual latitude over the Pacific Ocean, the eastern United States, and the western Atlantic. These winds were south of its normal position over the eastern Atlantic, Europe, and western North America (Posey, 1964). Note the corresponding southerly movement of the cloud fields [Figures A6(a) and A6(b)].

The storm activity continued well above normal in the Gulf of Alaska, as the monthly mean surface pressure ranged 5 to 9 mb below normal. However, the cyclones were less intense in this area than during October. There was considerable extratropical storm activity in the Pacific north of 35°N from Japan to the west coast of the United States, and off the northeast United States from 40°N to 60°N. These storm tracks are indicated by increased cloudiness and cold T_{BB} values in Figures A6(a) and A6(b).

Typhoons were not reported during November, hence there was a noticeable decrease in cloudiness in the western Pacific [Figure A6(a)]. The cloudy southwest monsoon has withdrawn almost completely from India. The cloudiness of the ITC off the southern tip of the peninsula, over Indonesia and New Guinea, and across the Central Pacific is in good qualitative agreement with the climatological data. Considerable storm activity is also shown over Central and South America and Africa which is related to the climatological data in that region [Figure A6(c)].

Over Australia, storm tracks penetrated farther north during this month than in October, and cyclonic activity decreased in the South Pacific from 180° to 110°W, 25° to 40°S [Figure A6(a)].

December 1963

Strong meridional flow marked the long wave pattern in the mean 700-mb circulation for the eastern Pacific and North America during December. The 700-mb trough formerly in the Gulf of Alaska in November retrograded to the Central Pacific and deepened, while a strong ridge developed from Alaska through the western United States (Stark, 1964).

This caused an abrupt change in weather patterns from the central and eastern United States in that the principal storm tracks passed in the vicinity of the Great Lakes. This month was the coldest on record for the middle and lower Mississippi Valley, the Ohio Valley, and parts of the Gulf Coast States, and record snowfall was reported in many Southern cities. Note the more southerly penetration into the Gulf of Mexico in December of the 0° to -5°C T_{BB} values [Figure A7(a)]; this was caused largely by low surface temperatures during clear sky periods following the snowstorms as documented by the cloud observations [Figure 7(b)].

The Aleutian low was well developed during December, and very extensive low-pressure systems often covered most of the North Pacific. Within these systems, smaller, vigorous secondary cyclones often developed. Note the increase in surface-observed cloudiness over the Gulf of Alaska during December [Figure A7(b)], and the larger area of higher clouds indicated by T_{BB} values of -10° to -25°C over the whole Northern Pacific [Figure A7(b)].

Above-normal storminess and heavy cloudiness occurred off the eastern United States because of the position of the 700-mb trough and maximum winds at that level [Figures A7(a) and A7(b)]. A strong ridge formed over northwestern Europe, with decreased cloudiness indicated in that region.

Typhoon Phyllis and tropical storm Rita developed off the Northern Philippines; their northerly tracks are shown by the T_{BB} values of 0° to -5°C connecting to the storm tracks southwest of Japan [Figure A7(b)].

India, in its post-monsoon period this month, generally had clearer skies, scattered showers, and occasional disruptive cyclones from the Bay of Bengal. Intensive cloudiness related to the ITC position in the Indian Ocean is shown straddling the equator and extending out across the Central Pacific Ocean. December starts the end of the spring season in South America; an apparent decrease in cloudiness during this month is noted.

Moderate cloudiness is indicated over the northwest coast of Australia which is related to a convergence line shown in the climatological chart and radiation data [Figures A7(a) and A7(b)]. Australia is in the midst of the summer season, during which storm tracks usually pass well to the south of the continent. The relatively low T_{BB} values, $+5^{\circ}$ to $+15^{\circ}\text{C}$, are due mainly to day-night averaging, although variable local convective cloudiness may contribute to the observed equivalent blackbody temperatures over this continent.

January 1964

During this month, a broad trough persisted over the Bering Sea, and the Pacific subtropical high was stronger and positioned farther north than normal (Andrews, 1964). Note the large amount of surface-observed cloudiness in the Pacific Ocean, the presence of a strong jet stream aloft between 35° and 40°N , [Figure A8(b)], and the cold T_{BB} values (-15° to -25°C) shown in the TIROS VII radiation analysis [Figure A8(a)].

A small-amplitude trough persisted over the central United States and eastern Canada during January 1964. The above-normal rainfall along the Gulf and southeast coasts and in the Pacific northwest is associated with the 700-mb jet. Note increased cloudiness and cold T_{BB} values in these areas [Figures A8(a) and A8(b)].

The flow over the Atlantic Ocean was meridional, and a strong blocking ridge was observed over Europe with an associated deep trough located over north central Russia. As a result of strong anticyclonic circulation, unusually dry weather prevailed over much of Europe. Note that the curved shape of the -10°C T_{BB} isotherm indicates the edge of high cloudiness which follows the bell shape of this ridge [Figures A8(a) and A8(b)].

India, the Arabian Sea, the Bay of Bengal, and Southeast Asia are relatively cloud-free, with T_{BB} values of 0° to $+15^{\circ}\text{C}$; and are within their dry season, which is caused by the northeast monsoon. An exception is seen over southeast China, where broken to overcast clouds were observed [Figure 8(b)]. These cloud conditions are related to the "Crachin weather" which consists of widespread low-level fog and drizzle or light rain, with ceilings below 1,500 feet and visibilities less

than two miles, and stratiform cloud decks with tops near 6,000 feet. There is little cloudiness other than thin cirrus in the dry air above this undercast, hence the radiation analysis indicates warm (+5° to -5°C) T_{BB} values [Figure A8(a)].

Central China is dominated by the intensely cold and dry Siberian High, and is relatively cloudless. The T_{BB} values of -15° to -30°C relate to the surface snow cover over the Tibetan Plateau and the China Mainland which was intermittently covered by scattered clouds [Figures A8(a) and A8(b)].

The cloudy Intertropical Zone of Convergence over the Indian Ocean and Indonesia is shown by the "window" radiation (-5° to -15°C, T_{BB} values) and appears to be north of its mean Southern Hemisphere climatological position [Figures A8(a) and A8(c)].

In the eastern Pacific, the clouds east of 100°W from 0° to 10°N are probably more stratiform, as confirmed by the warmer (+5° to +10°C) T_{BB} values.

The ITC region from 110° to 160°W along the 0° to 10°N latitude band indicates clouds of more vertical development (0° to -10°C, T_{BB} values) which overlie the warmer Equatorial Countercurrent water. The stratiform cloudiness over the cooler California and North Equatorial Current is indicated by surface observations and the T_{BB} values of 0° to -5°C [Figures A8(b) and A8(a)]. The location of the cool Peru and South Equatorial Current, which flows westward between 5°N and 10°S, is well delineated by the lack of significant cloudiness in Figure A8(a).

Heavy high cloudiness over central South America is evidenced by the cold (-20° to -30°C) T_{BB} values shown in Figure A8(a). From 35°S, 25°W the -10°C T_{BB} isoline generally moves southeastward to approximately 55°S, 125°W. This isotherm is essentially the edge of high cloudiness associated with cyclone tracks in the Southern Hemisphere in the summer months, January through March, previously described by Van Loon (1966) and Taljaard (1967). There is also a pronounced cloudy zone east of New Zealand from 180° to 110°W, with T_{BB} values of 0° to -10°C, shown in Figure A8(a). The Great Sandy Central Australian Desert is generally cloud-free in the summer season; hence T_{BB} values of +10° to +15°C are noted. An exception to this seasonal condition is the north coast, where cloudiness related to the convergence line is detected by the "window" channel.

February 1964

During February, the strength of the ridges at 700 mb was abnormally amplified along the west coast of North America, Europe and Central Asia. Troughs were anomalously deepened and near their normal locations near the east coast of North America and in Central Europe, while the Pacific trough was about 20° of longitude east of its normal position (O'Connor, 1964). The Atlantic surface low south of Greenland at 50°N was 9 mb lower than normal. Note the heavy cloudiness and cold T_{BB} values (-20° to -25°C) at 55° to 65°W and 160°E to 160°W between 35° to 45°N in Figures A9(a) and A9(b) which are related to the jet stream axis, the U. S. East Coast trough and mid-Pacific trough, respectively.

The mean jet axis at 700 mb was farther north than its usual position in the ridge areas, and farther south than normal in the trough areas. The principal storm tracks over North America

were closely related to the position of this jet axis and were located approximately 5° to the north of this referenced position (O'Connor, 1964).

February was relatively dry in the United States and cloud-free west of the Appalachian Mountains, as shown in Figure A9(b). The T_{BB} values of -5° to -10°C are related to the equivalent black-body temperatures of the cold ground in the clear sky regions. A cloudy zone in the eastern Pacific, related to the California and North Equatorial Current at 125° to 145°W, 10° to 35°N, is shown in conventional cloud observations [Figure A9(b)] and radiation analysis [Figure A9(a)].

The center of the surface Siberian High near Lake Baikal, in Russia, reached a record average central pressure of 1,047.5 mb. Note the absence of clouds in this area in Figure A9(b), and the T_{BB} values of -15° to -25°C, which are related to the cold ground temperatures.

Saudia Arabia, the Arabian Sea, Malaya, and the Philippines are relatively cloud-free and under the influence of the northeast monsoon. Two weak easterly waves moved westward across Ceylon and the southern tip of India and caused scattered thunderstorms to occur (Indian Journal of Meteorology, 1964b). Note the T_{BB} values of 0° to -5°C, related to cloudiness in this region [Figure A9(a)].

The ITC with associated cloudiness (0° to -15°C, T_{BB} values) in its annually most southern position (5° to 15°S) in the Indian Ocean is in good agreement with the climatological position [Figures A9(a) and A9(c)].

A large area of cloudiness (T_{BB} values of -10° to -35°C) from 160°E to 175°W, 10°N to 20°S, is shown over the ITC [Figure A9(a)], where it begins to recurve across the equator and extend into the Northern Hemisphere. Another distinctive area of cloudiness (T_{BB} values of -10° to -25°C) from 160°E to 180°, 10°N to 40°S is shown in Figure A9(a). This "cold" area lies between the two South Pacific highs and is a climatological frontal stagnation zone, or Southern Hemisphere Convergence Zone, previously discussed by Hill (1963).

The clouds over the northern portion of South America are related to the southern position of the ITC and the tropical convergence troughs which oscillate east to west, oriented northeast-southwest in the north central portion of the continent.

March 1964

A large change occurred in the 700-mb flow during the month of March. The ridge ordinarily over western North America was displayed offshore over the Pacific with an indicated +320 feet height anomaly. Two major troughs, one from eastern Canada to northern Mexico and the other extending southeastward from the Davis Strait to the Central Atlantic (Posey, 1964), are shown in Figure A10(b). The 700-mb jet stream over the United States was displaced far to the south, and heavy rains and flooding occurred in the Ohio and Mississippi valleys east of the deep trough. Cyclonic activity caused above-normal precipitation in the Northwest. Note in Figures A10(a) and A10(b) the cold T_{BB} values (-15° to -25°C) over the Ohio Valley and over the northwest United States, which are related to high-level cirrus clouds that accompanied the storms over these regions.

A blocking ridge formed over Norway and Sweden with related decreased cloudiness [Figure A10(b)]. The west-to-east storm tracks increased in number in the central Pacific. Note the presence of clouds as indicated by the cold T_{BB} values (-20° to -25°C) in this region from 180° to 160°W , 40° to 45°N [Figure A10(a) and A10(b)]. Very cold T_{BB} values (-30° to -45°C) are shown over the Himalayas, related to the build-up of clouds in that region. Saudi Arabia, the Arabian Sea, India, and Malaya are under the influence of the winter monsoon and are relatively free of clouds, as shown by Figure A10(a).

The ITC is in a southern position (5° to 15°S) in the Indian Ocean, but is less active than in February 1964. Increased cloudiness is noted in the ITC south of the Philippines and the northern Australia region. This is in agreement with the climatological position of the ITC in Figure A10(c). The ITC cloudiness in the eastern Pacific is similar to the moderate intensity and cloud organization which occurred in the previous January.

The heavy cloudiness over north central South America is related to the extreme southerly limit of the ITC and to the intersection of tropical convergence troughs in that region.

Central Australia exhibits warm T_{BB} values ($+15^{\circ}$ to $+25^{\circ}\text{C}$), which are related to cloud-free conditions.

The boundary of high clouds (-10°C , T_{BB} value) in the Southern Hemisphere in March is located at approximately 42°S in the South Atlantic and the Indian Ocean, and drops to 48°S east of New Zealand in the South Pacific. This shows a similarity to January, although the high cloud edge is more east-west in orientation.

April 1964

Two 700-mb troughs, one extending NE/SW from the Great Lakes to Baja California and the other NNE/SSW off Newfoundland, affected the weather over the United States and the western Atlantic. Most of the eastern half of the United States was subject to southerly 700-mb flow, which caused the advection of low-level heat and moisture from the Gulf of Mexico and resulted in wide-spread instability, severe storms, and major flooding in Mississippi, Alabama, and the Ohio Valley (Stark, 1964). Note the increased cloudiness in this region, Figures A11(a) and A11(b).

The 700-mb circulation in the Pacific consisted of a trough NE/SW off Kamchatka Peninsula and Japan and a pronounced ridge with a +400 feet height anomaly in the eastern Pacific. Note the lack of high clouds under this ridge, as indicated by the T_{BB} values of 0° to -10°C .

The trough off the British Isles was weak, and a slight ridge existed over western Europe. The "cool" T_{BB} values (0° to -5°C) in Figure A11(a) are related to the low clouds and/or low amounts of clouds in this weak ridge and trough area. The weak trough east of the Caspian Sea is reflected in the T_{BB} values of -10° to -15°C .

Saudi Arabia, the Arabian Sea, and southeast Asia are relatively cloud-free during this transition season from winter to summer monsoon, while the Philippines are under the influence of the

Pacific subtropical anticyclone. Note the high T_{BB} values (+15° to +30°C) in this region in Figure A11(a). From March to April there was an increase of +15°C in the radiation temperatures (T_{BB}) over India.

The ITC shows an increase in intensity from 0° to 10°N off the west coast of Africa [Figure A11(a)]. This location is in good agreement with the climatological position [Figure A11(c)]. A gradual northerly movement of the ITC is noted in the Indian Ocean and Indonesia, with a corresponding decrease in higher cloudiness.

The ITC is better organized in April in the western and central Pacific, and is connected to low cloudiness over the California Current southwest of Baja California [Figure A11(a)].

Note the presence of a climatological precipitation area shown from 0° to 10°S in the eastern tropical Pacific [Figure A11(c)]. The location of this secondary zone is slightly indicated by a dip in the +10°C T_{BB} values, in Figure A11(a). Kornfield and Hanson (1968) also noted this double structure of the ITC in the ATS-1 data in the eastern Pacific Ocean.

The decreased cloudiness over north central South America shows a gradual northward movement from 20°S to 12°S which indicates the onset of the fall season. This is in agreement with the climatological data in Figure A11(c).

A more intense cyclonic activity is indicated over southeast Australia during this month compared with March 1964.

The boundary of high clouds, T_{BB} values of -10° to -15°, which is the edge of the storm tracks in the Southern Hemisphere, shows a gradual slope from 43°, in the South Atlantic, to 49°S, south of New Zealand.

May 1964

The most prominent feature of the 700-mb circulation in the Northern Hemisphere is the strong ridge over the Aleutian Islands and the Bering Sea. This height anomaly (+520 feet) had not been equaled in more than 30 years of record (Green, 1964). The sea level pressure in this region was 17 mb higher than normal, which was a 15-year record. The mean jet core was displaced more than 1,000 miles north of its normal position in the North Pacific Ocean. The edge of the high clouds, T_{BB} values of -10° to -15°C in this region [Figure A12(a)], reaches to approximately 50°N, a northward movement of 10° from the April radiation map [Figure A11(a)]. Two troughs were located over the east and west coasts, with a weak ridge over the central United States. The anti-cyclonic upper air flow affected the mean cloudiness over the U. S., which was at a minimum. These clear sky conditions were reflected by the T_{BB} values of +5° to +20°C shown in Figure A12(a). East of the trough, scattered shower activity is indicated by cloudiness over eastern Mexico and West Texas and north to Wyoming [Figures A12(a) and A12(b)]. A serious shortage of rainfall existed along the southeast coast and in the midwestern and southwestern United States.

A ridge covered western Europe, and is shown by a decrease in cloudiness in that region [Figures A12(a) and A12(b)]. Cloudiness east of the trough in the vicinity of the Black Sea is indicated

by T_{BB} values of -5° to -20°C in Figure A12(a). T_{BB} values over the Himalayas appear to have increased from -45°C in March to -25°C in May [Figures A10(a) and A12(a)] as a result of seasonal surface warming and/or lower cloud heights. Unusually disturbed cloudy conditions exist from 10° to 20°N from 20° to 15°W over northwest Africa, but the ITC appears to be located in its normal position [Figure A12(c)].

Saudi Arabia and India are still cloud-free; but the onset of the southwest monsoon is noted over the Bay of Bengal, Malaya, and Vietnam, where heavy clouds were observed in Figure A12(a) (Indian Journal of Meteorology, 1964c). Two areas of convergence appeared in the Indian Ocean, at 0° to 10°N and 0° to 10°S (0° to -30°C , T_{BB} values), and have the appearance of a double trough on either side of the equator. The ITC in the west Pacific is shown in the February radiation data [Figure A9(a)] at 2° to 5°S over New Guinea. It surged to 2° to 10°N in the Philippines [Figure A12(a)] in May. This movement is in agreement with the climatological data [Figure A12(c)].

Increased cloudiness, with T_{BB} values of -10° to -25°C , which is related to trough positions located off the east coast of Japan, is shown between 25° and 45°N in Figures A12(a) and A12(b).

The ITC appears to have strengthened in the eastern Pacific and also moved northward along the south coast of Panama and Costa Rica, as shown in Figure A12(a), in agreement with climatological data shown in Figure A12(c).

The central portion of South America is relatively cloud-free because of the intrusion of the South Atlantic High into that region. Trough and frontal cloudiness are indicated in the north and south regions, respectively [Figure A12(a)].

The main storm tracks appear to have shifted from 35°S to 45°S off southern Australia, while the northwest coast still remains relatively cloud-free ($+10^{\circ}$ to $+15^{\circ}\text{C}$, T_{BB} values) [Figure A12(a)].

June 1964

A large readjustment of the circulation in the mid-Pacific Ocean occurred during this month. Monthly mean 700-mb heights in the Pacific had been anomalously above normal since February, and the large Pacific height fall (-600 feet) from May to June represented a sharp return to a normal condition (Dickson, 1964). The cloudiness in the North Pacific Ocean increased from May to June [Figure A13(b)], because of increased storm activity in that area; but the cloud tops appeared to have lowered significantly, as shown by the shrinking of areas of T_{BB} values below -10°C [Figure A13(a)].

Two troughs were positioned off the two coasts of the United States, with a minor ridge located between them. A series of upper-level troughs and accompanying surface systems brought record precipitation to the northwest United States. Note the high "cold" clouds (-10° to -20°C , T_{BB} values) in this region in Figure A13(a).

Strengthened ridges over western Europe, eastern Siberia, and central Canada are shown by decreased cloudiness and the T_{BB} values of 0° to $+10^{\circ}\text{C}$ shown in Figures A13(b) and A13(a).

Warm T_{BB} values (+15° to +25°C) are shown over the cloud-free "surface thermal low" areas of the Arabian, Iraq, Sahara, and Mexican deserts [Figures A13(a) and A13(b)].

The onset of the southwest monsoon over India was five days late during June. The monsoonal activity was normal except for spells of heavy rains leading to floods in Central India. Severe cyclonic storms in the Arabian Sea and Bay of Bengal did great damage to persons and property (Indian Journal of Meteorology, 1965a). High clouds (-10° to -15°C, T_{BB} values) are indicated in these regions [Figure 13(a)]. Dry weather prevailed over northwestern India during this period, as indicated by T_{BB} values of +5 to +15°C in this region.

The ITC appears to have weakened across the Central Pacific and intensified across the eastern Pacific Ocean. This agrees with the climatological records of measured precipitation from May to June in these regions. Evidence of typhoon tracks is shown in the cloudiness east of the Philippines [Figure A13(a)]. Increased storm activity is shown over the west central portion of South America, an anomalous condition for fall. Note the clearer sky conditions in June 1963 [Figure A1(a)] in this region that are more typical of the fair weather regime for this season.

The storm tracks surged northward over Australia during this month with the shift equatorward of the subtropical high-pressure belt. The 0°C T_{BB} isotherm reaches almost to 20°S during the height of the winter season over a major portion of Australia.

July 1964

An anomaly of the 700-mb circulation for July was the extremely deep low over the North Polar regions (Andrews, 1964). Increased cyclone development was reported in the North Pacific shipping lanes from Japan to the Gulf of Alaska, and was due to lower than normal pressure in that region. Note the heavy cloudiness in Figure A14(b) and varied high cloud tops (-10° to -20°C, T_{BB} values) in Figure A14(a) in this region.

Two troughs close to their normal positions are located in the eastern and western Pacific Ocean. The subtropical Pacific High was stronger than normal and the Pacific jet stream axis was well-defined zonally and strong [Figure A14(b)]. A ridge over the western United States caused persistent warm weather and clearer skies in the north central regions, while a trough along the east coast brought showers to the southeastern states [Figures A14(a) and A14(b)]. A ridge over western Europe is shown by decreased cloudiness and T_{BB} values of 0° to +10°C [Figures A14(a) and A14(b)].

Over India and Malaysia, the monsoonal rain activity was well maintained during July. Flooding and damage due to very heavy rains occurred in Central India, and heavy cloudiness is indicated by the T_{BB} values of -10° to -40°C [Figures A14(a) and A14(b)] (Indian Journal of Meteorology, 1965a).

Extremely warm (+15° to +40°C) T_{BB} values are shown over the Middle East deserts. The lack of sufficient monthly orbital coverage is indicated by dashed data lines, and hence these high T_{BB} values are not true monthly averages [Figure A14(a)].

The ITC appears discontinuous across the Central Pacific; this was caused in part by data gaps. A fair dry season weather regime with decreased cloudiness (T_{BB} values of +10° to +20°C) is indicated over central South America, and is in agreement with climatological data [Figures A14(a) and A14(b)].

Northwestern Australia and southern Indonesia are relatively cloud-free (+10° to +15°C, T_{BB} values), while cloud cover from transient Indian Ocean cyclones extends across the southern portion of Australia [Figure A14(a)].

August 1964

A large ridge replaced a negative (-500 feet) 700-mb anomaly over the North Polar Basin during August. In conjunction with a strong Pacific High and a negative height anomaly over the Bering Sea and Gulf of Alaska, the zonal westerlies were stronger than normal (Posey, 1964) [Figure A15(b)]. The Aleutian Low had slightly lower than normal pressure, and several extratropical cyclones were found migrating from the Aleutians to the Gulf of Alaska. In addition to the above storm tracks, the major trough east of Kamchatka (160° to 170°E) was also well indicated by cloudiness [Figures A15(a) and A15(b)].

Major long-wave troughs were located close to their normal positions on the west and east coasts of the United States, but are only weakly indicated in Figures A15(a) and A15(b). With the collapse of the ridge over North America in July, a more intense cyclonic activity in August brought rainfall to areas previously dry. Billings, Montana, reported the wettest August in 30 years. Note the T_{BB} values of -10° to -30°C, indicating heavy cloudiness over the northwest United States [Figure A15(a)].

The monsoon rain activity over India, the Bay of Bengal, and Malaya was well sustained during August, as shown by T_{BB} values of -10° to -25°C [Figure A15(a)] (Indian Journal of Meteorology, 1965a). Heavy cloudiness was also observed over the Tibetan Plateau. The deserts of the Middle East are outlined by high temperature values similar to those of June 1964 [Figures A13(a) and A15(a)].

The ITC appears more continuous and active in the entire Pacific and is in its more northerly position during this month [Figure A15(c)].

The tracks of three typhoons and two tropical storms are indicated by the cold (0° to -40°C) T_{BB} values in the western Pacific [Figure A15(a)].

An increase in storminess can be detected over South America, with particularly high cloudiness over the northwest and southeast regions [Figure A15(a)].

Australia exhibits a pattern of cloudiness in the south similar to that shown in July [Figures A14(a) and A15(a)].

September 1964

September 1964 was an unusual month in that an increased number of tropical storms occurred in both the Pacific and Atlantic oceans.

In the northern hemisphere, the subtropical highs were abnormally strong, the jet stream core was generally farther south than normal, and the low-latitude troughs were deeper than usual (Green, 1964). These features were conducive to faster than normal subtropical easterlies. In the northern Pacific and Atlantic oceans, more frequent and vigorous extratropical cyclones were reported in the major shipping lanes. The Aleutian Low and the Icelandic Low had deeper than normal pressures, and the 700-mb circulation showed related broad cyclonic regions with large negative height departures. Note the increase in cloudiness in these regions in Figures A16(a) and A16(b).

The formation of a Siberian High with a ridge of high pressure and clearer skies reaching almost to Japan is shown in Figures A16(a) and A16(b). This appears to signal the onset of the north-east monsoon along the eastern Asiatic coast.

Unfortunately, there was insufficient TIROS VII radiation coverage during September from 45°N to 45°S to document the ITC position, tropical storminess, and Indian monsoonal cloudiness [Figures A16(a) and A16(c)].

October 1964

The upper flow over the Western Hemisphere showed the development of a stronger than normal subtropical Pacific High, the deepening of the mean trough over the eastern United States and eastern Pacific, and the strengthening of the ridge over the western U. S. [Figure A17(b)]. Accompanying this was the northward shift of the west wind belt into southern Canada. The prevalence of this typical circulation pattern was a principal factor in the continuation of the long-term drought over the western and central United States from 1962 to 1965 (O'Connor, 1965).

However, over the southeastern United States, the remains of two hurricanes, Hilda and Isabel, produced October precipitation records. Note the cloudiness east of the trough along the east coast [Figures A17(a) and A17(b)].

Autumn weather was much in evidence as the severity and frequency of cyclonic storms increased in the North Pacific, central Canada, and the North Atlantic. Note the cloudiness related to the storm tracks in these regions [Figures A17(a) and A17(b)].

Over western Europe, a negative anomaly center, with accompanying cloudiness, is shown by the T_{BB} values of -20° to -25°C in Figures A17(a) and A17(b).

The southwest monsoon started to withdraw from northern and central India and remained confined to the southern peninsula during October (Indian Journal of Meteorology, 1965b). Note the decrease in cloudiness in the northern region in Figures A17(a) and A17(b).

The tracks of three typhoons and three tropical storms which formed in the western Pacific and the position of a more continuous ITC through the Central Pacific are indicated in Figures A17(a) and A17(c).

October is the onset of the South American spring season. A variety of weather disturbances such as active convergence troughs, and instability (air mass) storms do occur and create heavy cloudiness over the west central region [Figures A17(a) and A17(c)].

A greater portion of Australia appears to be cloud-free in its summer season (+10° to +20°C, T_{BB} values), as storm tracks keep well to the south of the continent [Figure A17(a)].

November 1964

- The 700-mb circulation of November revealed a complete reversal of planetary wave patterns from those of the preceding month. The development of a mean trough over the western states and a mean ridge over the eastern United States brought southerly flow and record precipitation from the south plains to the Great Lakes (Dickson, 1965). Note the T_{BB} values of 0° to -10°C in this region [Figure A18(a)].

Decreased extratropical cyclone activity was prevalent in the North Pacific, as the Aleutian Low was above normal and the westerlies decreased in velocity. Note the decrease in cloudiness over Alaska and the Bering Sea in Figure A18(b). A major trough east of Japan appears to have extended its cloudiness deep into the tropics, where it merges with the ITC [Figures A18(a) and A18(b)]. Distinct low-level cloudiness is shown over the California Current (120° to 140°W) [Figures A18(a) and A18(b)]. Four typhoons developed from six tropical storms in the vicinity of the Philippines, a greater frequency than normal [Figure A18(a)].

The Asian High intensified in this month, and as a result a period of decreased cloudiness developed in northeast Siberia [Figure A18(b)]. A trough over central Russia brought increased cloudiness into that region [Figures A18(a) and A18(b)].

The northeast monsoon was beginning to take effect over south central Asia, with a continued decrease in cloudiness over India and Pakistan [Figures A18(a) and A18(b)].

Very pronounced storm activity (-10° to -20°C, T_{BB} values) is noted over north central South America. A tropical convergence trough, which merged with an extratropical trough that extends NW/SE off the east coast, is typical of the spring season and is in agreement with climatological data. Southern Hemisphere storm tracks penetrated farther northward this month in the region 130° to 170°W, as indicated by cooler (-5° to -10°C) T_{BB} values [Figures A18(a) and A18(c)].

December 1964

The mean 700-mb circulation in the Pacific Ocean indicated that over the eastern portion a strong ridge had developed which extended northward to the Aleutians [Figure A19(b)]. The mid-latitude westerlies decreased generally in the Western Hemisphere, and the Aleutian Low, which

normally would be elongated from the Gulf of Alaska to the Aleutians, was fragmented into two cells. Many strong storms were reported in the North Pacific, but a majority were blocked by the intervening ridge in the Aleutians (Posey, 1965).

Two strong jet streams converged at the base of a major trough off the California coast, and warm moist southwesterly flow prevailed over the mountains. Heavy rains and disastrous floods in California and Oregon occurred in association with the cyclonic activity indicated by the jet maxima [Figure A19(b)].

Weather conditions over the Atlantic were less severe than normal, but most regions north of 30°N experienced occasional gale weather [Figures A19(a) and A19(b)].

The Siberian High is strongly developed, and the northeast monsoon is indicated by a diminished cloudiness in the south Asian area [Figure A19(b)].

The ITC, which appears weakened in the eastern Pacific, has moved southward into the Southern Hemisphere in the western Pacific [Figures A19(a) and A19(c)]. Only one typhoon was reported to have formed, cloudiness for this system (0° to -10°C , T_{BB} values) is seen at 8° to 10°N , 150° to 160°E [Figure A19(a)].

The "summer season" storm tracks in the Southern Hemisphere appeared to oscillate between 40° to 50°S , and to 60°S southeast of New Zealand [Figure A19(a)].

CONCLUSIONS

Measurements from satellites of total outgoing atmospheric and terrestrial radiation have derived their justification and main interest from their importance to the evaluation of the variations, over many different temporal and spatial scales, of the radiation budget of the earth-atmosphere system. Measurements in the atmospheric window spectral regions have been shown, among other uses, to provide cloud and cloud-top height indicators for mainly synoptic purposes, furnishing cloud information during day and nighttime conditions. In the present study, efforts were directed toward a search for uses of monthly averaged equivalent blackbody temperatures derived from window radiometric measurements in studying the global large-scale atmospheric circulation and its monthly changes. The meteorological details discussed in this paper are important for a full elucidation of this subject.

A simplified method was applied in the production of monthly averages because of the tremendous data volume and the computer effort involved. Thus, averaging was done without consideration of local time of measurements. This created some shortcomings in the interpretability of monthly averages as presented herein. In clear regions or in areas with a pronounced daily variation in amount and/or vertical extension of clouds, the mixture of day and nighttime data causes a noticeable smoothing. In the case of poorer temporal data coverage, strong bias may have been generated by the predominance of certain local times of observation. Such statistical effects explained some of the discussed month-to-month changes. Additionally, over high- and mid-latitude

continental regions in winter, particularly over snow-covered ground, cloudy and clear regions could not be discriminated in some cases because of low surface temperatures in the clear regions, such as near the United States in December 1964. Additional synoptic information on the cloud conditions is necessary in such cases.

However, apart from the latter singularities, and bearing in mind the complex nature of the presented mean values, it became evident from the cases discussed that cold equivalent blackbody temperature (T_{BB}) was associated with areas of dense high-level clouds. Where the ground was in view of the radiometer, the T_{BB} values were larger. Low-lying cloud decks, particularly above strong low-level inversions, may, however, be warmer than snow surfaces.

Since the T_{BB} values are functions of cloud-top height, cloud density, cloud amount, and earth surface temperature, there is no direct relationship between equivalent blackbody temperature and conventional average cloud cover. Interpretation of cloud amount made in this paper is therefore necessarily qualitative, and relative to the season and location in question and to the differential variation of the monthly T_{BB} values over different areas.

Within the zone of high- and mid-latitude westerlies, the extreme mobility of the cloud systems usually causes a large amount of smearing of any cloud data during the period of a month. But, nevertheless, because of the persistence and the characteristic association with certain patterns of cloudiness of the major troughs, ridges, and blocking systems, the major large-scale characteristics of atmospheric circulation were well reflected in the overall distribution of T_{BB} values. Strong correlations between the satellite radiometric data and large-scale circulation systems became evident from month-by-month comparison.

In the lower latitudes, relatively stationary circulation systems seem to dominate the picture, although synoptic processes unquestionably are also deeply involved in the production of characteristic monthly cloud patterns. Development of continental heat lows and monsoonal flow is indicated by the increase and decrease, respectively, of T_{BB} values. These systems are qualitatively discussed in the text. In particular, the relative distribution and intensity of the Indian monsoonal rain activity are impressively characterized by the quantitative distribution of the monthly mean equivalent blackbody temperature.

The location and structure of the cloudiness associated with the intertropical convergence (ITC) are a prominent feature in all the radiation maps. The quasi-stationariness within a month's period of the ITC permits quite detailed insight into the local and temporal behavior of the tropical circulation, particularly over oceanic areas, where comparable information was largely missing until the availability of satellite observations. Over the Pacific Ocean, for example, the existence of a cloud band associated with an upper tropospheric trough appears to be evident almost permanently throughout the year, stretching from west of Easter Island northwestward toward the equator. This cloud zone, identical with the trough described by Hill (1963), usually merges with the ITC between Canton Island ($170^{\circ}W$) and New Guinea ($150^{\circ}E$), and is documented also by television cloud data over many years (Bjerknes et al., 1969). This trough obviously cuts through the subtropical high-pressure belt and represents a direct link between the tropical and extratropical circulation.

This southern mid-Pacific trough which, in the period of this study, was most strongly developed in February 1964, is apparently a counterpart to the mid-Pacific trough over the North Pacific Ocean found and described by Sadler (1968). But, as indicated by the satellite observations, the Southern Hemisphere trough seems to be an even more permanent as well as a more intense circulation phenomenon than the northern one. It should also be noted that usually the ITC cloudiness is most strongly developed where such troughs (which are, at least at times, also present in other geographic areas) reach equatorial regions and merge with the ITC, as has already been seen in TIROS III data (Allison et al., 1964). The second most frequent trough of this type appears, for example, over the South Atlantic Ocean, where a distinct cloud band exists between 50°S and central Brazil, southeast-northwest-oriented during most of the months covered in this study and being most intensely pronounced in November 1964.

The ITC positions shown in the (b) charts of Appendix A are over maritime areas, and are based solely on surface wind data. Variation in position of the areas of maximum precipitation frequency from surface ITC position may indicate that the ITC is sloped; or, more likely, that specific meteorological and oceanographic phenomena, like sea surface temperature distribution and its effect on vertical stability and convection of the overlying air, form the internal structure and the weather development within the ITC cloud zone.

The information content of the data established from TIROS VII measurements and documented in this volume is far from exhausted by the few examples of interpretation presented in this paper. As indicated in the title, the goal of this study was to explore the applicability of the satellite radiation data for general atmospheric circulation research and to draw the attention of researchers to this possibility of making additional use of radiation observations from meteorological satellites. The TIROS VII radiation experiment, which as of this writing has operated longer in orbit than any other, exhibited a number of difficulties in data interpretation due to spacecraft orbital and scanning geometry. They have, however, already been overcome by the Nimbus generation of meteorological satellites, which, therefore, promise information that should be even more reliable and interpretable on global circulation phenomena and their variations.

ACKNOWLEDGMENTS

The authors wish to thank William R. Bandeen, Goddard Space Flight Center, for his helpful comments and suggestions in the review of this paper. We are particularly grateful to the USAF Environmental Technical Applications Center, Washington, D. C., for providing the monthly surface cloud observations used in this study.

Goddard Space Flight Center
National Aeronautics and Space Administration
Greenbelt, Maryland, October 15, 1969
160-44-03-02-51

REFERENCES

- Air France, Division Navigation Infrastructure, *Climatologie Afrique* Département des Vols, Doc Nav Infra, No. M. 3, December 1963.
- Air France, Division Navigation Infrastructure, *Climatologie Amérique du Sud*, Département des Vols, Doc Nav Infra, 2nd Edition, No. M. 2, April 1965.
- Allison, L. J., Gray, T. L., and Warnecke, G., "A Quasi-Global Presentation of TIROS III Radiation Data," NASA Special Publication SP-53, 1964.
- Allison, L. J., Nicholas, G. W., and Kennedy, J. S., "Example of the Meteorological Capability of the High Resolution Infrared Radiometer on the Nimbus I Satellite," *Journal of Applied Meteorology* 5(3), June 1966.
- Allison, L. J., and Warnecke, G., "Synoptic Interpretation of TIROS III Radiation Data Recorded on 16 July 1961," *Bulletin of the American Meteorological Society* 47, No. 5, pp. 374-383, May 1966.
- Allison, L. J., and Warnecke, G., "A Synoptic World Weather Analysis of TIROS VII Radiation Data," NASA Technical Note D-3787, June 1967.
- Anderson, R. K., Ferguson, E. W., and Oliver, V. J., "The Use of Satellite Pictures in Weather Analysis and Forecasting," World Meteorological Organization Technical Note No. 75, Geneva, Switzerland, 1966.
- Andrews, J. F., "The Weather and Circulation of January 1964," *Monthly Weather Review* 92(4): pp. 189-194, April 1964.
- Andrews, J. F., "The Weather and Circulation of July 1964," *Monthly Weather Review* 92(10): pp. 477-482, October 1964.
- Bandeen, W. R., Halev, M., and Strange, I., "A Radiation Climatology in the Visible and Infrared from the TIROS Meteorological Satellites," NASA Technical Note D-2534, June 1965.
- Berliner Wetterkarte*, Institut für Meteorologie und Geophysik der Freien Universität Berline, 19 June 1963 to 31 December 1964.
- Bjerknes, J., Allison, L. J., Kreins, E. R., Godshall, F. A., and Warnecke, G., "Satellite Mapping of the Pacific Tropical Cloudiness," *Bulletin of the American Meteorological Society* 50(5): pp. 313-322, May 1969.
- Deutscher Wetterdienst, Hamburg 4, *Seewetteramt Die Witterung in Übersee* 11:1963, Germany (Federal Republic) Bern, Nöchstr 76, June 1963.
- Dickson, R. R., "The Weather and Circulation of June 1963," *Monthly Weather Review* 91(9): pp. 468-473, September 1963.

- Dickson, R. R., "The Weather and Circulation of June 1964," *Monthly Weather Review* 92(9): pp. 428-432, September 1964.
- Dickson, R. R., "The Weather and Circulation of November 1964," *Monthly Weather Review* 93(2): pp. 123-126, February 1965.
- Fritz, S., and Winston, J. S., "Synoptic Use of Radiation Measurements from Satellite TIROS II," *Monthly Weather Review* 90(1): pp. 1-9, January 1962.
- Fujita, T. T., "Formation and Structure of Equatorial Anticyclones Caused by Large-Scale Cross-Equatorial Flows Determined by ATS-1 Photographs," SMRP Research Paper No. 78, University of Chicago, January 1969.
- Gabites, J. F., "Weather Analysis in the Tropical South Pacific," Preliminary Note, Miscellaneous Meteorological Notes No. 1, New Zealand Directorate of Meteorological Services, Wellington, New Zealand, 10 pp., 1943.
- Godshall, F. A., and Shenk, W., private communication.
- Godshall, F. A., "Intertropical Convergence Zone and Mean Cloud Amount in the Tropical Pacific Ocean," *Monthly Weather Review* 96(3): pp. 172-175, March 1968.
- Green, R. A., "The Weather and Circulation of October 1963," *Monthly Weather Review* 92(1): pp. 37-42, January 1964.
- Green, R. A., "The Weather and Circulation of May 1964," *Monthly Weather Review* 92(8): pp. 374-380, August 1964.
- Green, R. A., "The Weather and Circulation of September 1964," *Monthly Weather Review* 92(12): pp. 601-606, December 1964.
- Hanson, K. J., Vonder Haar, T. H., Suomi, V. E., "Reflection of Sunlight to Space and Absorption by the Earth and Atmosphere over the United States During Spring 1962," *Monthly Weather Review* 95, pp. 345-362, 1967.
- Hill, H. W., "The Weather in Lower Latitudes of the Southwest Pacific Associated with the Passage of Disturbances in the Middle Latitude Westerlies," Proceedings, Symposium of Tropical Meteorology, New Zealand, 1963, pp. 352-365.
- House, F. B., "The Radiation Balance of the Earth from a Satellite," Thesis, Department of Meteorology, University of Wisconsin, 1965.
- Indian Journal of Meteorology and Geophysics, Weather:
- Vol. 15, No. 1, January 1964, a
- Vol. 15, No. 3, July 1964, b

Vol. 15, No. 4, October 1964, c

Vol. 16, No. 1, January 1965, a

Vol. 16, No. 2, April 1965, b.

Johnson, H. M., "Motions in the Upper Troposphere as Revealed by Satellite-Observed Cirrus Formations," NES Report 39, Environmental Science Services Administration, October 1966.

Kornfield, J., and Hanson, K., "On the Double Structure of Cloud Distribution in the Equatorial Pacific," The ATS-1 Volume, University of Wisconsin Press, 1968.

Kreins, E. R., and Allison, L. J., "An Atlas of TIROS VII Monthly Maps of Emitted Radiation in the 8-12 Micron Atmospheric Window Over the Indian Ocean Area," NASA Technical Note D-5101, February 1969.

Meteorologische Abhandlungen, Institut für Meteorologie und Geophysik der Freien Universität Berlin, 35, No. 5-12, 45, No. 1-r, June 1963 to December 1964.

Möller, F., "Eine Karte der Strahlungsbilanz des Systems Erde-Atmosphäre für einen 14tägigen Zeitraum, *Meteorol. Rundschau*, Vol. 20, pp. 97-98, 1967.

O'Connor, J. F., "The Weather and Circulation of July, August, and September 1963," *Monthly Weather Review* 91(10-12): pp. 737-748, October-November-December 1963.

O'Connor, J. F., "The Weather and Circulation of February 1964," *Monthly Weather Review* 92(5): pp. 255-262, May 1964.

O'Connor, J. F., "The Weather and Circulation of October 1964," *Monthly Weather Review* 93(1): pp. 59-66, January 1965.

Posey, J. W., "The Weather and Circulation of November 1963," *Monthly Weather Review* 92(2): pp. 85-89, February 1964.

Posey, J. W., "The Weather and Circulation of March 1964," *Monthly Weather Review* 92(6): pp. 333-338, June 1964.

Posey, J. W., "The Weather and Circulation of August 1964," *Monthly Weather Review* 92(11): pp. 535-542, November 1964.

Posey, J. W., "The Weather and Circulation of December 1964," *Monthly Weather Review* 93(3): pp. 189-194, March 1965.

Ramage, C. S., "The Summer Atmospheric Circulation over the Arabian Sea," *Journal of the Atmospheric Sciences* 23(2): pp. 144-150, March 1966.

Rao, P., and Winston, J. S., "An Investigation of Some Synoptic Capabilities of Atmospheric 'Window' Measurements from TIROS II," *Journal of Applied Meteorology* 2, pp. 12-23, 1963.

Raschke, E., Möller, F., and Bandeen, W. R., "The Radiation Balance of the Earth-Atmosphere System over Both Polar Regions Obtained from Radiation Measurements of the Nimbus II Meteorological Satellite," *Meddelanden, Serie B.*, Nr. 28, Sveriges Meteorologiska och Hydrologiska Institut, Stockholm, 1968.

Raschke, E., "The Radiation Balance of the Earth-Atmosphere System from Radiation Measurement of the Nimbus II Meteorological Satellite," NASA Technical Note D-4589, July 1968.

Sadler, J. C., "Average Cloudiness in the Tropics through Satellite Observations," *Indian Ocean Monograph #2*, Indian Ocean Expedition, East-West Center Press, Honolulu, Hawaii, 1968.

Sikha, D. R., private communication, Institute of Tropical Meteorology, Poona, India, 1964.

Simpson, R. H., Frank, N., Shideler, D., and Johnson, H. M., "Atlantic Tropical Disturbances, 1967," *Monthly Weather Review* 96(4): pp. 251-259, April 1968.

Staff Members, Goddard Space Flight Center, 1964, 1965, 1966: *TIROS VII Radiation Data Catalog and User's Manual*:

Vol. 1, September 30, 1964(a)

Vol. 2, December 31, 1964(b)

Vol. 3, October 15, 1965

Vol. 4, January 15, 1966.

Stark, L. P., "The Weather and Circulation of December 1963," *Monthly Weather Review* 92(3): pp. 139-146, March 1964.

Stark, L. P., "The Weather and Circulation of April, 1964," *Monthly Weather Review* 92(7): pp. 357-362, July 1964.

Taljaard, J. J., "Development, Distribution, and Movement of Cyclones and Anticyclones in the Southern Hemisphere During the IGY," *Journal of Applied Meteorology* 6(6): pp. 973-987, December 1967.

Taylor, V. Ray, and Winston, Jay S., *Monthly and Seasonal Mean Global Charts of Brightness from ESSA III and ESSA V Digitized Pictures*, February 1967-February 1968, TR-NESC #46, ESSA, U. S. Department of Commerce, Washington, D. C., November 1968.

Van Loon, H., "On the Annual Temperature Range Over the Southern Oceans," *Geographical Review* LVI(4): pp. 497-515, 1966.

Vonder Haar, T. H., "Variations of the Earth's Radiation Budget," Thesis, Department of Meteorology, University of Wisconsin, 1968.

Warnecke, G., Allison, L. J., Kreins, E. R., and McMillin, L., "A Satellite View of Typhoon Marie 1966 Development," NASA Technical Note D-4757, November 1968.

- Widger, W. K., Barnes, J. C., Merritt, E. S., and Smith, R. B., "Meteorological Interpretation of Nimbus High Resolution Infrared (HRIR) Data," NASA CR-352, 1966.
- Winston, J. S., "Planetary-Scale Characteristics of Monthly Mean Long-Wave Radiation and Albedo and Some Year-to-Year Variations," *Monthly Weather Review* 95, pp. 235-256, 1967.
- Winston, J. S., and Krishna Rao, P., "Preliminary Study of Planetary-Scale Outgoing Long-Wave Radiation as Derived from TIROS II Measurements," *Monthly Weather Review* 90, pp. 307-310, 1962.
- Winston, J. S., and Taylor, V. R., "Atlas of World Maps of Long-Wave Radiation and Albedo for Seasons and Months Based on Measurements from TIROS IV and TIROS VII," ESSA Technical Report, NESC 43, 1967.
- Winston, J. S., "Global Distribution of Cloudiness and Radiation as Measured from Weather Satellites," *Climate of the Free Atmosphere*, D. F. Rex, (ed), World Survey of Climatology, Volume 4, Elsevier Publishing Co., Amsterdam, 1969.

Page intentionally left blank

Page intentionally left blank

Appendix A

- (a) Maps of monthly mean equivalent blackbody temperature, June 1963-December 1964, from TIROS VII radiometric measurements in the 8-12 micron window.
- (b) Maps of mean monthly cloud coverage from surface observations, of the monthly range of the position of the ITC, of the principal axes of the 700-mb maximum winds with isotachs (except June 1963), and of the mean monthly trough positions, June 1963-December 1964.
- (c) Monthly mean surface streamlines in the tropics, ITC positions, and precipitation frequency and amounts, based upon long-term climatological data.

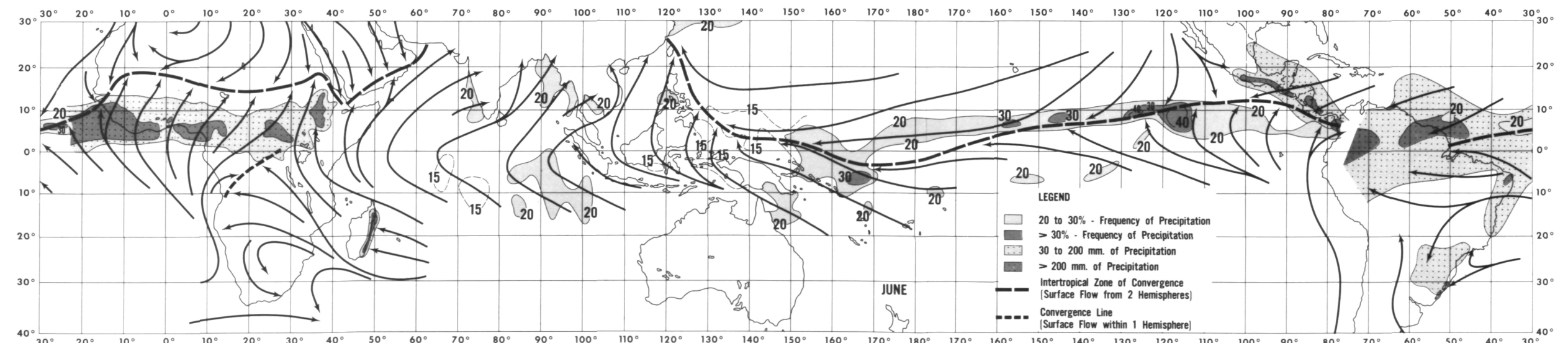
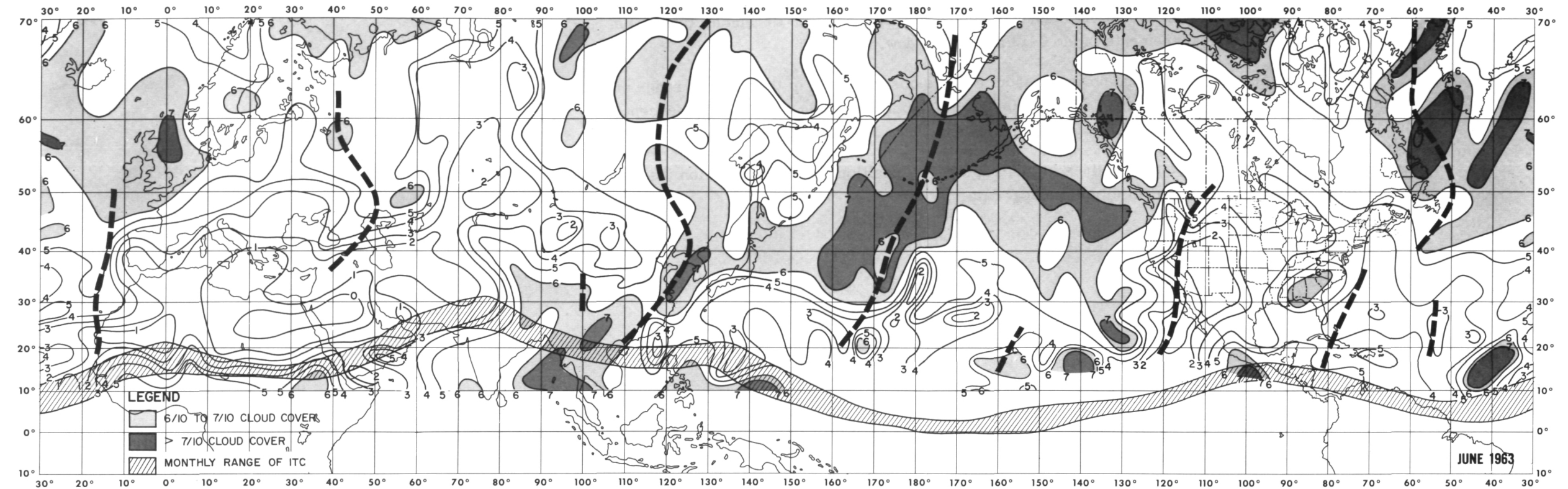
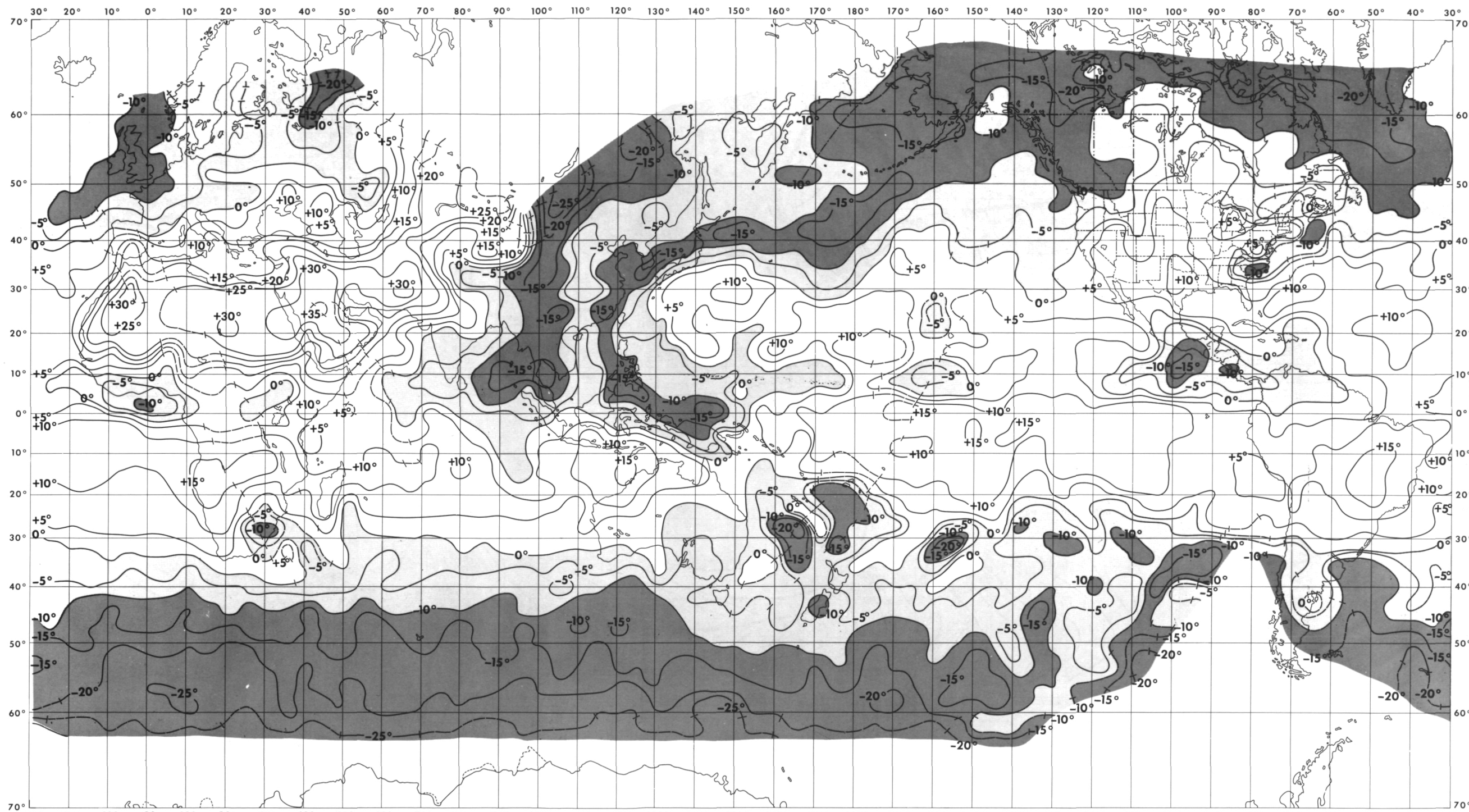


Figure A1(b) top — A1(c) bottom.



JUNE 1963 MONTHLY AVERAGE OF
EQUIVALENT BLACKBODY TEMPERATURE ($^{\circ}$ C)
TIROS VII , 8 - 12 μ CORRECTED FOR DEGRADATION

Figure A1(a).

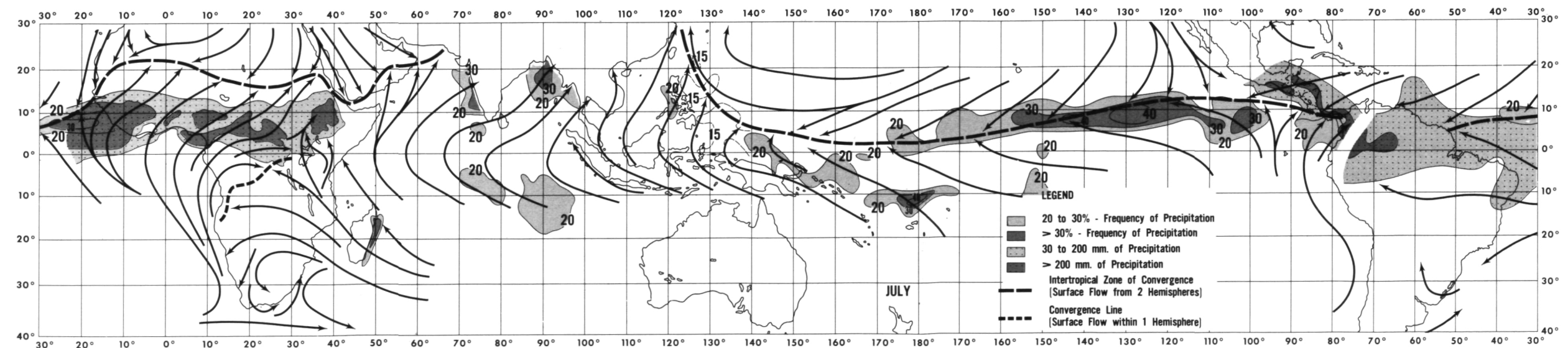
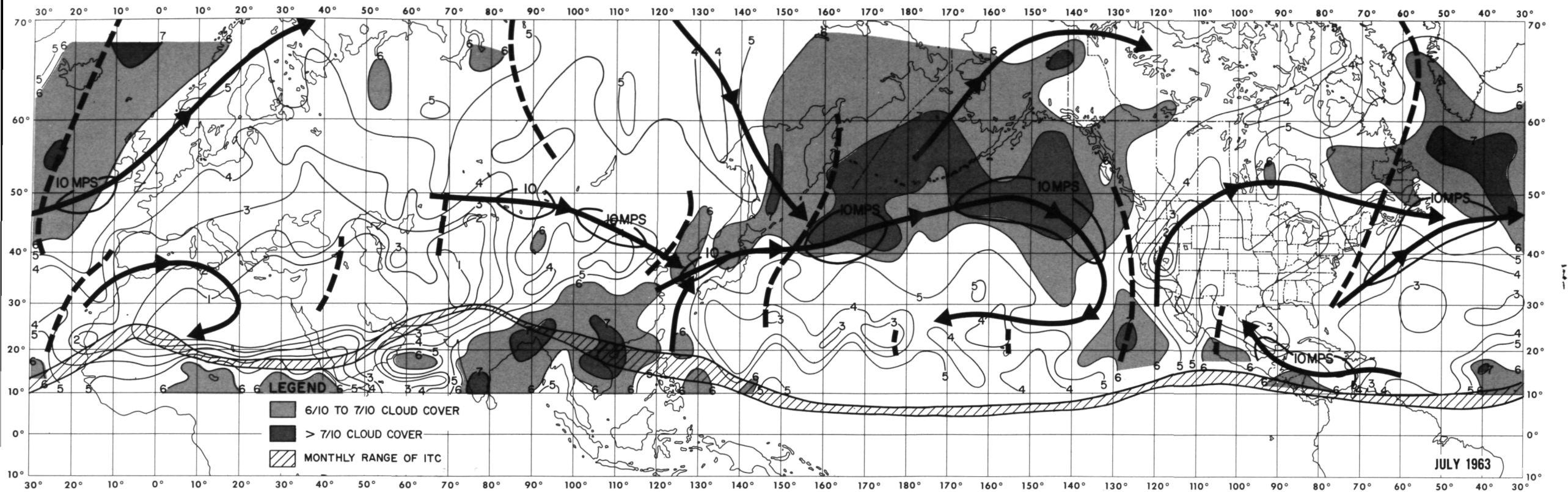
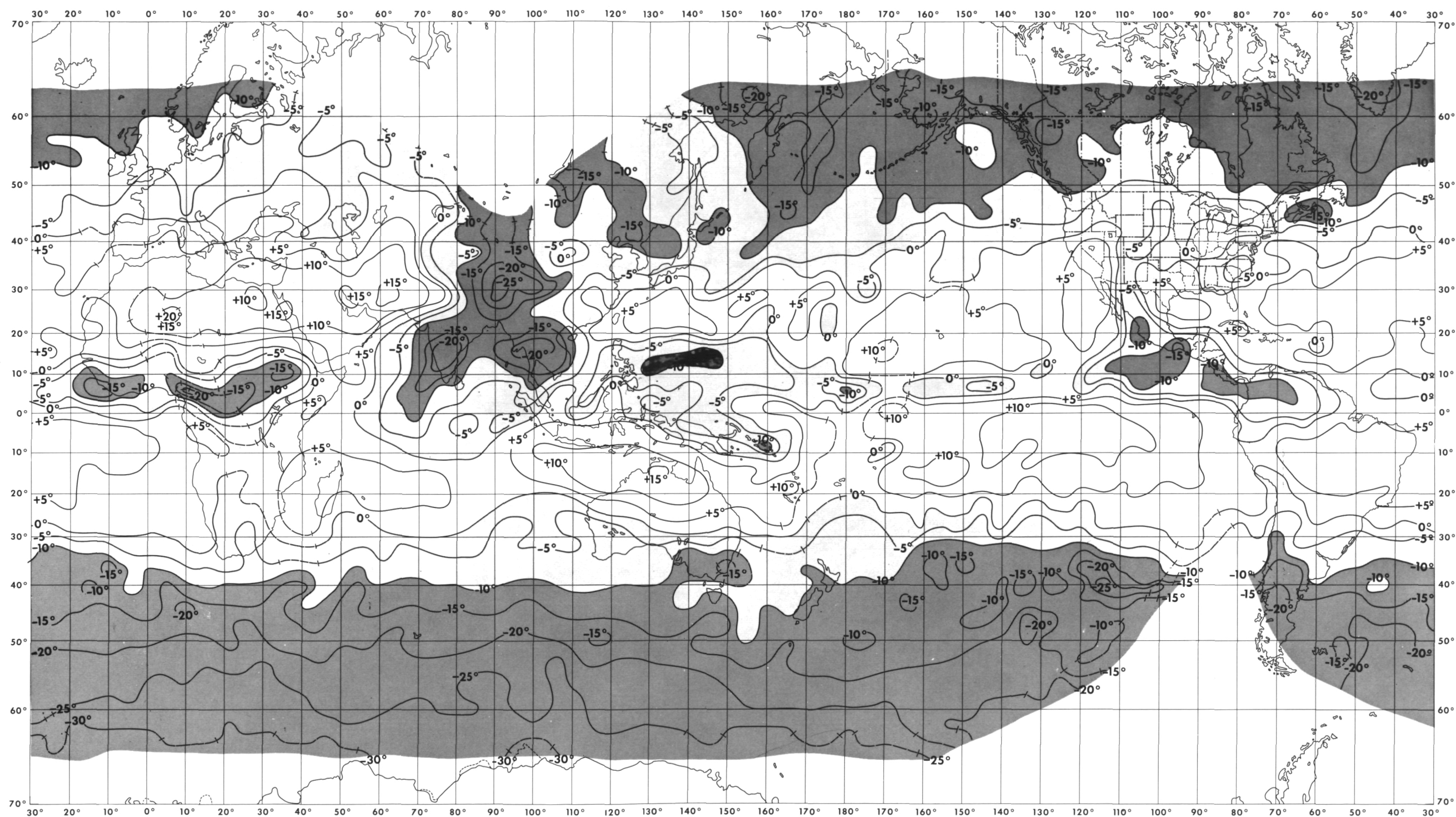


Figure A2(b) top — A2(c) bottom.



JULY 1963 MONTHLY AVERAGE OF
EQUIVALENT BLACKBODY TEMPERATURE ($^{\circ}$ C)
TIROS VII , 8 - 12 μ CORRECTED FOR DEGRADATION

Figure A2(a).

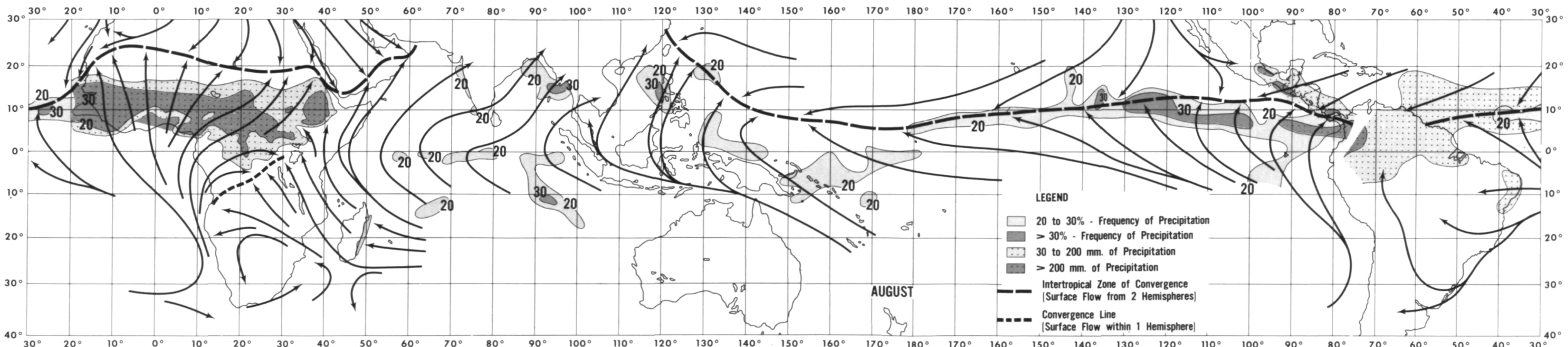
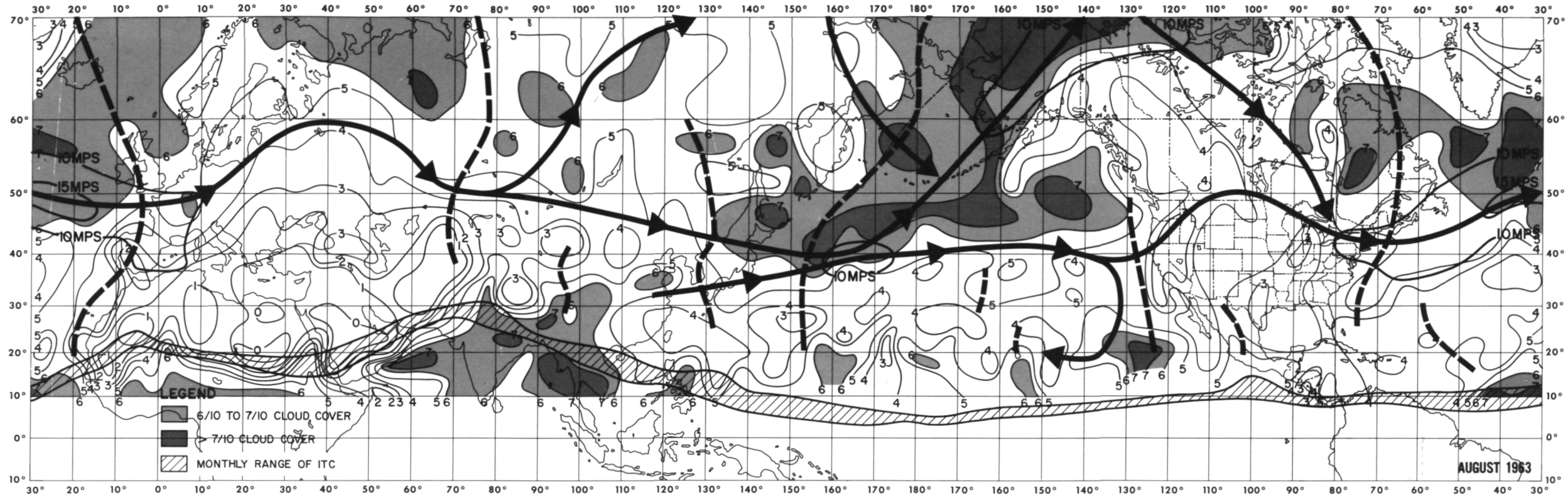
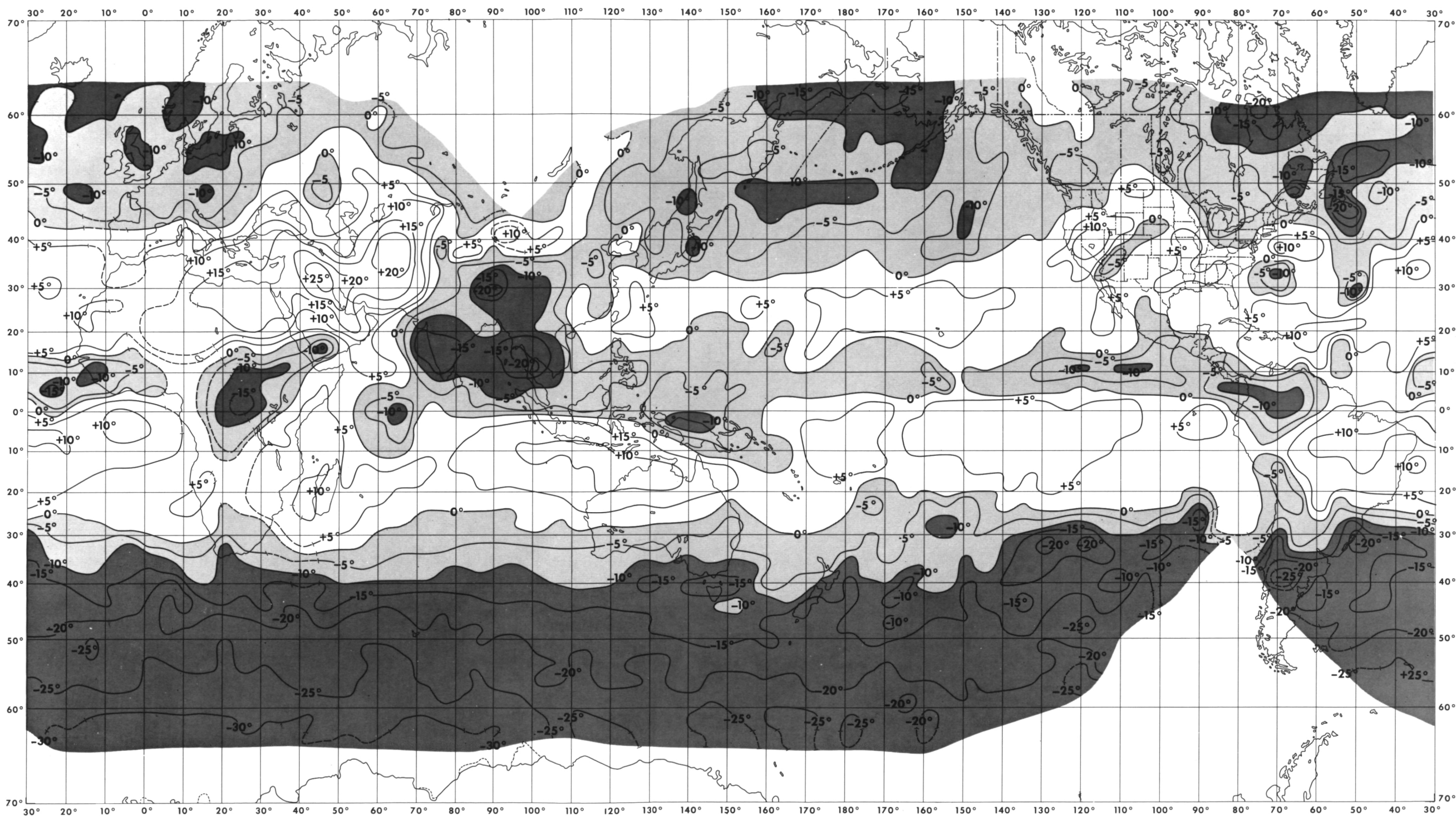


Figure A3(b) top — A3(c) bottom.



AUGUST 1963 MONTHLY AVERAGE OF
EQUIVALENT BLACKBODY TEMPERATURE (°C)
TIROS VII , 8 - 12 μ CORRECTED FOR DEGRADATION

Figure A3(a).

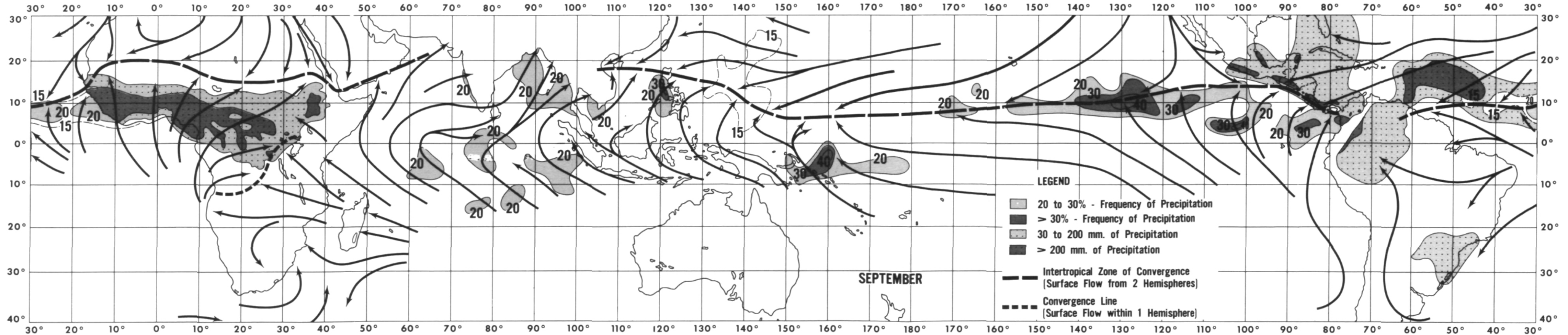
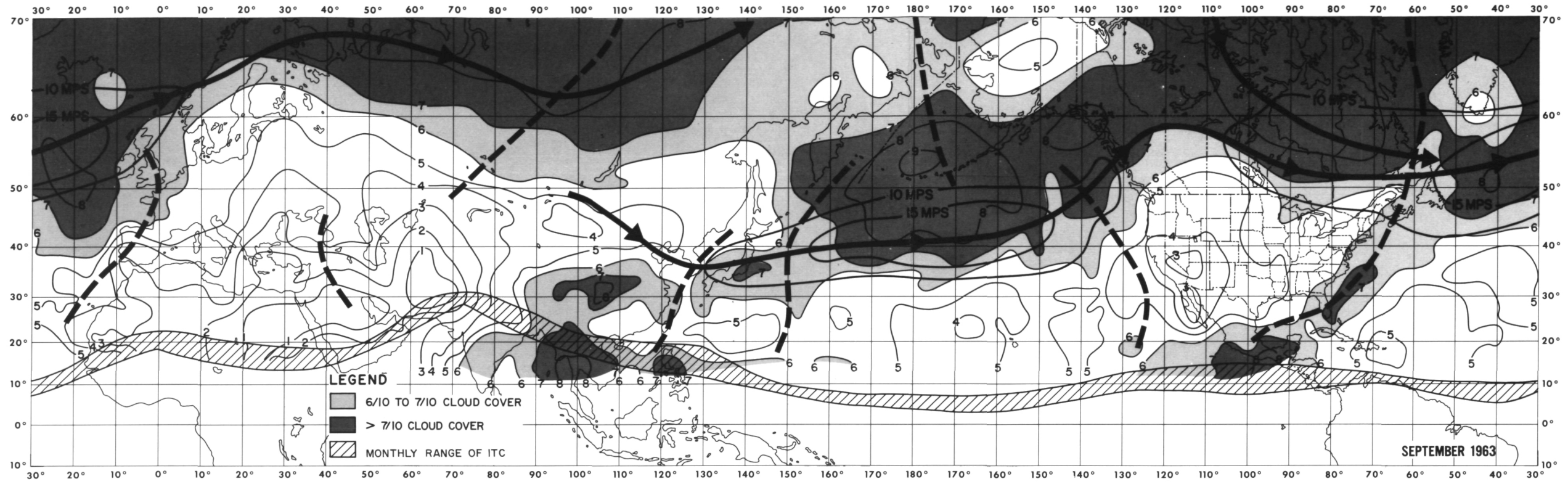
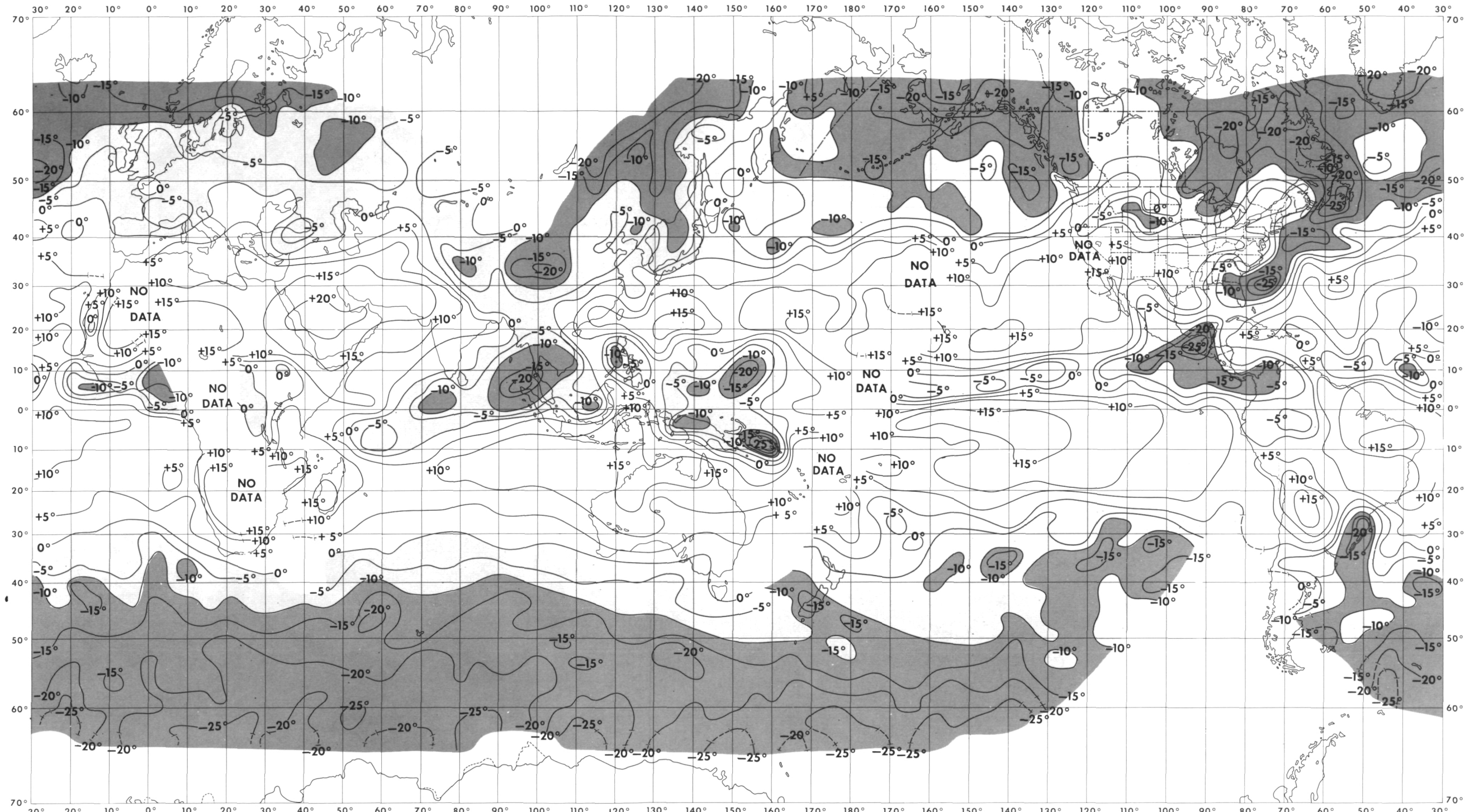


Figure A4(b) top — A4(c) bottom.



SEPTEMBER 1963 MONTHLY AVERAGE OF
EQUIVALENT BLACKBODY TEMPERATURE ($^{\circ}$ C)
TIROS VII , 8 - 12 μ CORRECTED FOR DEGRADATION

Figure A4(a).

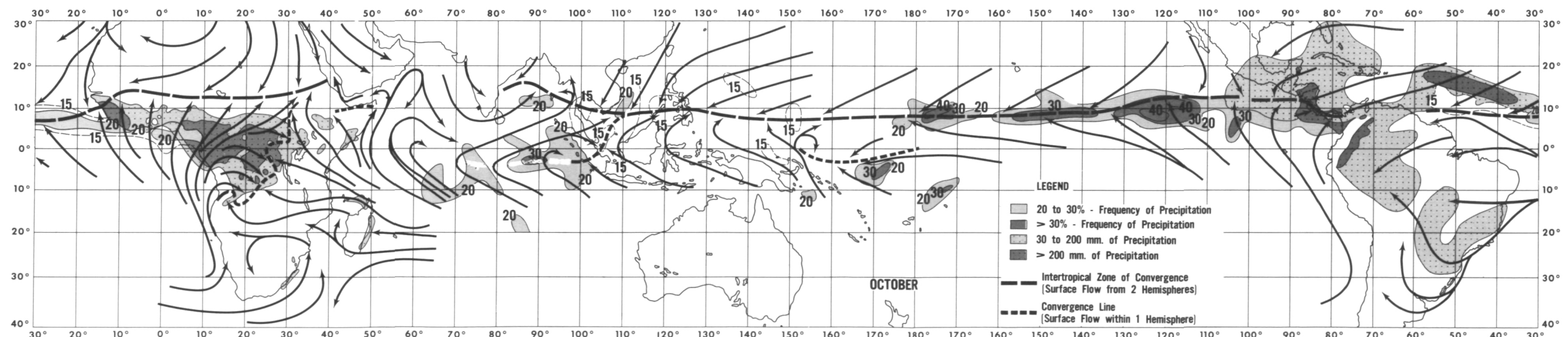
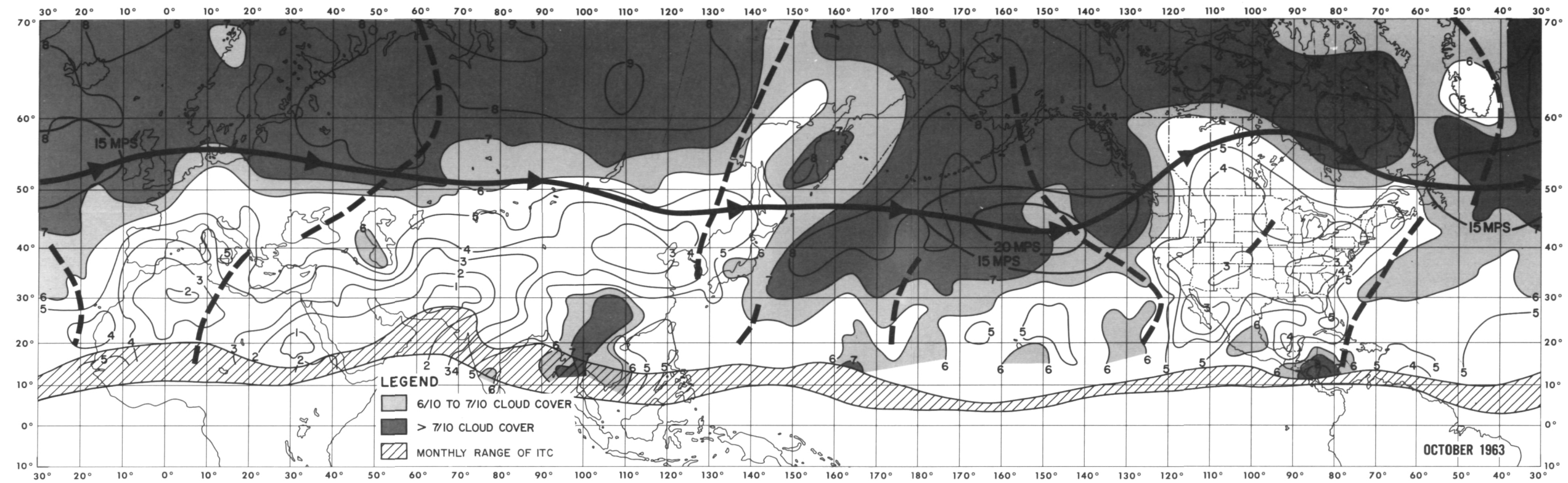
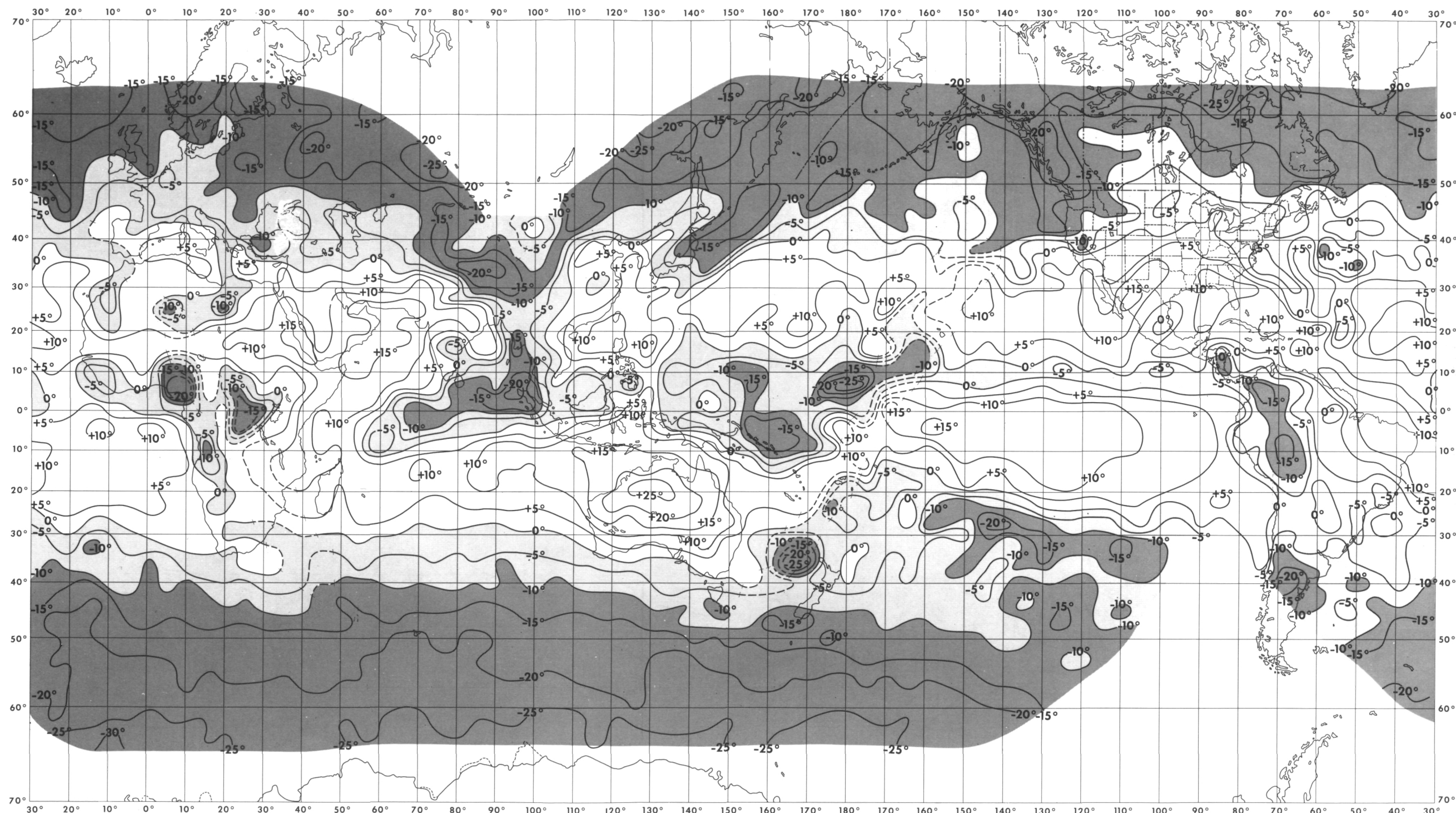


Figure A5(b) top — A5(c) bottom.



OCTOBER 1963 MONTHLY AVERAGE OF
EQUIVALENT BLACKBODY TEMPERATURE ($^{\circ}$ C)
TIROS VII , 8 - 12 μ CORRECTED FOR DEGRADATION

Figure A5(a).

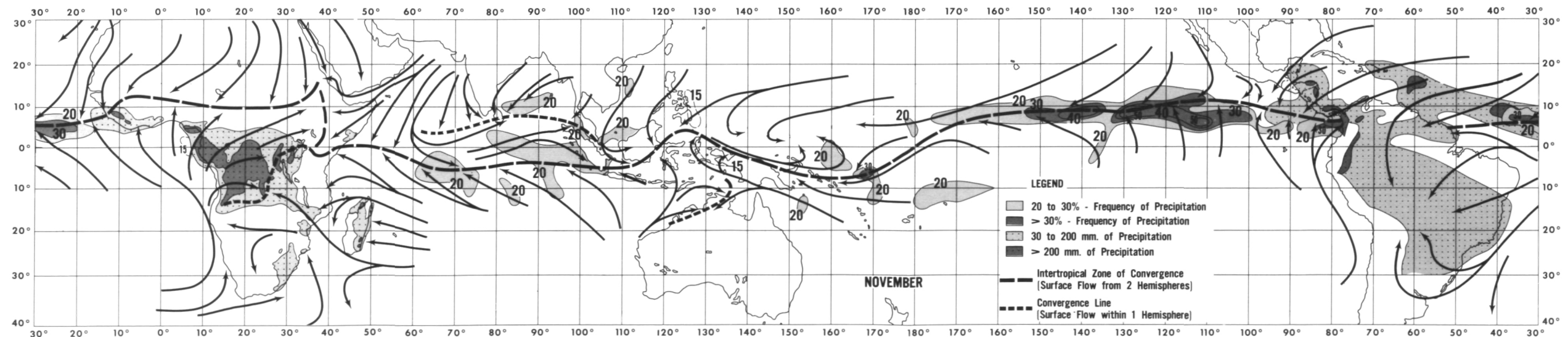
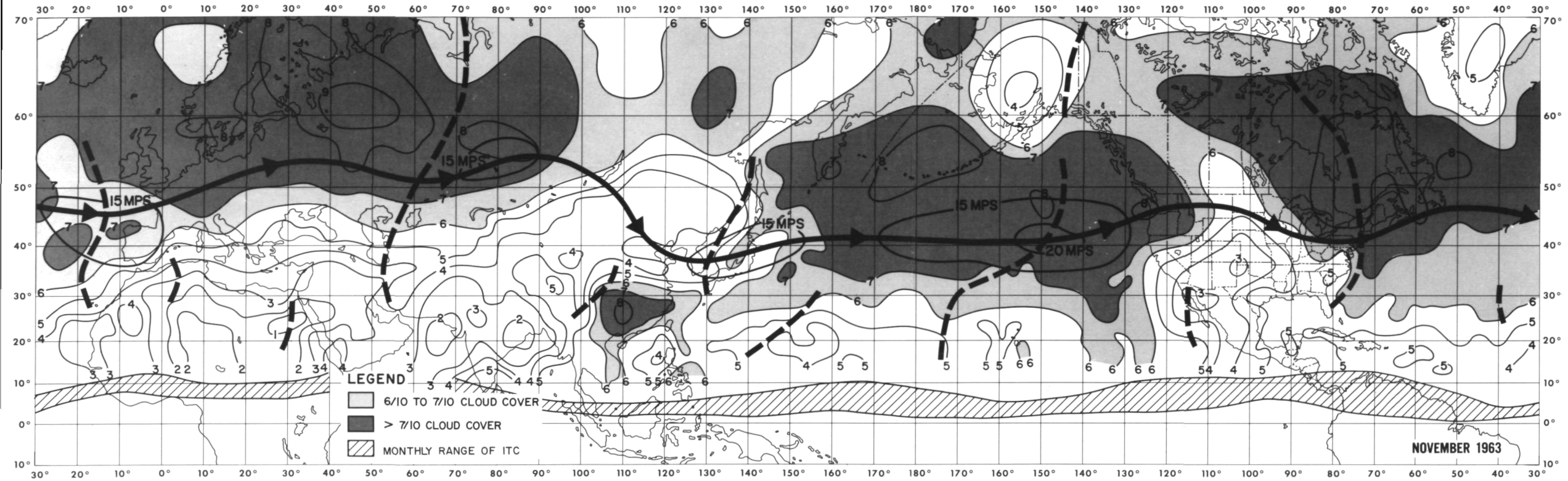
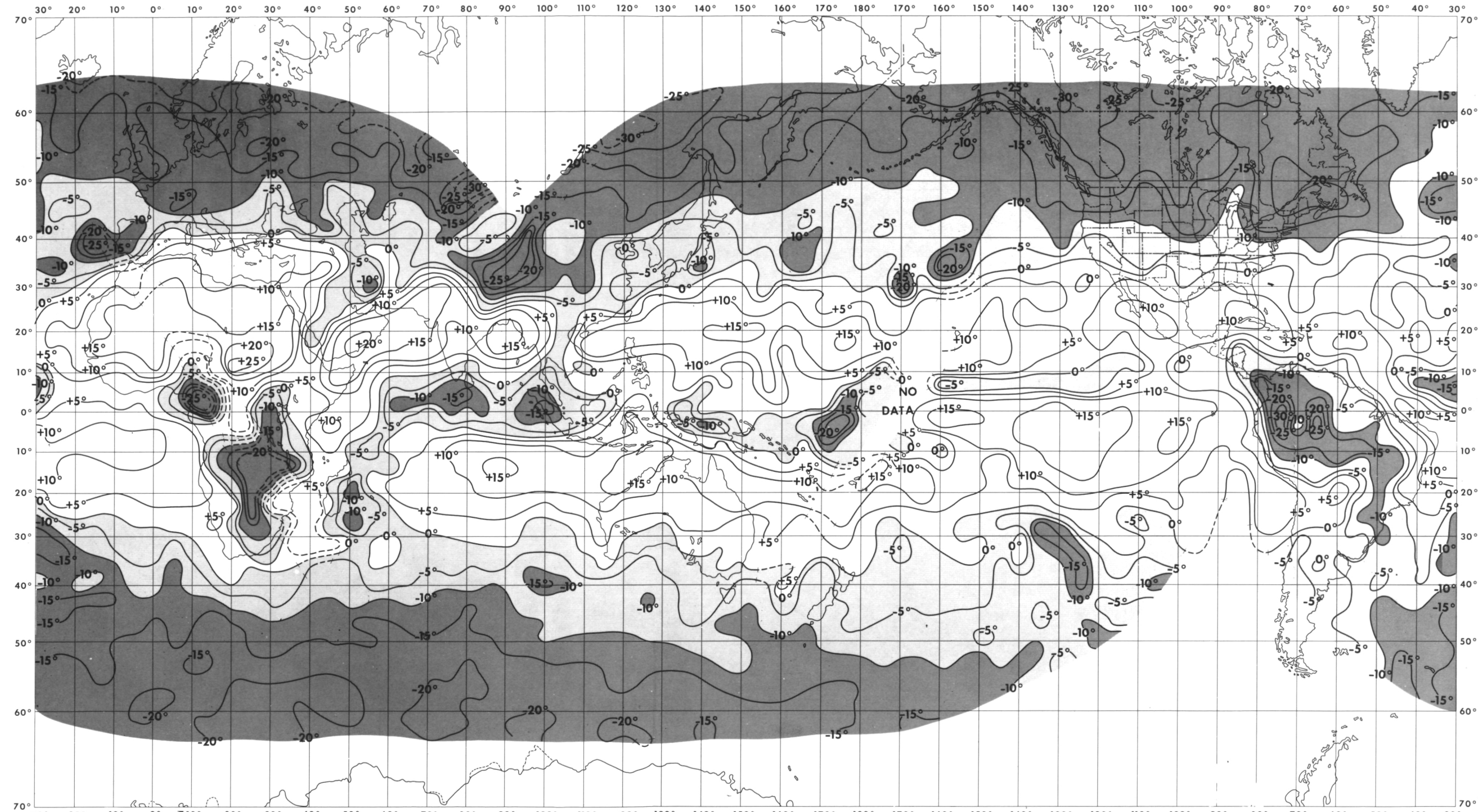


Figure A6(b) top — A6(c) bottom.



NOVEMBER 1963 MONTHLY AVERAGE OF
EQUIVALENT BLACKBODY TEMPERATURE ($^{\circ}\text{C}$)
TIROS VII , 8 - 12μ CORRECTED FOR DEGRADATION

Figure A6(a).

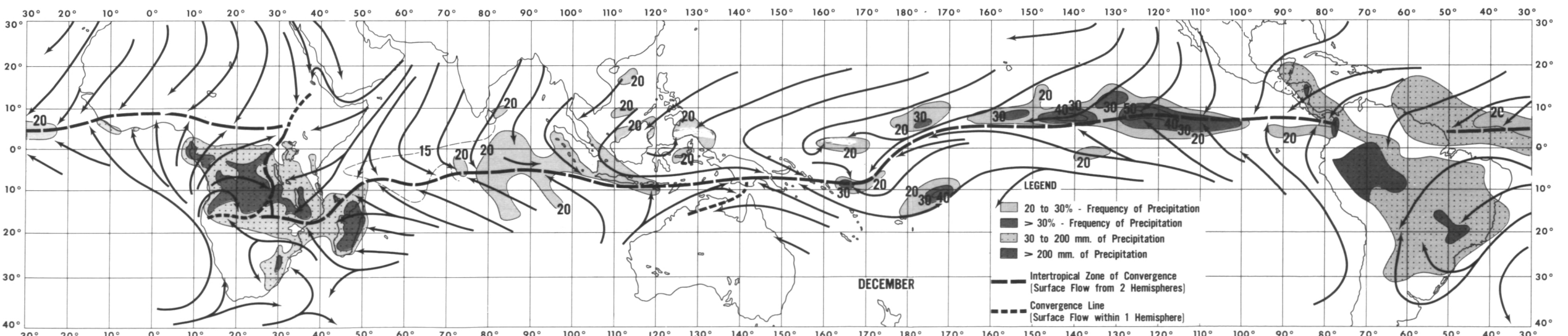
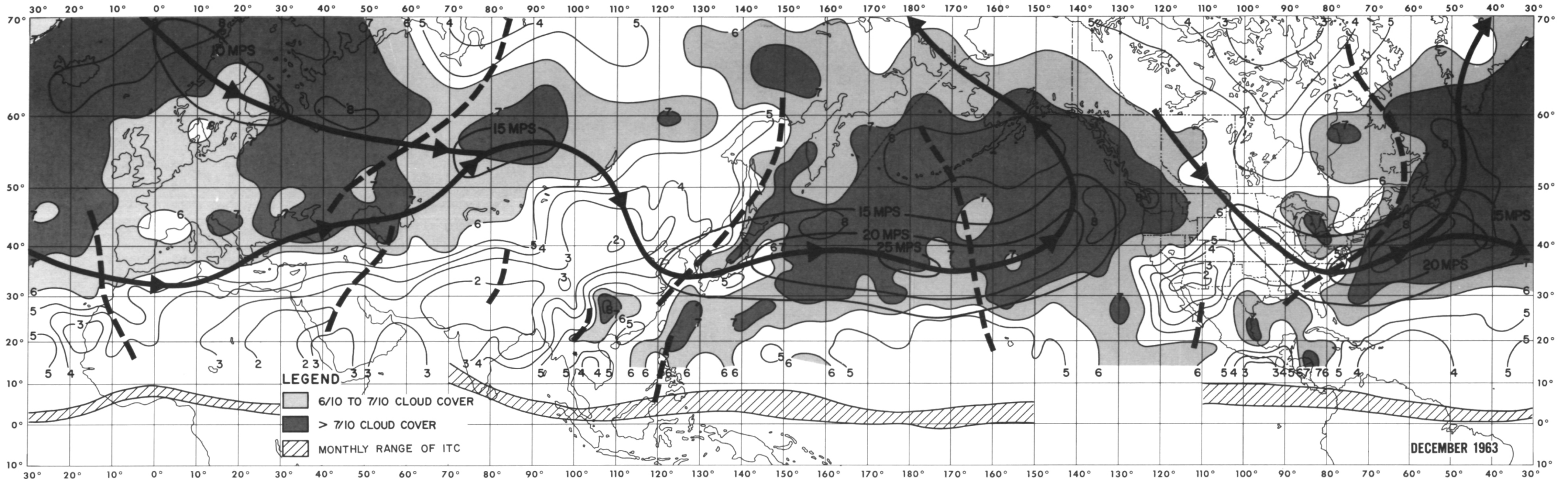


Figure A7(b) top — A7(c) bottom.

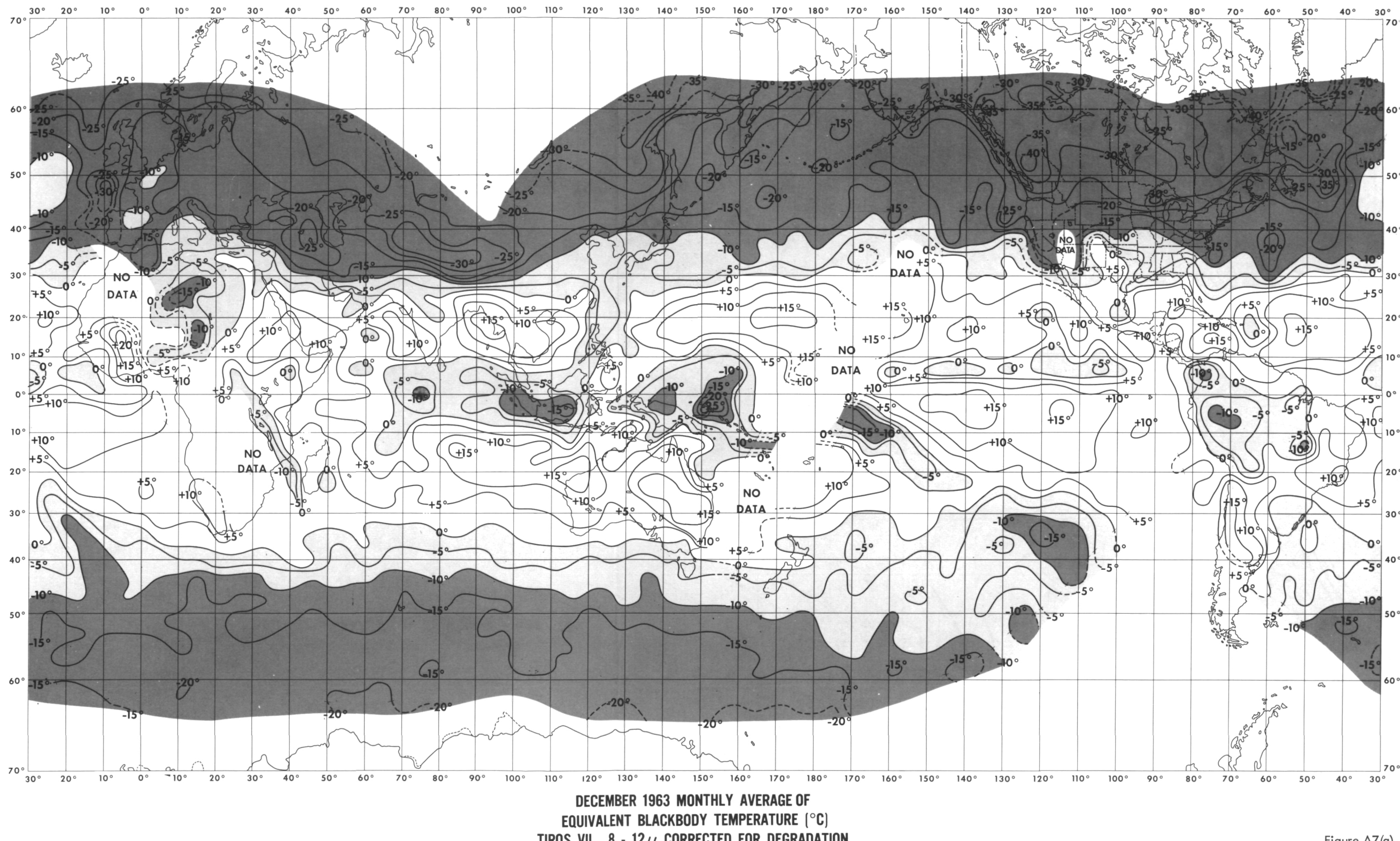


Figure A7(a).

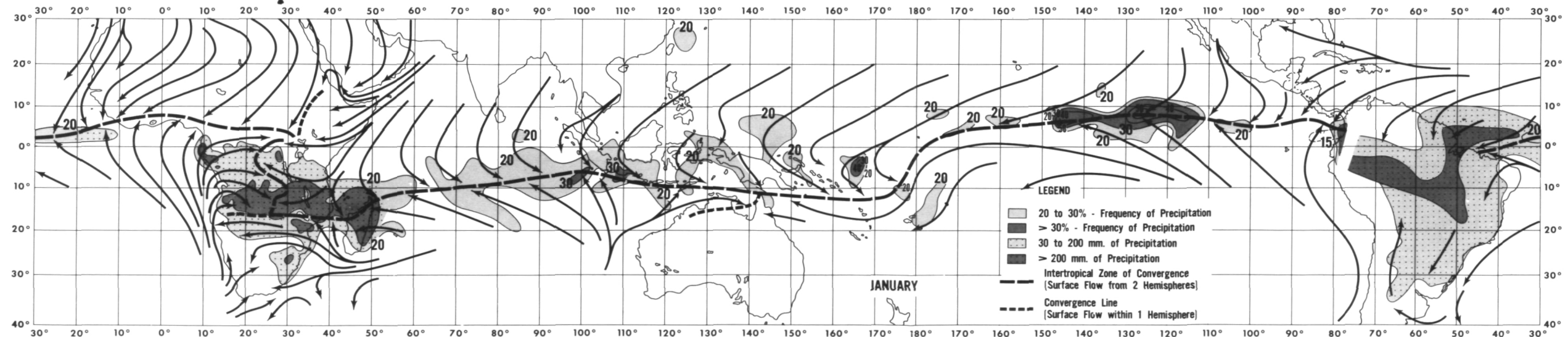
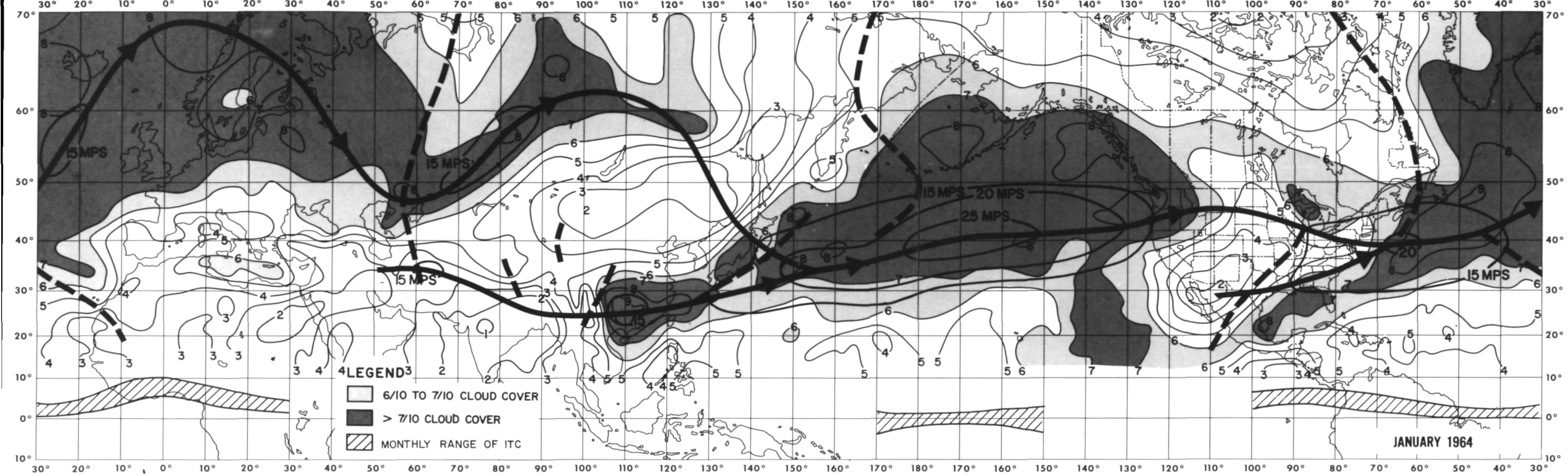


Figure A8(b) top — A8(c) bottom.

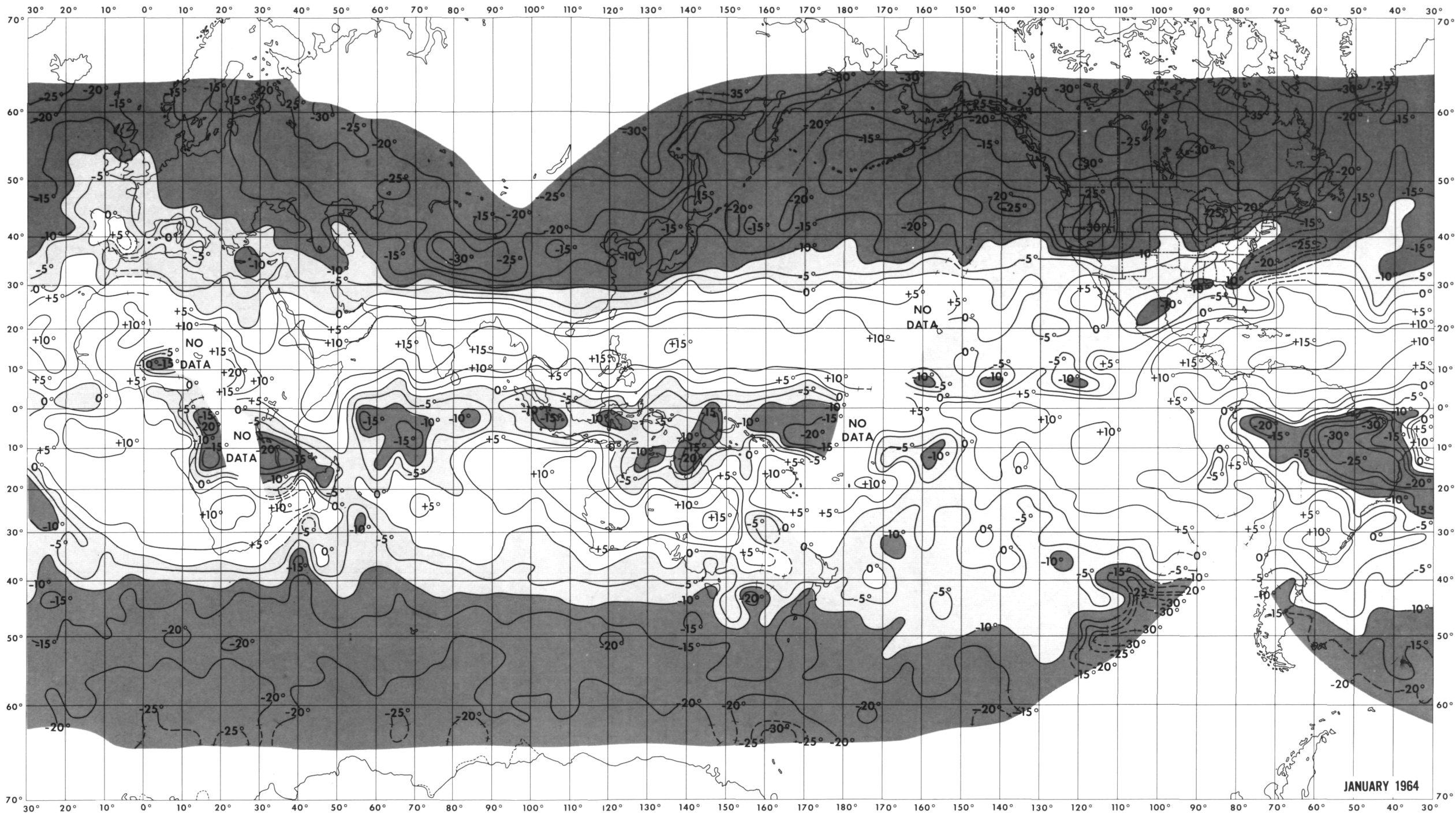


Figure A8(a).

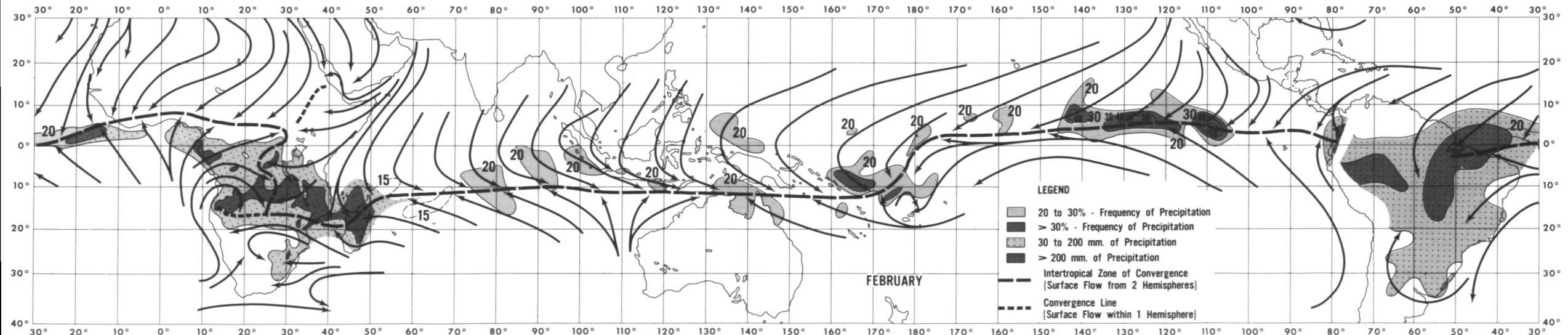
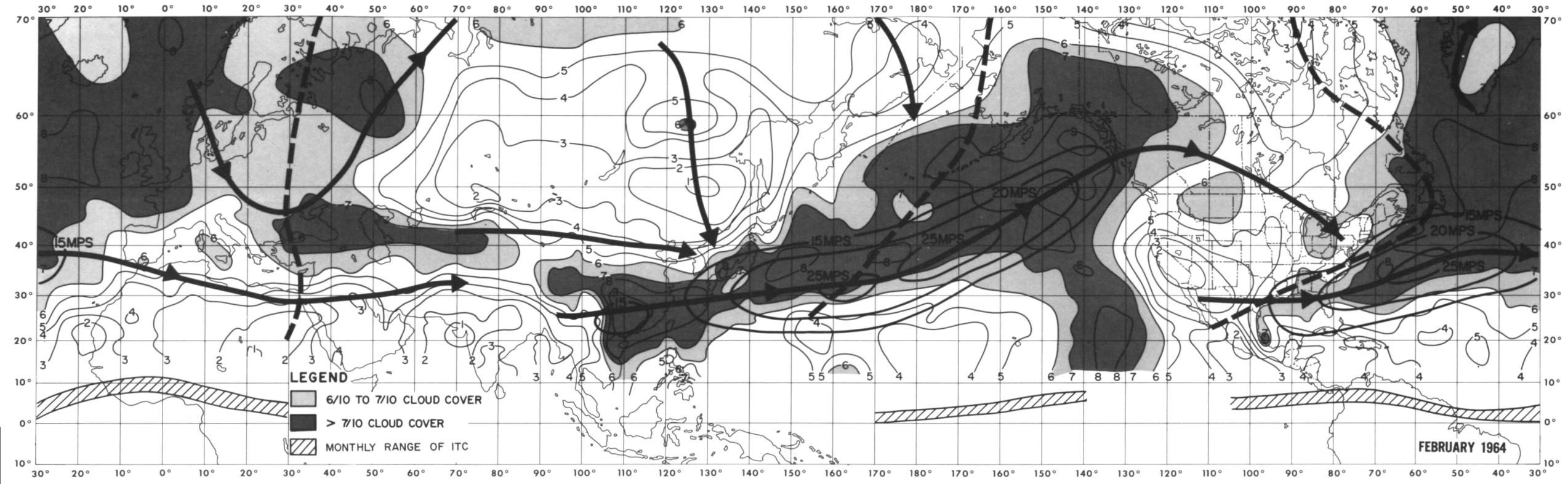


Figure A9(b) top — A9(c) bottom.

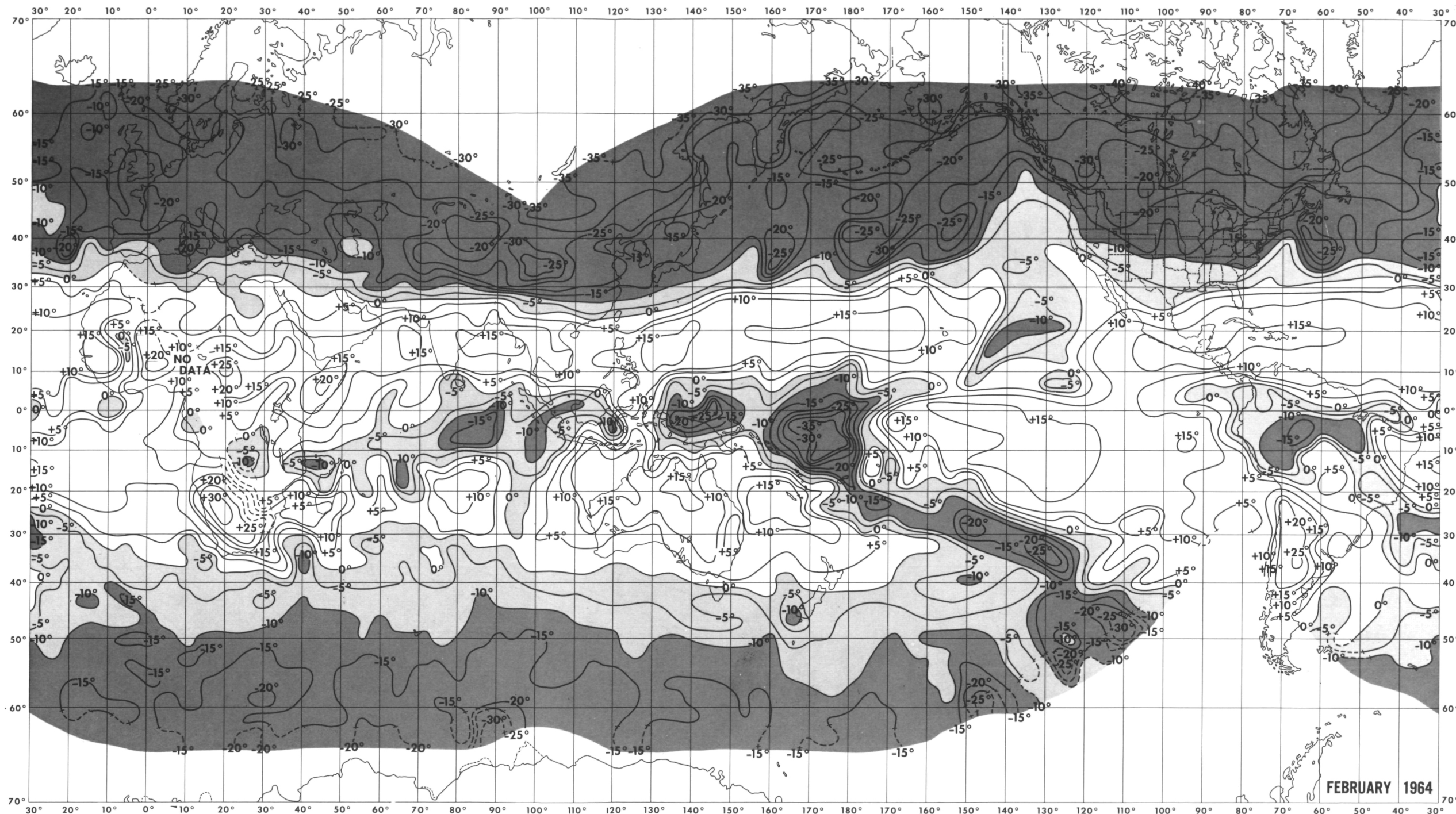


Figure A9(a).

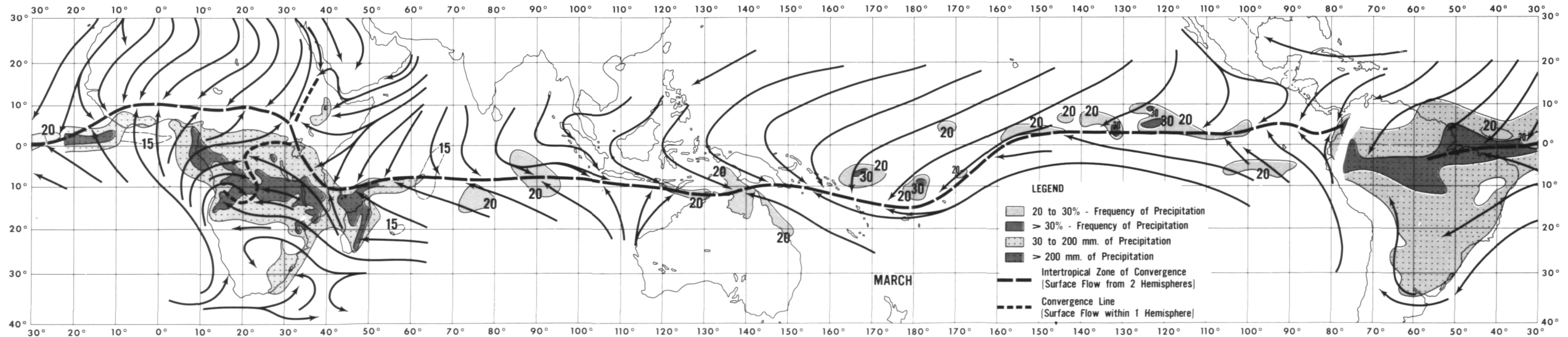
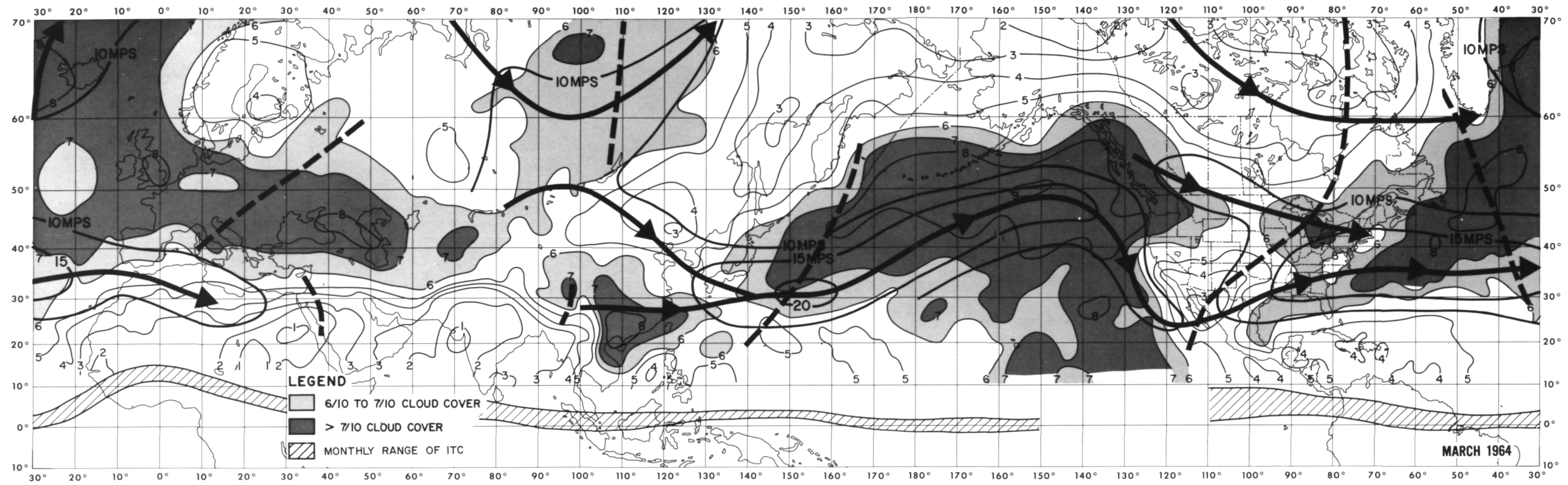


Figure A10(b) top — A10(c) bottom.

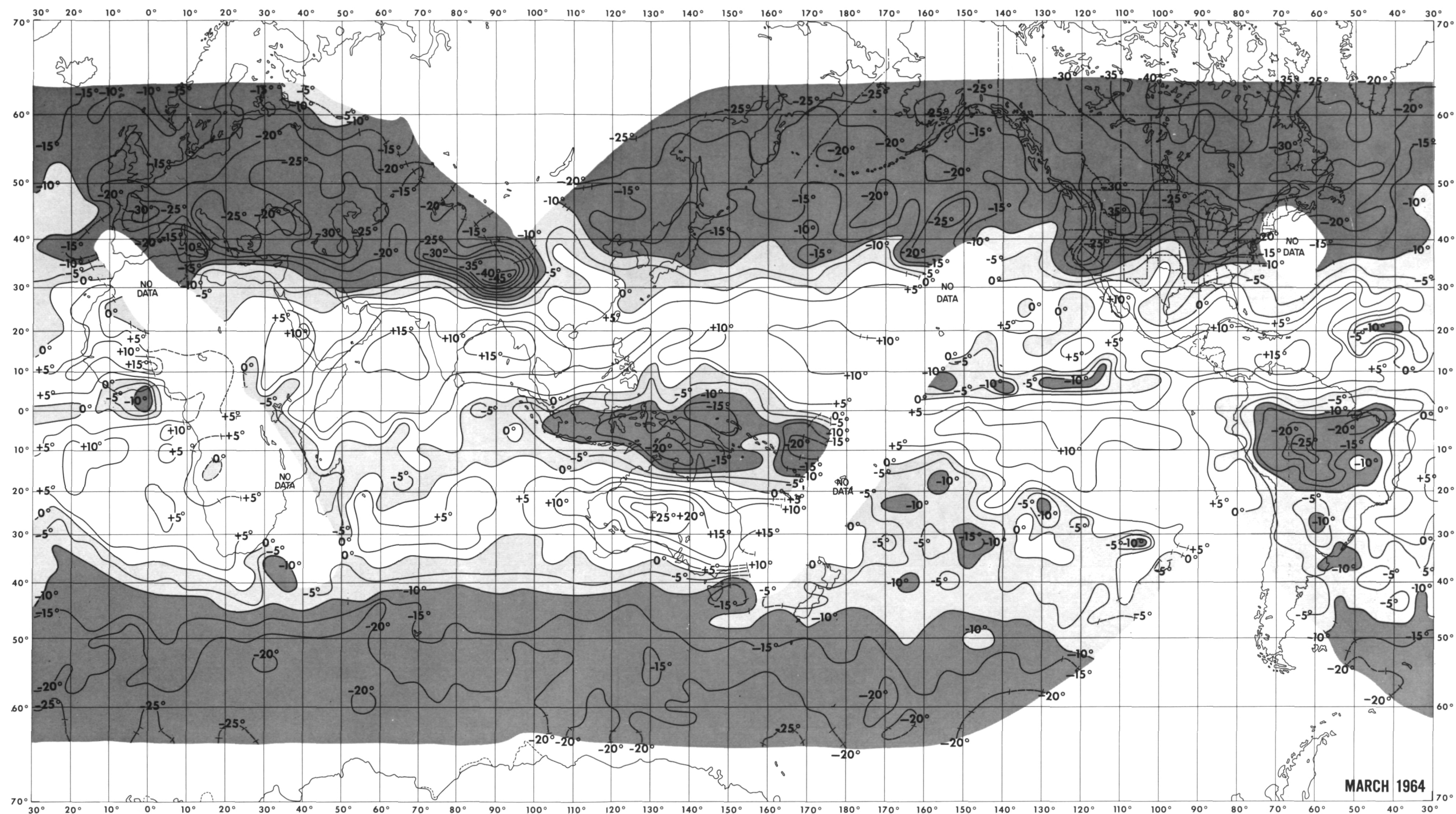


Figure A10(a).

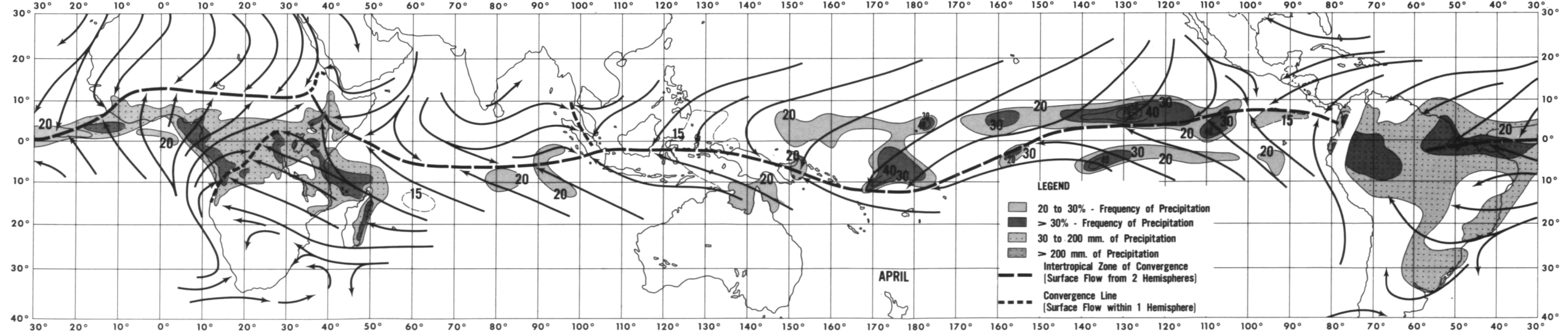
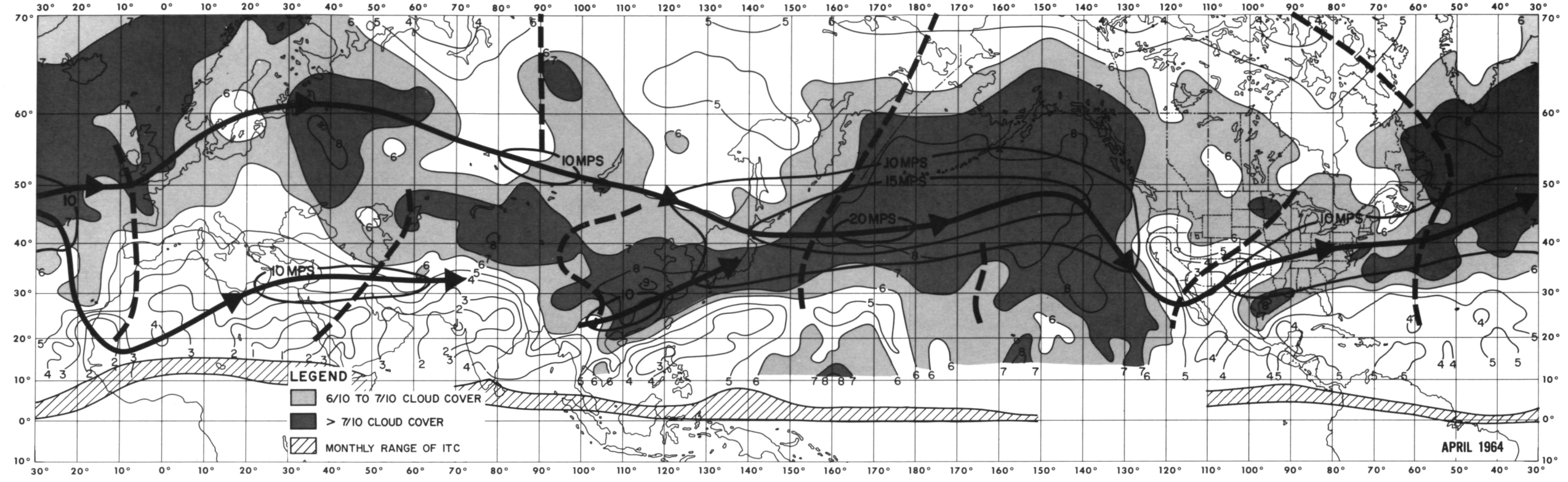
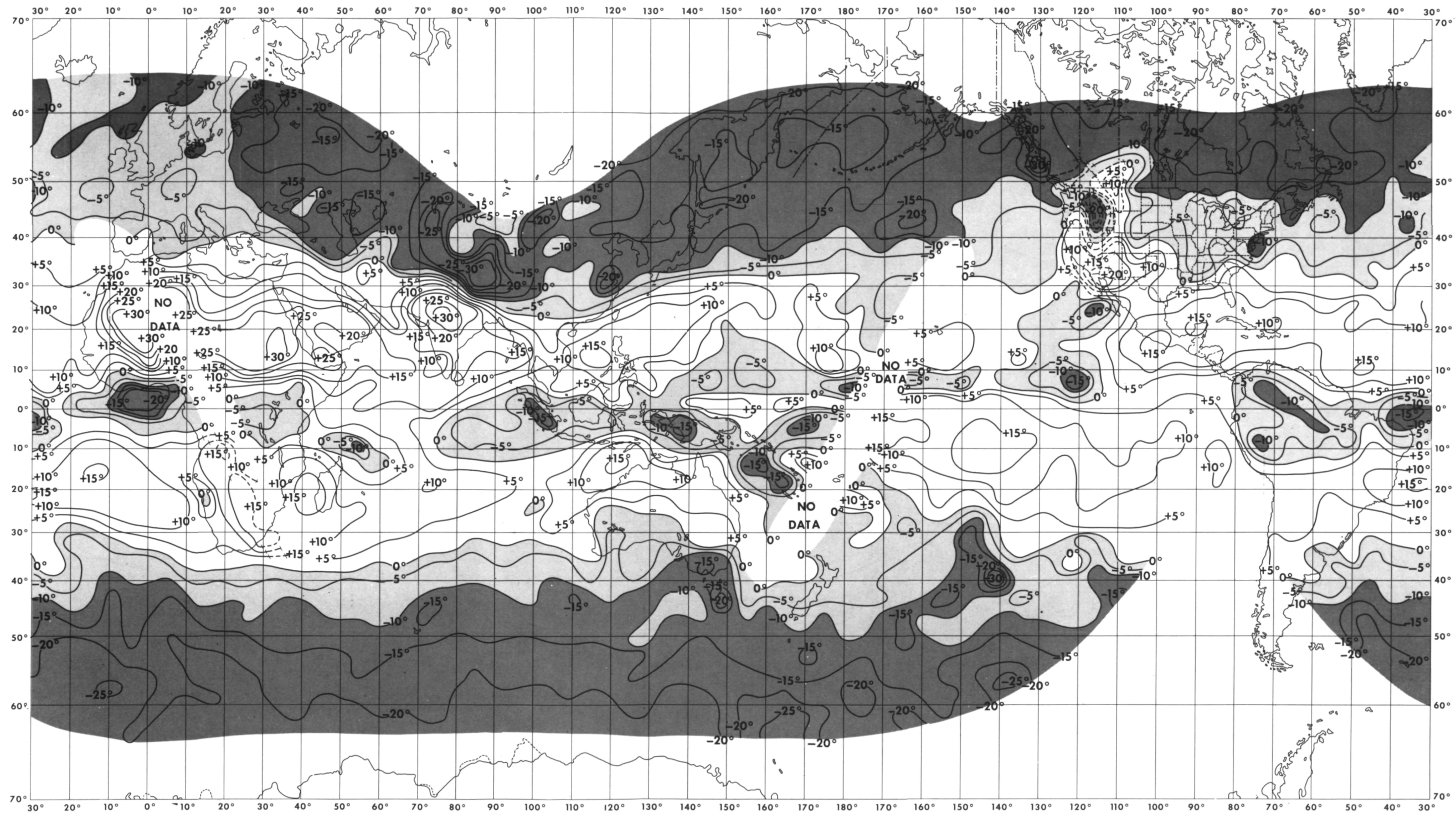


Figure A11(b) top – A11(c) bottom.



APRIL 1964 MONTHLY AVERAGE OF
EQUIVALENT BLACKBODY TEMPERATURE ($^{\circ}$ C)
TIROS VII , 8 - 12 μ CORRECTED FOR DEGRADATION

Figure A11(a).

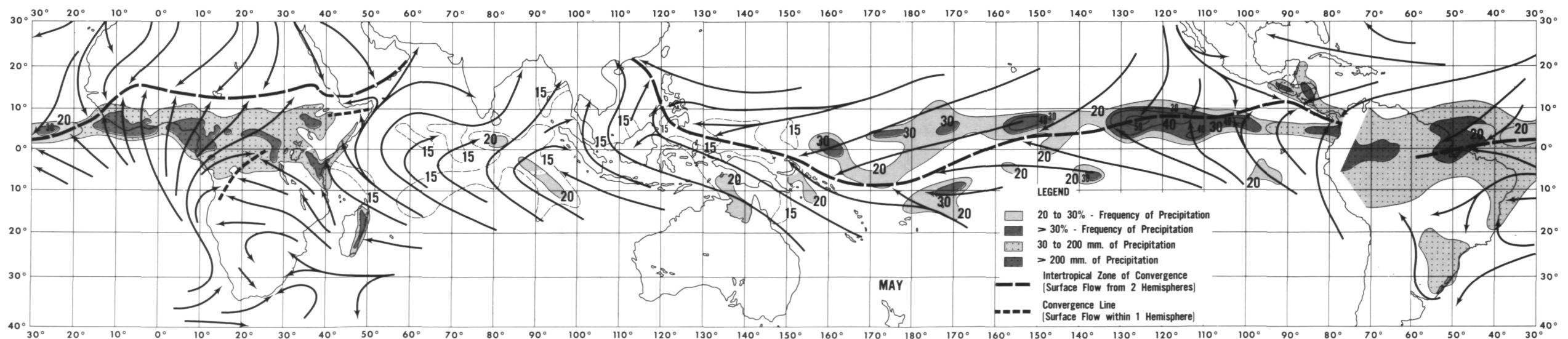
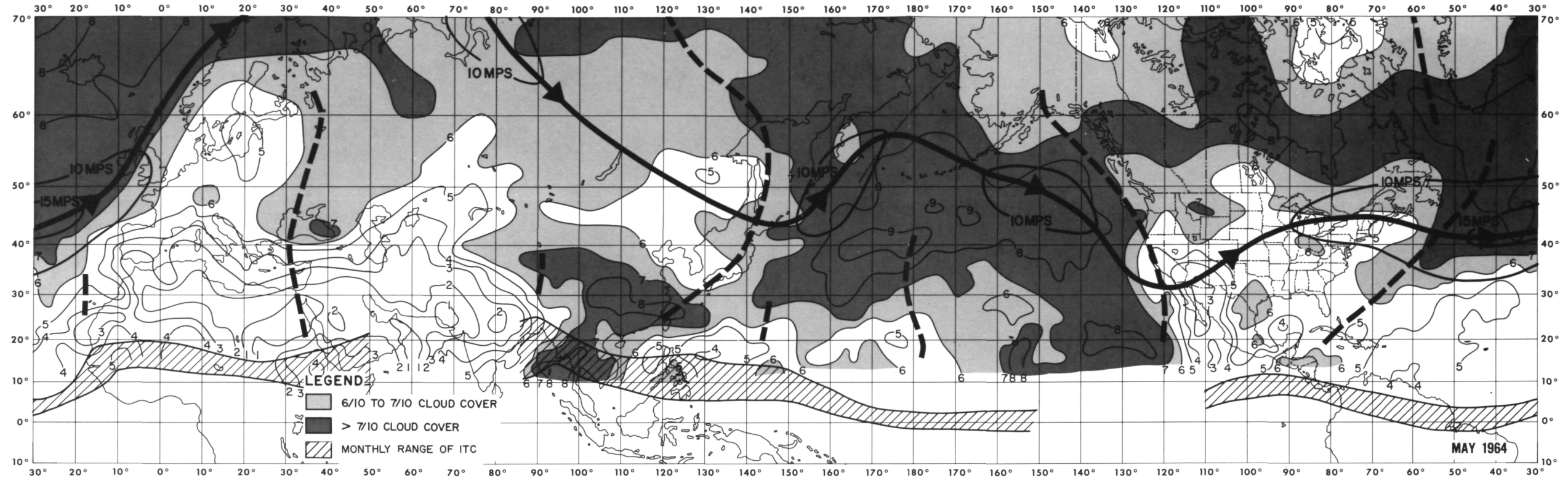


Figure A12(b) top — A12(c) bottom.

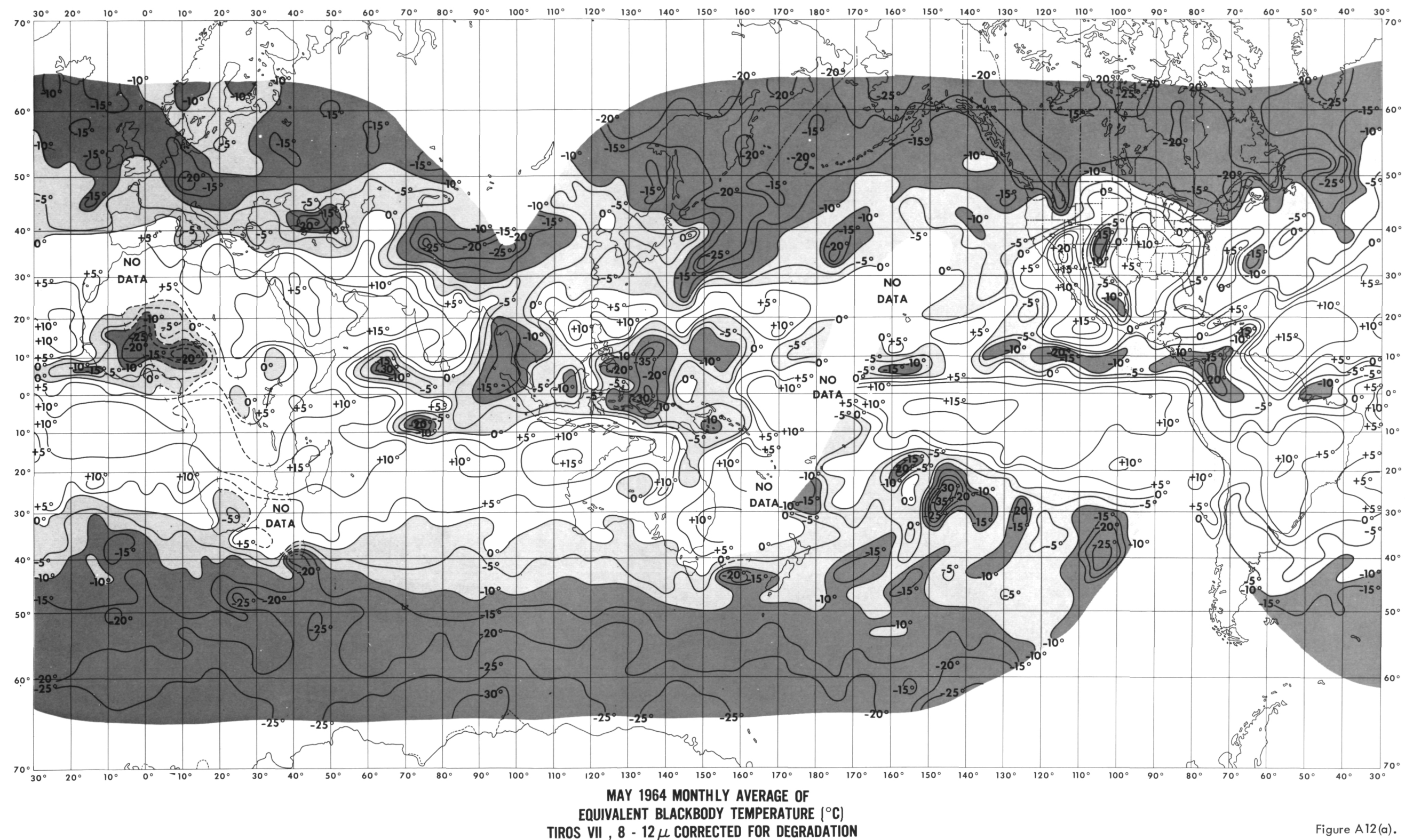


Figure A12(a).

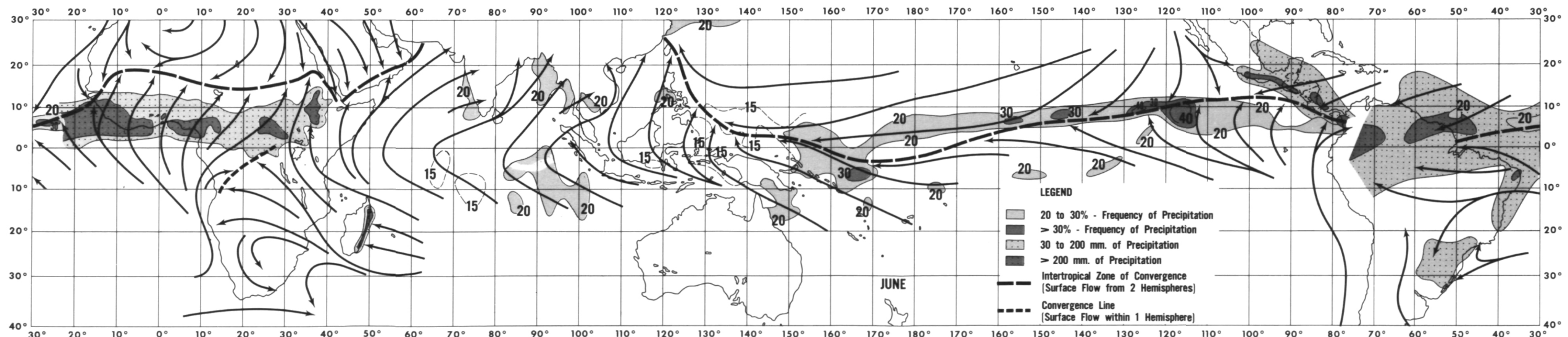
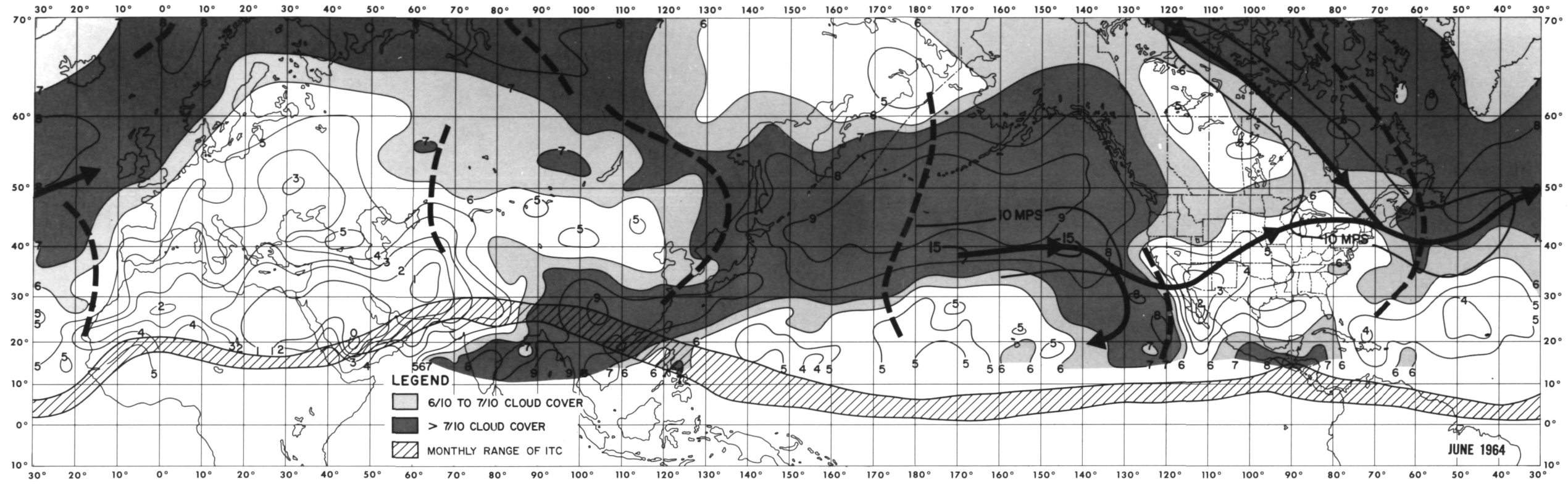


Figure A13(b) top — A13(c) bottom.

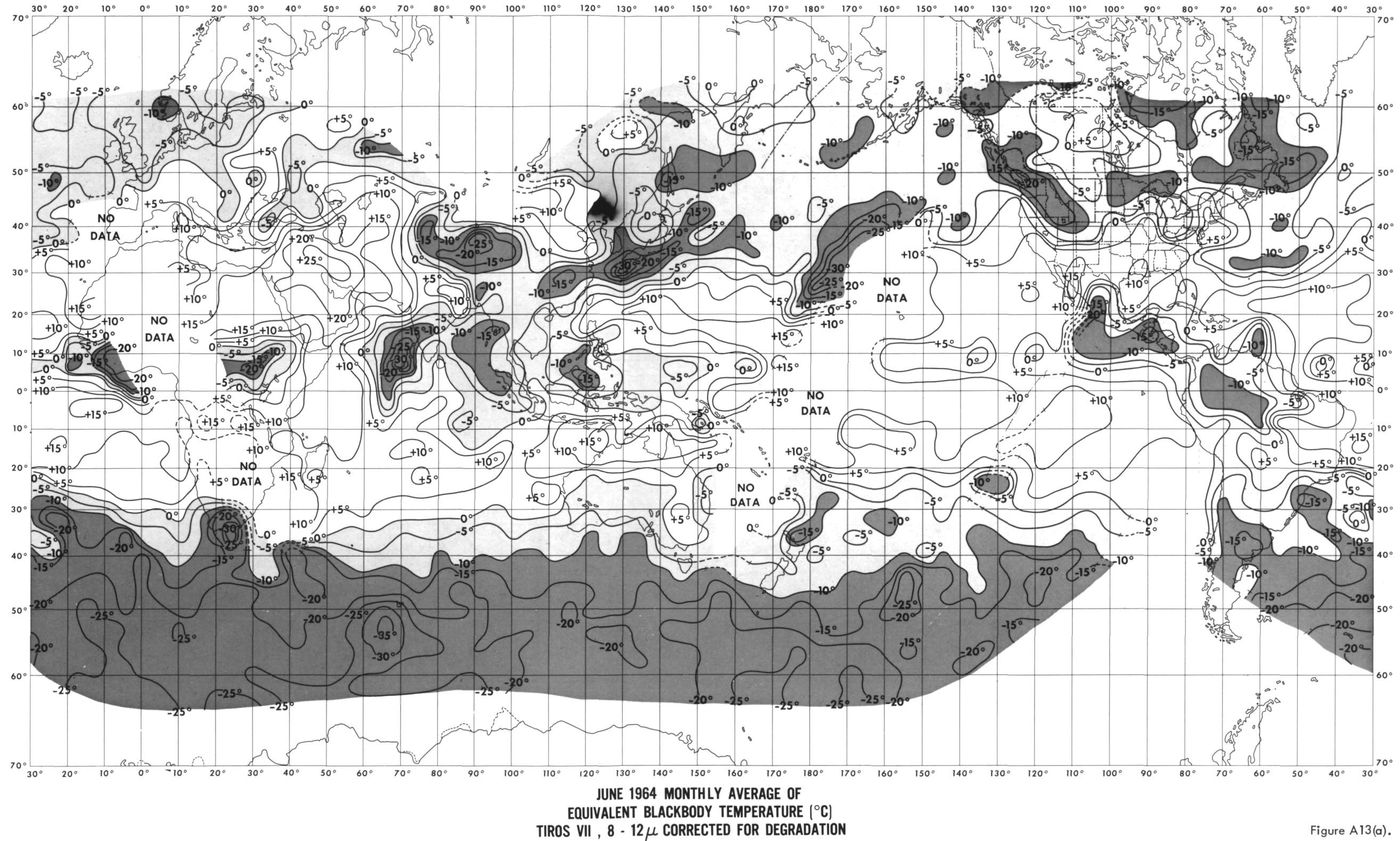


Figure A13(a).

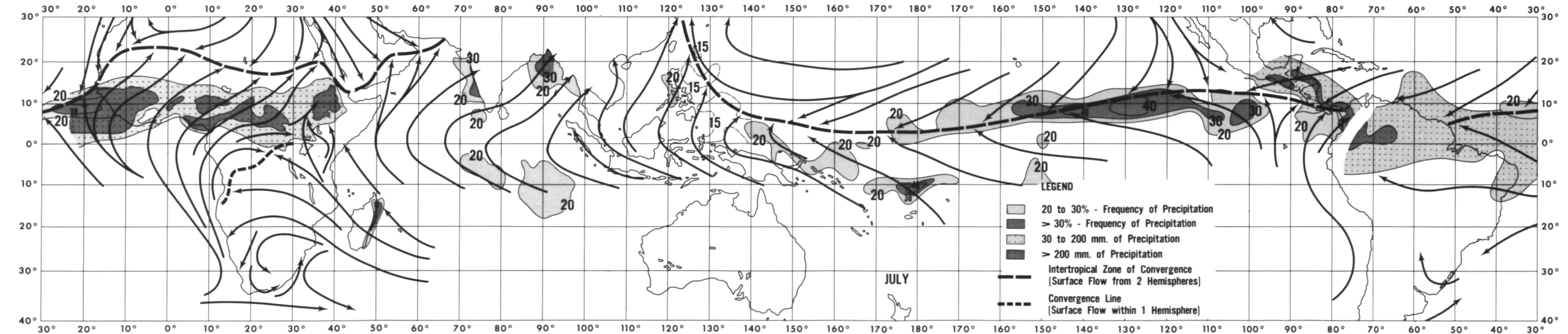
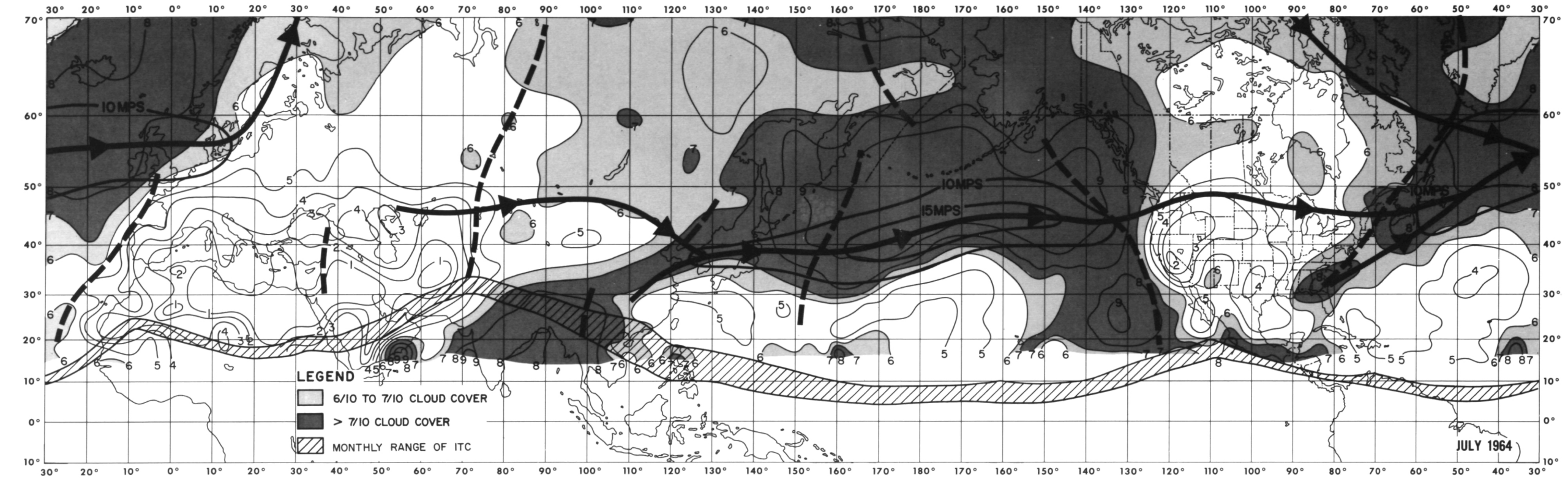
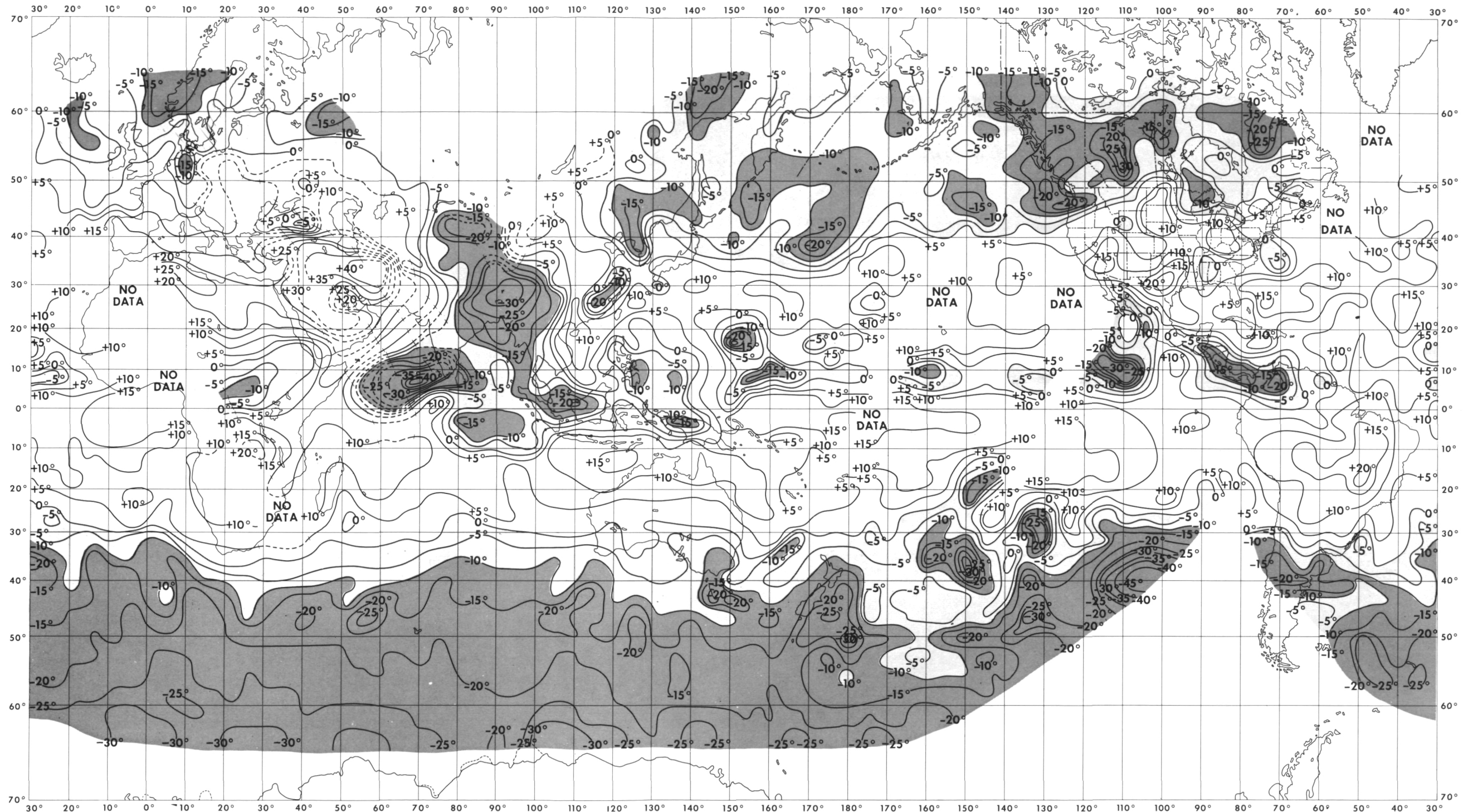


Figure A14(b) top — A14(c) bottom.



JULY 1964 MONTHLY AVERAGE OF
EQUIVALENT BLACKBODY TEMPERATURE [°C]
TIROS VII , 8 - 12 μ CORRECTED FOR DEGRADATION

Figure A14(a).

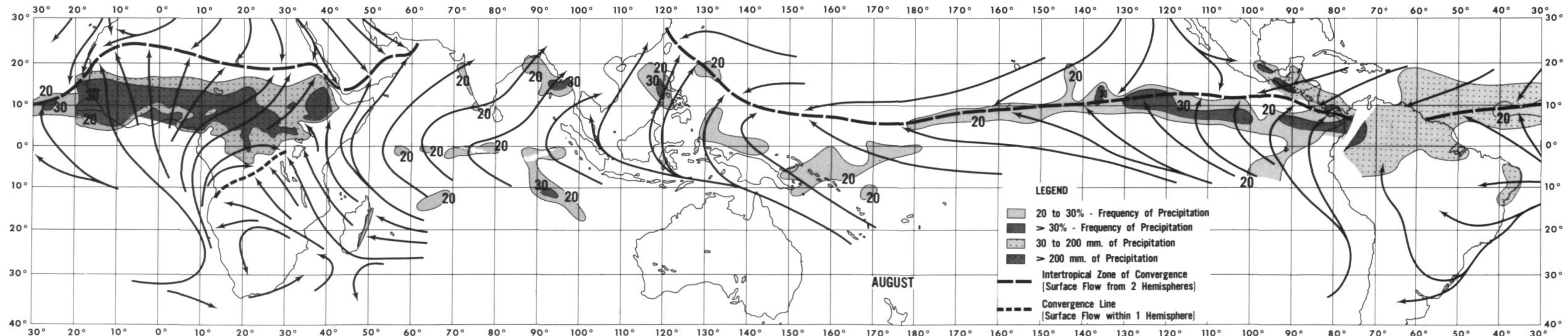
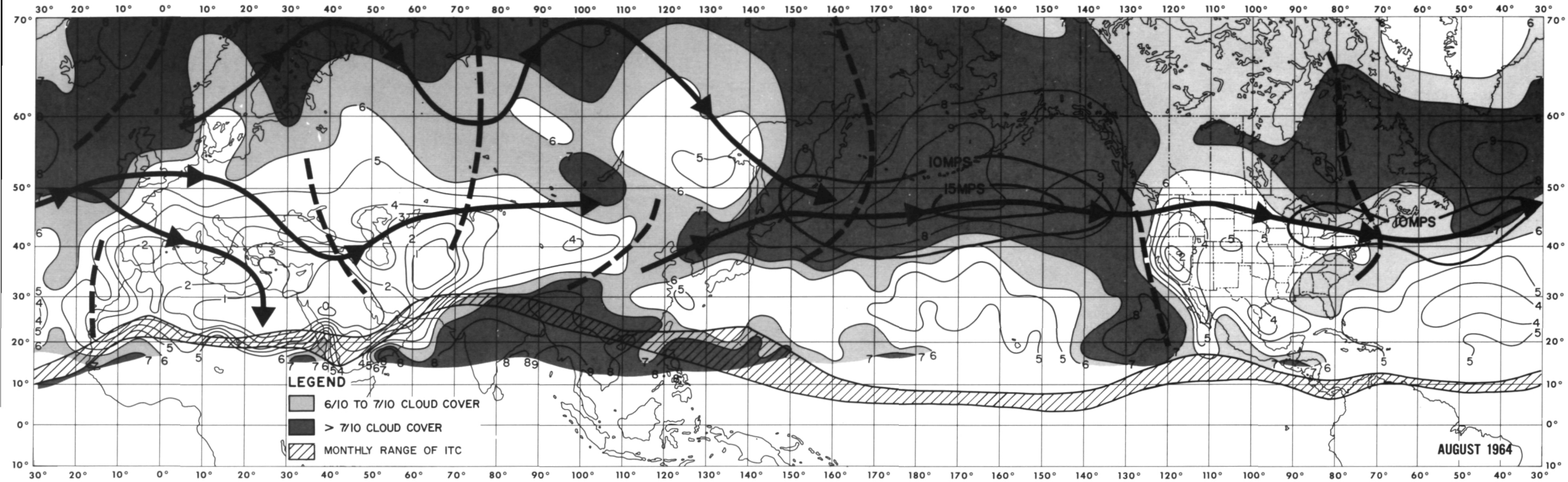
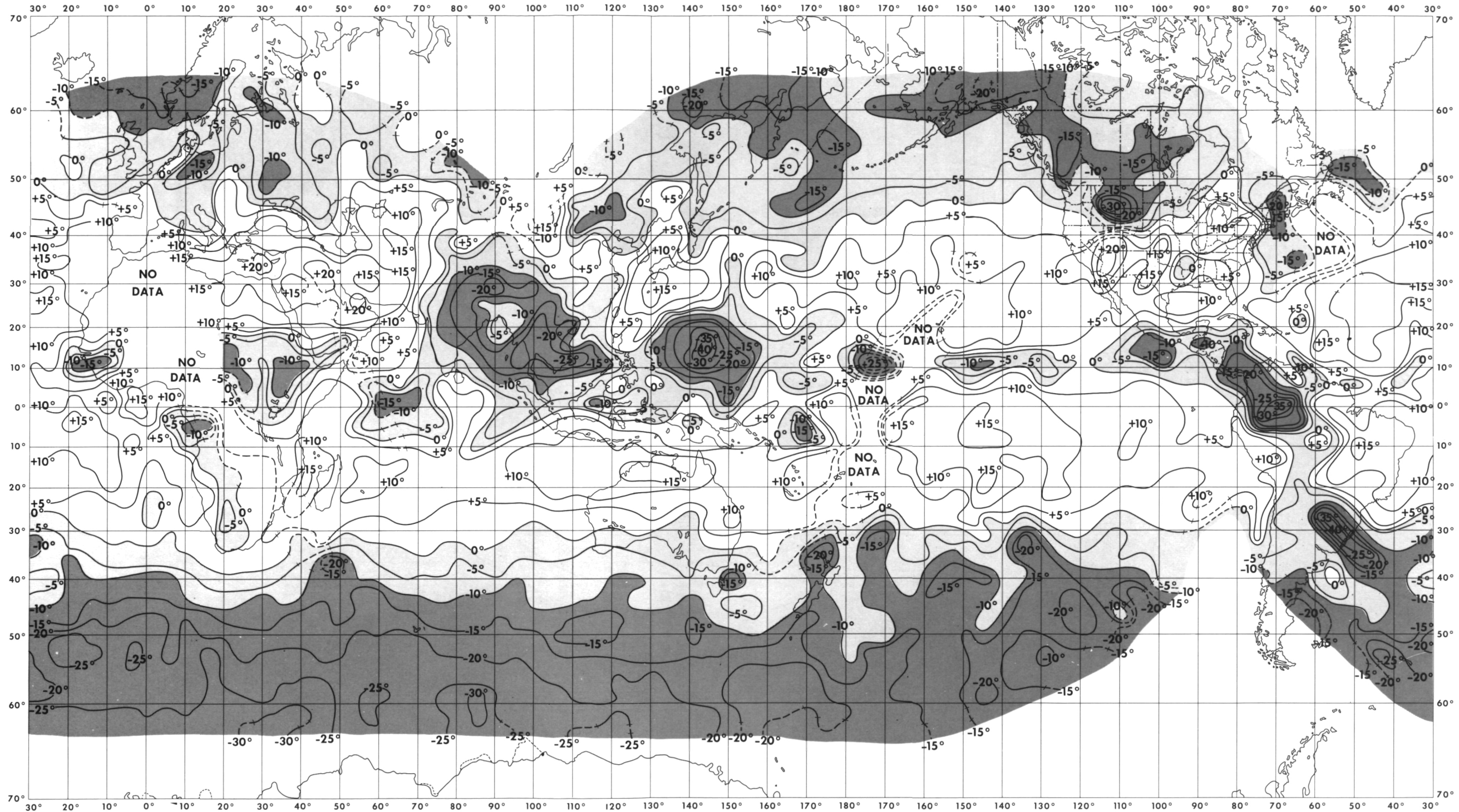


Figure A15(b) top — A15(c) bottom.



AUGUST 1964 MONTHLY AVERAGE OF
EQUIVALENT BLACKBODY TEMPERATURE ($^{\circ}$ C)
TIROS VII , 8 - 12 μ CORRECTED FOR DEGRADATION

Figure A15(a).

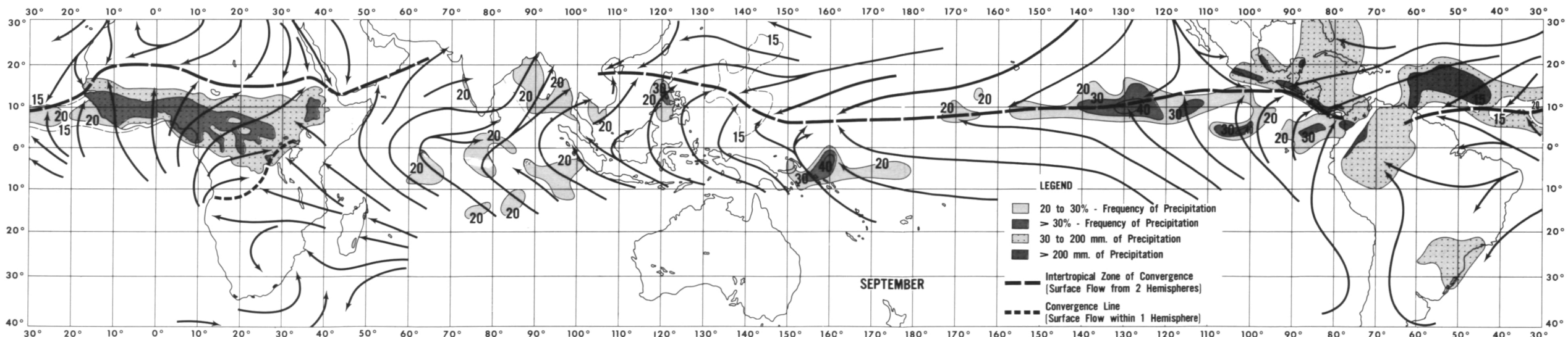
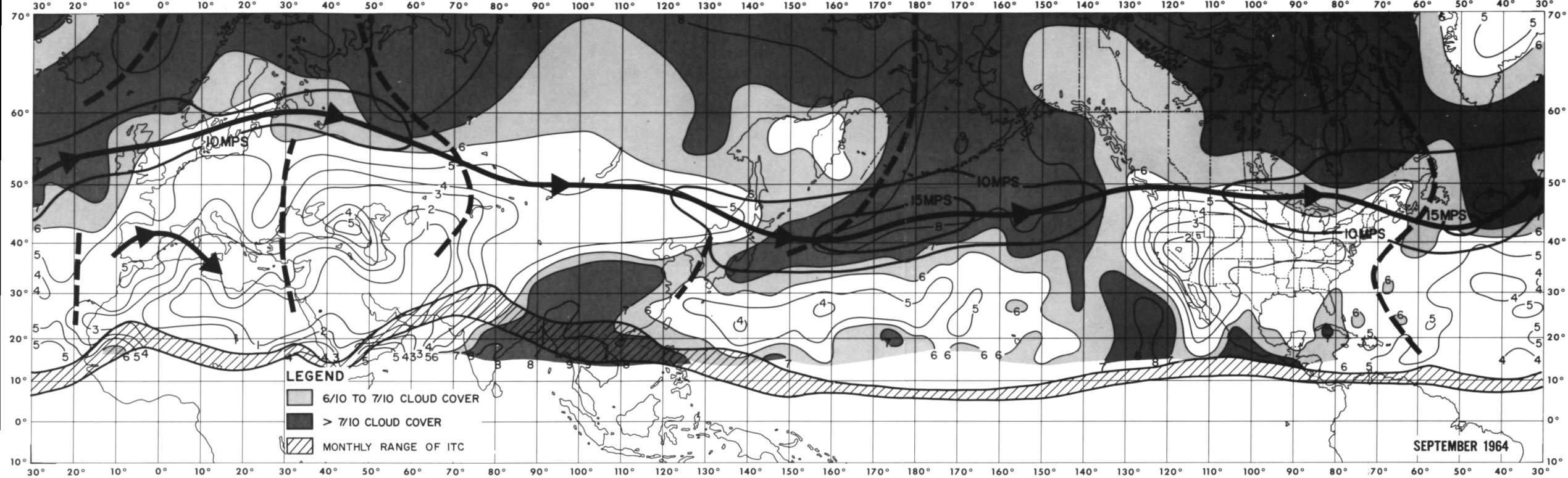
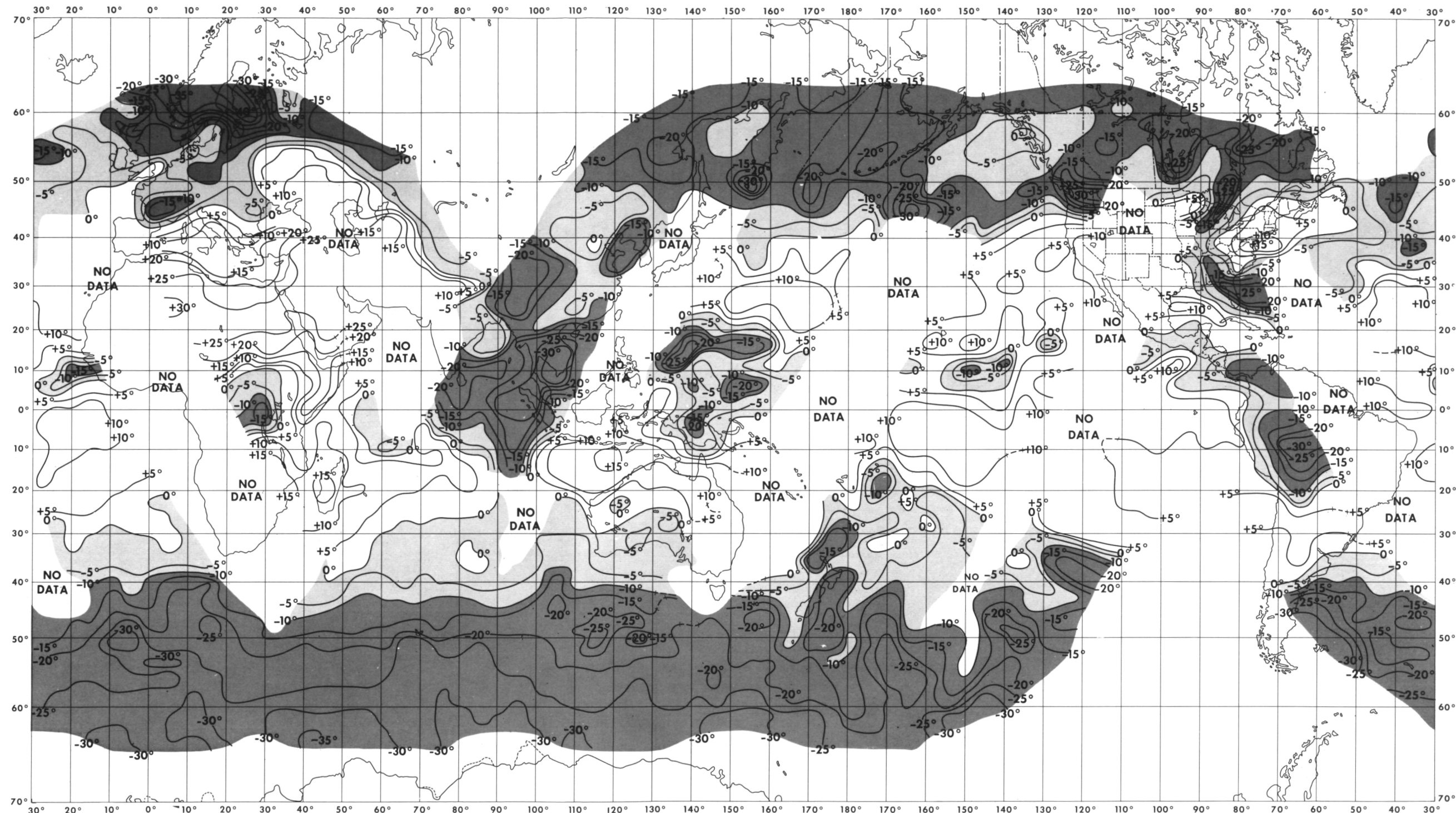


Figure A16(b) top — A16(c) bottom.



SEPTEMBER 1964 MONTHLY AVERAGE OF
EQUIVALENT BLACKBODY TEMPERATURE ($^{\circ}\text{C}$)
TIROS VII , 8 - 12μ CORRECTED FOR DEGRADATION

Figure A16(a).

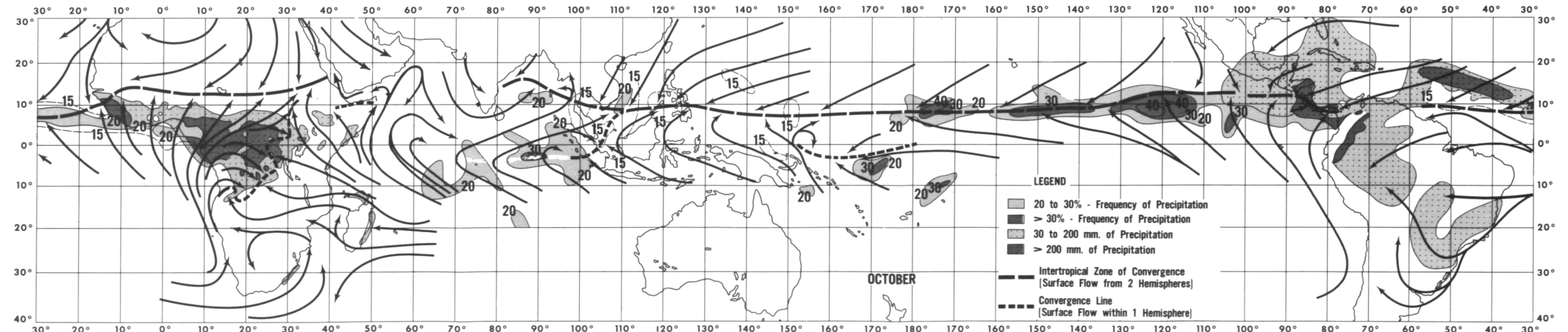
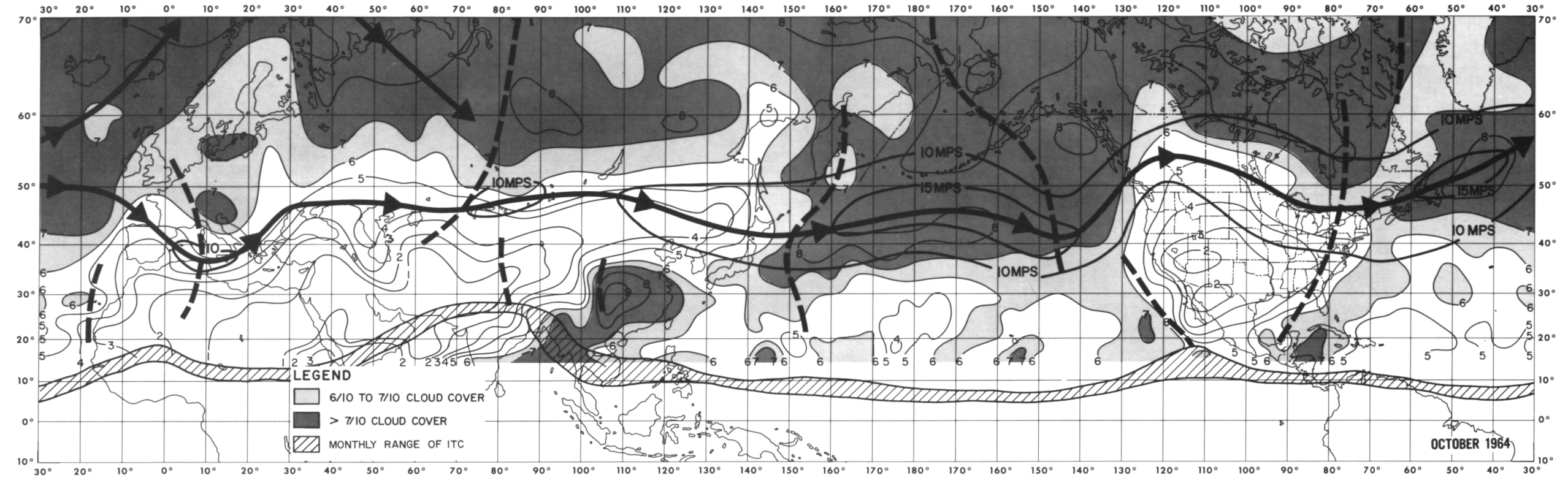
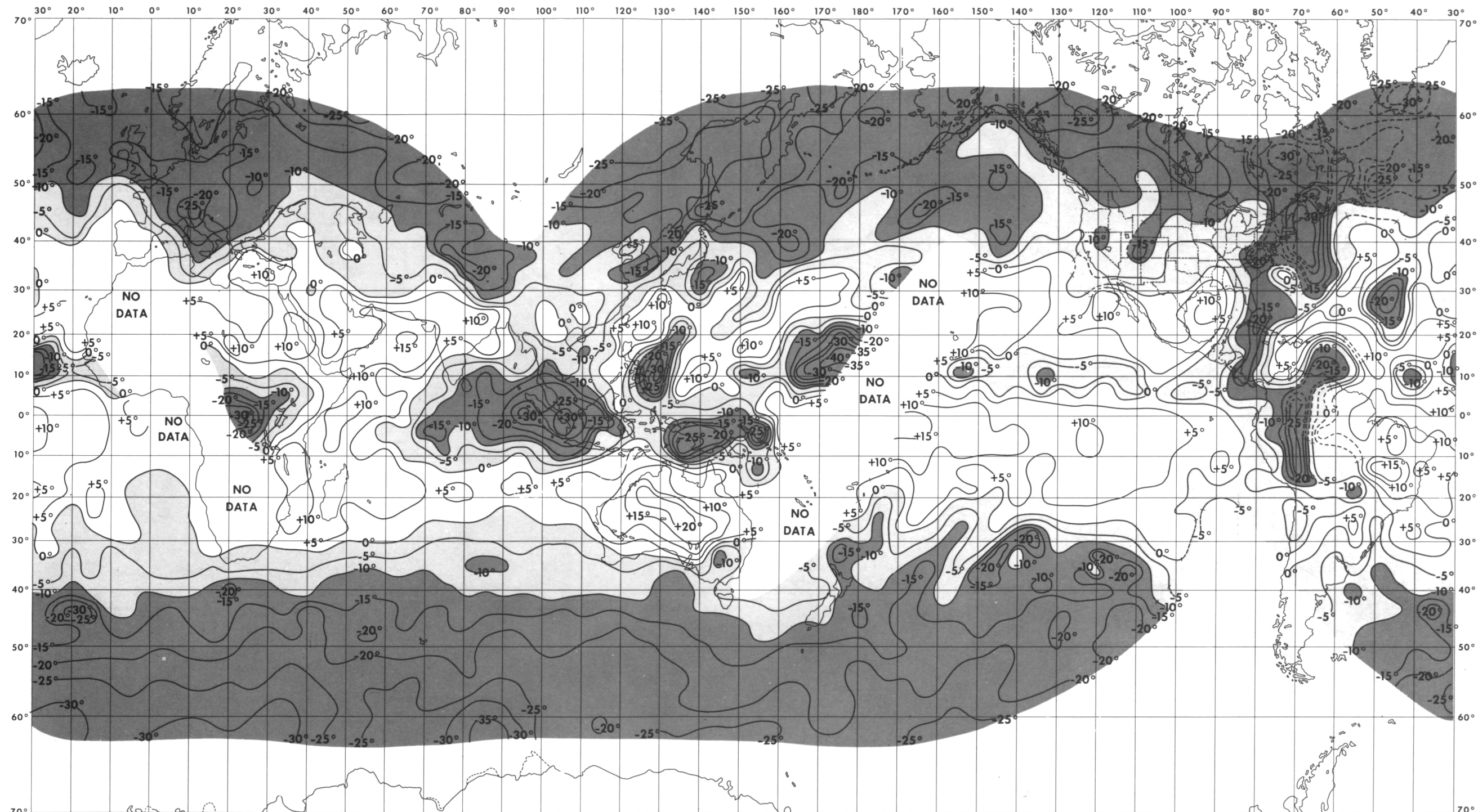


Figure A17(b) top — A17(c) bottom.



OCTOBER 1964 MONTHLY AVERAGE OF
EQUIVALENT BLACKBODY TEMPERATURE ($^{\circ}$ C)
TIROS VII , 8 - 12 μ CORRECTED FOR DEGRADATION

Figure A17(a).

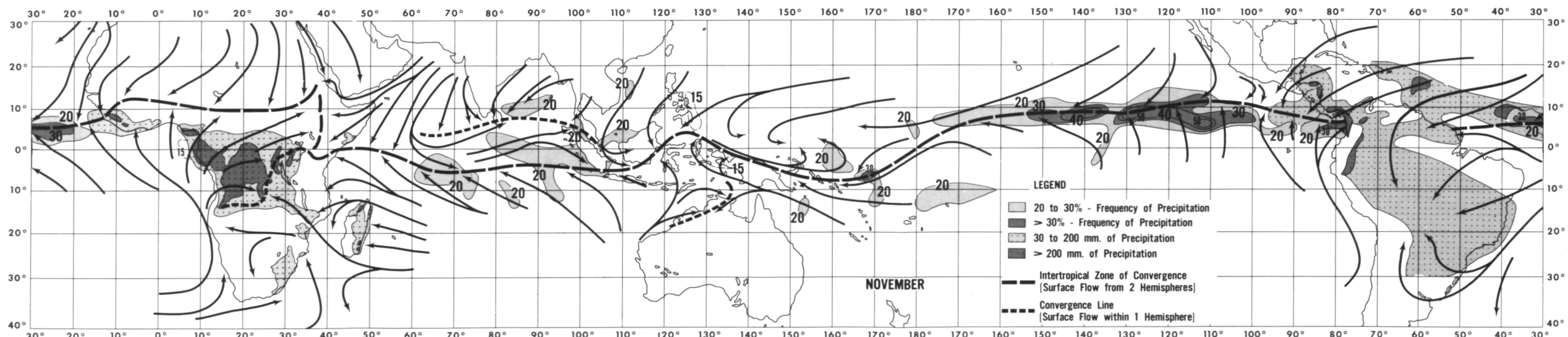
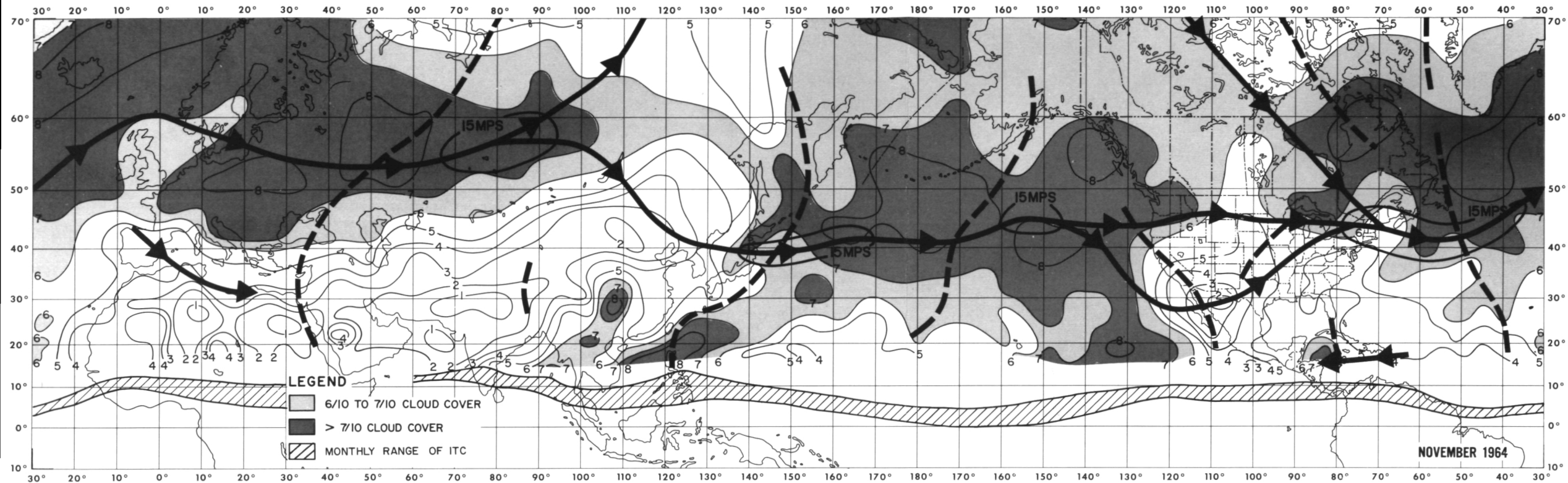
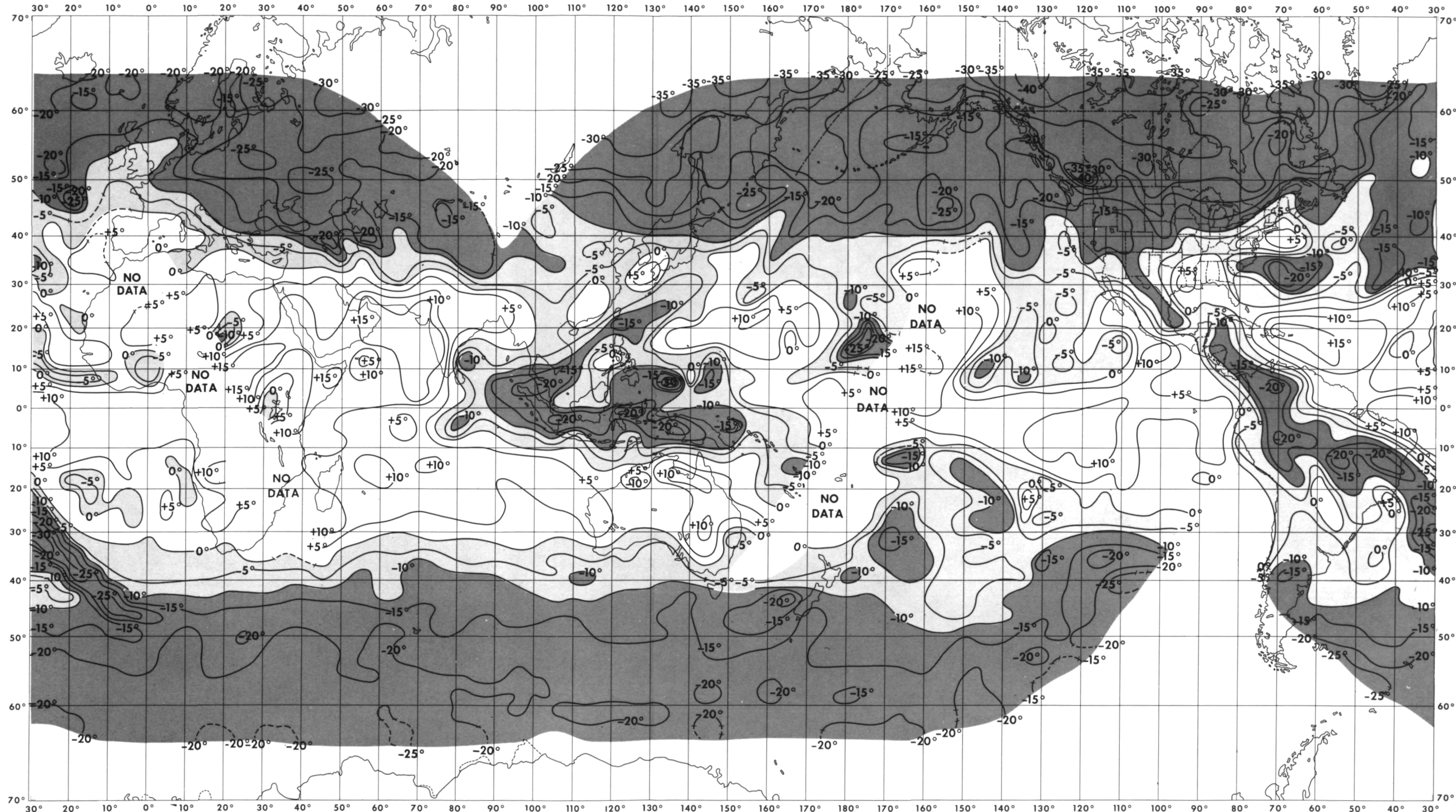


Figure A18(b) top — A18(c) bottom.



NOVEMBER 1964 MONTHLY AVERAGE OF
EQUIVALENT BLACKBODY TEMPERATURE ($^{\circ}\text{C}$)
TIROS VII, 8 - 12 μ CORRECTED FOR DEGRADATION

Figure A18(a).

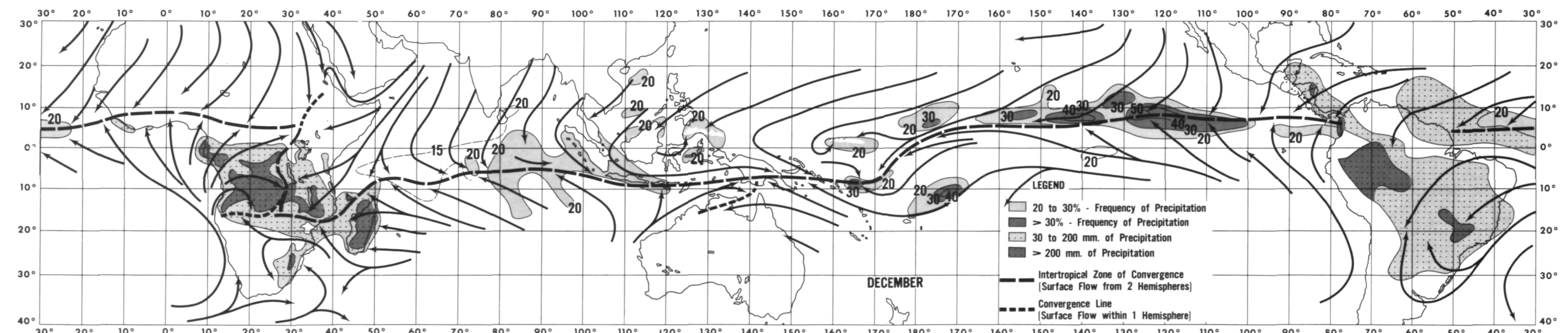
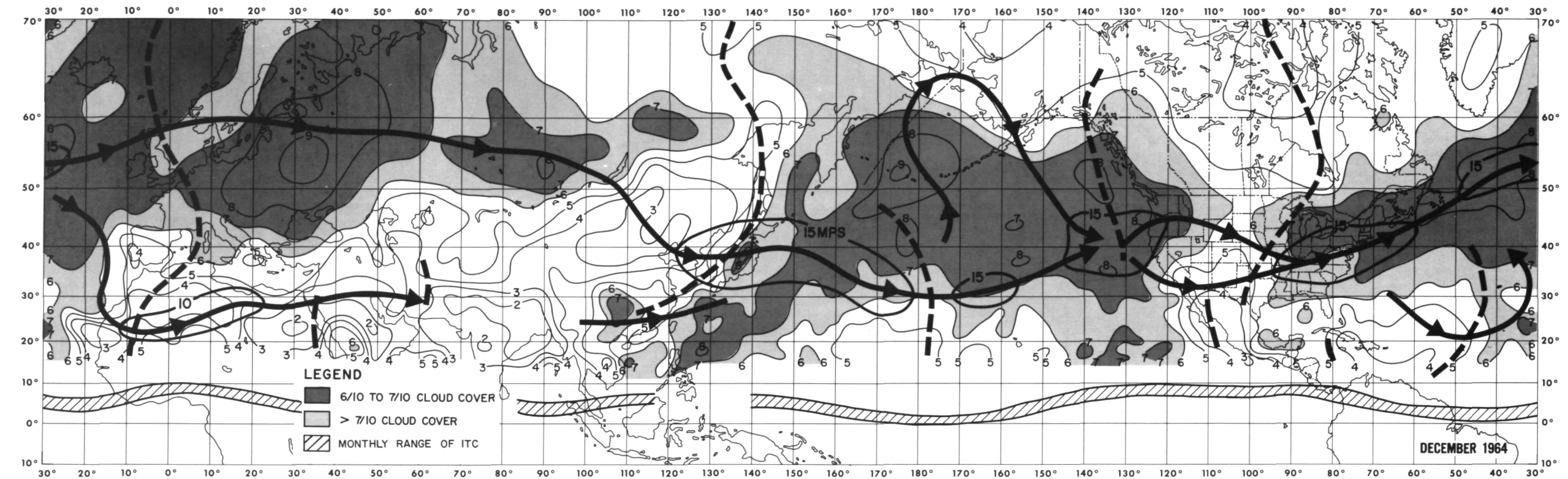
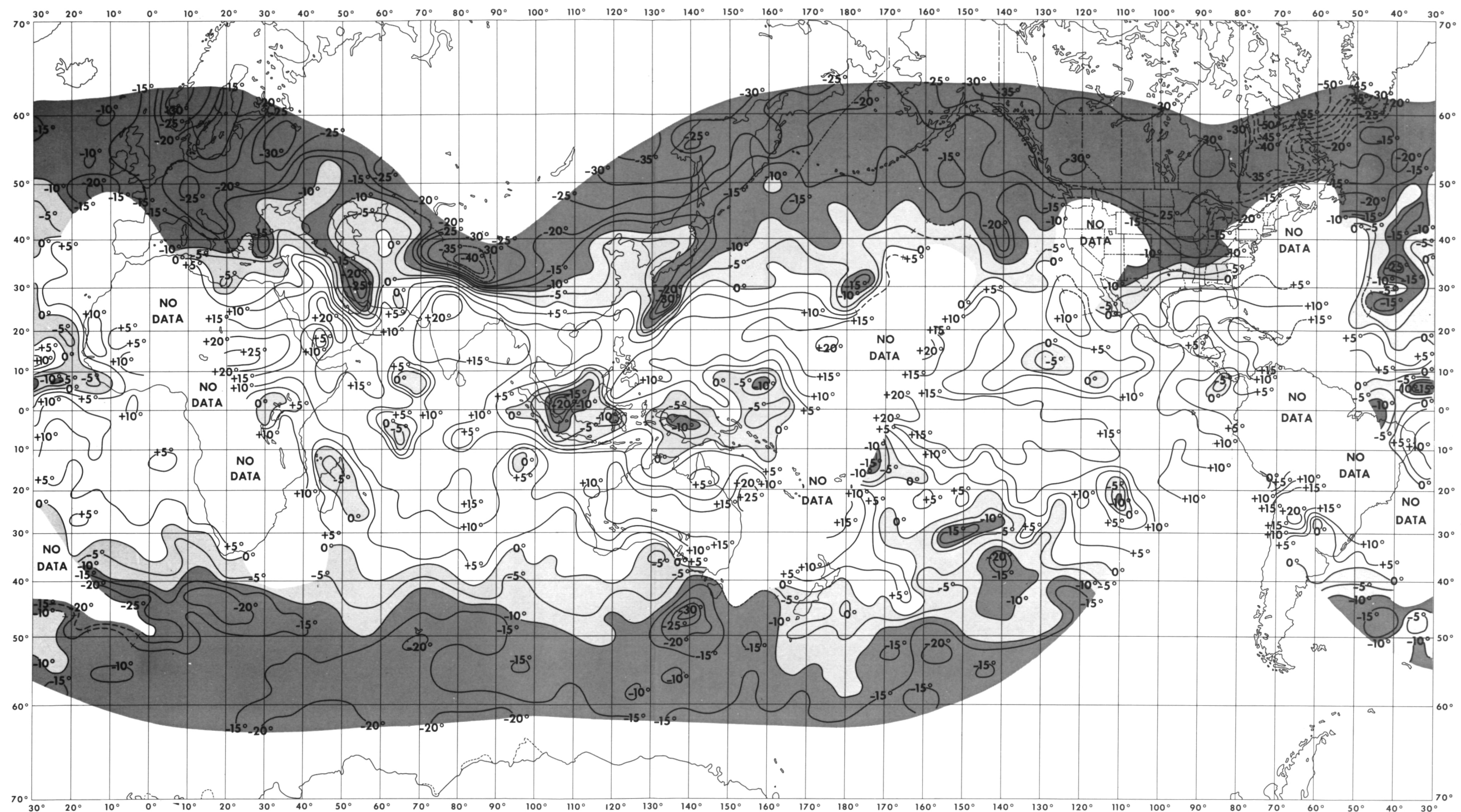


Figure A19(b) top — A19(c) bottom.



DECEMBER 1964 MONTHLY AVERAGE OF
EQUIVALENT BLACKBODY TEMPERATURE ($^{\circ}\text{C}$)
TIROS VII , 8 - 12μ CORRECTED FOR DEGRADATION

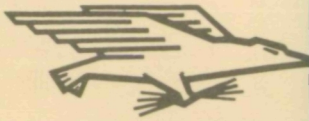
Figure A19(a).

NATIONAL AERONAUTICS AND SPACE ADMINISTRATION

WASHINGTON, D.C. 20546

OFFICIAL BUSINESS

FIRST CLASS MAIL



POSTAGE AND FEES PAID
NATIONAL AERONAUTICS AND
SPACE ADMINISTRATION

POSTMASTER: If Undeliverable (Section 158
Postal Manual) Do Not Return

"The aeronautical and space activities of the United States shall be conducted so as to contribute . . . to the expansion of human knowledge of phenomena in the atmosphere and space. The Administration shall provide for the widest practicable and appropriate dissemination of information concerning its activities and the results thereof."

— NATIONAL AERONAUTICS AND SPACE ACT OF 1958

NASA SCIENTIFIC AND TECHNICAL PUBLICATIONS

TECHNICAL REPORTS: Scientific and technical information considered important, complete, and a lasting contribution to existing knowledge.

TECHNICAL NOTES: Information less broad in scope but nevertheless of importance as a contribution to existing knowledge.

TECHNICAL MEMORANDUMS: Information receiving limited distribution because of preliminary data, security classification, or other reasons.

CONTRACTOR REPORTS: Scientific and technical information generated under a NASA contract or grant and considered an important contribution to existing knowledge.

TECHNICAL TRANSLATIONS: Information published in a foreign language considered to merit NASA distribution in English.

SPECIAL PUBLICATIONS: Information derived from or of value to NASA activities. Publications include conference proceedings, monographs, data compilations, handbooks, sourcebooks, and special bibliographies.

TECHNOLOGY UTILIZATION PUBLICATIONS: Information on technology used by NASA that may be of particular interest in commercial and other non-aerospace applications. Publications include Tech Briefs, Technology Utilization Reports and Technology Surveys.

Details on the availability of these publications may be obtained from:

SCIENTIFIC AND TECHNICAL INFORMATION DIVISION

NATIONAL AERONAUTICS AND SPACE ADMINISTRATION

Washington, D.C. 20546